UNIVERSITAT DE BARCELONA

Lipid raft association and subcellular localization of UNC5 Netrin-1 receptors

Associació als lípids raft i localització subcel·lular de la familia de receptors de la Netrina-1 UNC5

Marc Hernaiz Llorens

UNIVERSITY OF BARCELONA

FACULTY OF BIOLOGY

DEPARTMENT OF CELLULAR BIOLOGY, PHYSIOLOGY AND IMMUNOLOGY

BARCELONA SCIENCE PARK

Lipid raft association and subcellular localization of UNC5 family Netrin-1 receptors

Marc Hernaiz Llorens

Barcelona, September 2019

PhD program in Biomedicine

UNIVERSITAT DE BARCELONA

FACULTAT DE BIOLOGIA

DEPARTAMENT DE BIOLOGIA CEL·LULAR, FISIOLOGIA I IMMUNOLOGIA

PARC CIENTÍFIC DE BARCELONA

Lipid raft association and subcellular localization of UNC5 family Netrin-1 receptors

Associació als *lipid raft* i localització subcel·lular de la família de receptors de la Netrina-1 UNC5

Memòria presentada per **Marc Hernaiz Llorens**, graduat en Biologia, per optar al grau de Doctor per la Universitat de Barcelona.

Els estudis de tercer cicle s'han emmarcat dins el programa de Doctorat en Biomedicina de la Universitat de Barcelona. El projecte de Tesi Doctoral està inscrit al Departament de Biologia Cel·lular, Fisiologia i Immunologia de la Facultat de Biologia de la Universitat de Barcelona. El treball experimental i la redacció de la memòria han estat dirigits pel **Dr. Eduardo Soriano García**, Professor Catedràtic de la Universitat de Barcelona i pel **Dr. Ramón Martínez Mármol**, investigador Postdoctoral de la Universitat de Queensland.

Barcelona,

Verificat i amb la conformitat dels directors:

Dr. Eduardo Soriano García

Dr. Ramón Martínez Mármol

Marc Hernaiz Llorens

® Thesis cover illustration: Anna Llorens

Christina's World

Andrew Wyeth (1917-1989)

Tempera on gypsum. 1948

MUSEUM OF MODERN ART (MOMA): NEW YORK

This painting shows Christina Olson, an American girl from Cushing, Maine, who suffered from poliomyelitis. Andrew Wyeth was a friend of Christina's parents and stayed at their house on several occasions. There, Wyeth met Christina and witnessed her extraordinary strenght and willpower when it came to getting about, despite that she was unable to walk due to her illness. Wyeth said of her that she was "*an admirable woman*". With great difficulty, in this painting Christina drags herself across the lawn to reach the house.

Andrew Wyeth was born in Chadds Ford, Pennsylvania in 1917. He devoted himself above all to watercolors and tempera on gypsum. His oeuvre is realistic, depicting mainly scenes from rural American day life, in which sentiment dominate each of his paintings.

"*OBSERVED VULGARITY BECOMES ROMANTIC*" ANDREW WYETH

To Victor and Anna,

ABSTRACT

During brain development, UNC5 receptors play a key role in controlling axonal extension through their sensing of the guidance molecule Netrin-1. The correct positioning of receptors into specific cholesterol-enriched membrane raft microdomains is of crucial importance for the efficient transduction of the recognized signal. Whether such microdomains are required for the appropriate axonal guidance mediated by UNC5 receptors remains unknown. Here, we extend the classical biochemical characterization of raft microdomains by performing confocal microscopy, live cell FRAP analysis and sptPALM of fluorescently-tagged UNC5 receptors and we reveal for the first time differences into their membrane mobility properties. Using a combination of pharmacological and genetical approaches in primary neuronal cultures and brain cerebellar explants we further demonstrate that disrupting raft microdomains inhibit the chemorepulsive response of growth cones and axons against Netrin-1. Together, our findings indicate that the distribution of all UNC5 receptors into cholesterol-enriched raft microdomains is heterogeneous and that their specific localization have functional consequences for the axonal chemorepulsion against Netrin-1.

Alternative splicing is a key mechanism in which a variety of proteins is achieved from "cut and paste" mRNA. The plethora of proteins resulting from alternative splicing processes is crucial for the proper function of certain protein isoforms. In this thesis we have detected alternative splicing in the UNC5A receptor in the nervous system. The resulting product is a UNC5A isoform that lacks the first TSPI repeat, uncovered here, to be important for cell membrane targeting. We have further analyzed the implications of losing the first TSPI repeat.

TABLE OF CONTENTS

ABREVIATIONS

ABCA1	ATP-binding cassette A1
ADD	Addiction/dependence domain
Atoh1	Atonal BHLH Transcription Factor 1
Bcl-2	B-cell lymphoma 2
BDNF	Brain derived neurotrophic factor
BMP	Bone Morphogenetic Protein
CAM	Cell adhesion molecule
cav	Caveolin
C-domain	Central domain
ChoA	Cholesterol oxidase
CHX	Cycloheximide
CNS	Central nervous system
CoA	Coenzyme A
CTxB	Cholera toxin B-subunit
CYP27A1	Sterol 27-hydroxylase
CYP46A1	Cholesterol 24-hydroxylase
DAPK	Serine/threonine kinase death-associated protein kinase
DB	DCC binding
DCC	Deleted in Colorectal Cancer
DD	Death domain
DIP13	DCC interacting protein 13
DRM	Detergent resistant membrane
DSCAM	Down syndrome cell adhesion molecule
DSM	Detergent soluble membrane
E	Embryonic day

EGF	Epidermal growth factor
EGL	External granular layer
Eph	Erythropoietin-producing hepatocellular carcinoma
ER	Endoplasmatic reticulum
F-actin	Filamentous actin
FAD	Flavin adenine dinucleotide
FNIII	Fibronectin type III
GAP	GTPases activating protein
Gbx2	Gastrulation brain homeobox 2
GDI	Guanine nucleotide dissociation inhibitors
GDNF	Glial cell line-derived neurotrophic factor
GDP	Guanosine-5'-diphosphate
GEF	Guanine nucleotide exchange factors
GFP	Green Fluorescent Protein
GM_1	Monosialotetrahexosylganglioside
GPI	Glycosylphosphatidylinositol
GTP	Guanosine-5'-triphosphate
GUV	Giant unilamellar vesicle
HEK293T	Human Embryonic Kidney 293T
HRP	Horseradish peroxidase
ICM	Inner cell mass
Ig	Immunoglobulin
IGL	Internal granular layer
kD	kiloDalton
L_d	Liquid disordered
LDLR	Low-Density Lipoprotein Receptor

lEGL	Lower external granular layer
L_o	Liquid ordered
MBS	Membrane blocking solution
Mf	Mobile fraction
MHB	Midbrain/hindbrain boundary
ML	Molecular layer
MT	Microtubule
MβCD	Methyl-β-cyclodextrin
NGF	Nerve growth factor
NgR	Nogo receptor
P	Postnatal day
P-domain	Peripheral domain
PIP_3	Phosphatidylinositol-3, 4, 5-triphosphate
PKB	Protein kinase B
r1	Rhombomere 1
RFP	Red Fluorescent Protein
Rho	Ras homologous
Robo	Roundabout
ROI	Region of interest
Otx	Orthodenticle
Sema3A	Semaphorin3A
Sema3B	Semaphorin3B
Sema3F	Semaphorin3F
Shh	Sonic Hedgehog
SR-BI	Scavenger receptor class B type 1
TIRFM	Total internal reflection fluorescence microscopy

TSPI	Thrombospondin type I
T-zone	Transition zone
uEGL	Upper external granular layer
UNC5	Uncoordinated-5 homolog
UPR	Unfolded protein response
Wnt	Wingless
YFP	Yellow Fluorescent Protein
ZU5	Zona ocludens/UNC5

INTRODUCTION

The human brain is perhaps the most complex organ in our body. It is composed by billions of cells and trillions of connections, that make this organ a treasure of enormous proportions. Nowadays, we are far to comprehend how this intricate machinery works, but the study of the cellular constituents, neurons and glia, have been a productive field over the past decades. Cells in the brain are able to communicate between them to generate an immensely vast range of outcomes, from voluntary movement to maintaining vegetative functions in our body or complex features like sensations, thoughts and behavior. To comprehend all these processes, we must first understand how neuronal cells are first identified and how the complex circuitry of the brain is established.

It is important then, to take into consideration that the construction of the brain is the result of a series of very finely tuned developmental stages, starting with the decision of few embryonic cells to undergo neuronal cells to the continuously shaping and rewiring of neuronal connections due to environmental inputs.

1. DEVELOPMENT OF THE MAMMAL NERVOUS SYSTEM

1. 1. EARLY STAGES OF EMBRYONIC DEVELOPMENT

The cells of mammals are organized into differentiated layers. These layers are generated from the egg cell through a series of synchronized cell divisions and subsequent rearrangements. Once fertilized by the sperm, the egg undergoes a series of rapid cell divisions, known as cleavages and defining the morula stage (Fig. 1A). Once cleavages are completed, all resulting cells are equal in their potential. After a sufficient number of cell divisions, two regions are determined, trophoblasts, that will give rise to extra-embryonic tissues and the inner cell mass (ICM), which are cells inside the hollow ball, which is called blastula at this stage (Fig. 1A). After this stage, mammalian embryos undergo a process of gastrulation, in which the developing mesodermal cells migrate through the primitive streak that runs along the anterior-posterior

axis. The ectoderm, laying above the entering mesodermal cells, will ultimately become the neural tube. As development continues, the streak elongates until reaching maximum length. The distal tip of the streak is known as the node. The node works as an organizer and it resembles the Hensen's node in chick[1].

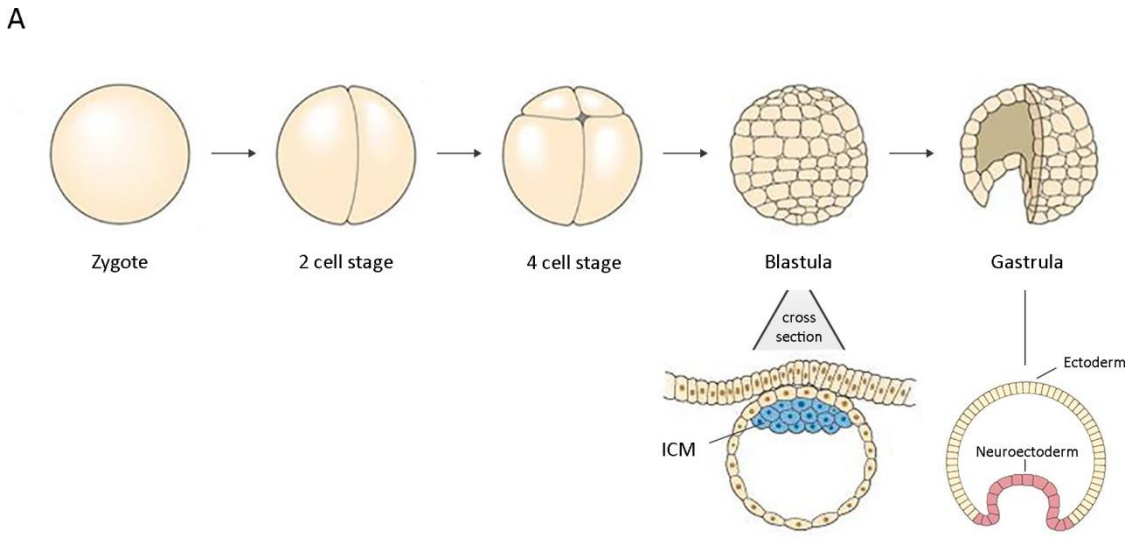

Figure 1 | Early stages during animal development. The early processes during animal development share a conserved sequence. After fertilization, a series of cleavage divisions, divide the egg into a multicellular blastula (**A**). At this point some cells (ICM) are found inside the blastula (**A**). During the process of gastrulation, some cells from the surface of the embryo migrate inside to generate the three layered structure, common to most multicellular animals (**A**). At some point after gastrulation, a subset of the ectoderm is specified as neuroectoderm, which will ultimately give rise to the CNS. ICM: Inner cell mass.

1. 2. THE NEURAL INDUCTION

The three basic layers of the embryo, the endoderm, mesoderm and ectoderm, arise through movements of the gastrulation, which create new tissue contacts and relations. The ectoderm is the outermost of the three germ layers, which will give rise to the entire central nervous system and other organs and embryonic structures. The neural induction is the process where a subset of the ectoderm is determined to develop into the nervous system. A subset of cells of the ectoderm will become the neuroectoderm, which is induced by the inhibition of the Bone Morphogenetic Protein (BMP) pathway (Fig. 1A). Other critical cues to determine and maintain neural fate of the prospecting nervous system are the Fibroblast Growth Factor (FGF)

family and the Wingless (Wnt) family of transcription factors. The process of neural induction results in a plate of cells that cover the rostrocaudal length of the whole embryo.

1. 3. NEURULATION

The neural plate is a thickened region of the ectoderm located medially in the embryo. This thickening of the neural plate, is an intrinsic property of the ectodermal cells, once they have been induced as neural cells[2]. During the shaping of the neural plate, several cell behaviors like cell elongation, convergent extension and cell division, along with a regression of the primitive streak[3], convert the neural plate from a relatively short structure to a long and narrow. This process is mainly driven by the notochord, a common feature of all chordate animals. Notochord derives from cells in the mesoderm and mainly secretes Sonic Hedgehog (Shh), thought to be crucial for neural plate cells fate determination.

Once the neural plate has become a narrow and lengthen structure, there is a localized deformation and elevation of the two flanks of the cells of the neuroepithelium, converting the neural plate to a neural groove[2]. Subsequently, this neural groove undergoes closure by bringing the two tips of the neural folds into close contact, which will attach and fuse. The non-neural epithelium will form a continuous sheet above the neural tube and the cells of the neural crest.

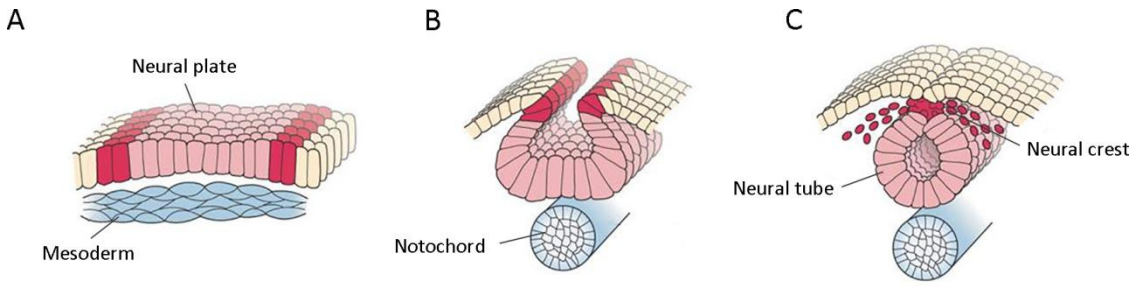

Figure 2 | Specification of the neural tube. When the neural tube is specified, it begins to fold to separate from the ectoderm (light red) (**A**). A subset of involuting cells derived from the mesoderm, condense to form the notochord (blue) (**B**). This structure, specifies the identity of the cells conforming the neural plate (**B**). When the neural plate rolls up, both dorsal margins fuse and from this fusion point neural crest cells arise (red) (**C**).

1. 4. REGIONALIZATION OF THE CENTRAL NERVOUS SYSTEM

In the mammal embryo, most of the neural tube will give rise to the spinal cord. The rostral part of the neural tube enlarges to form the three primary brain vesicles: the prosencephalon (forebrain), the mesencephalon (midbrain) and the rhombencephalon (hindbrain). The three primary brain vesicles are further subdivided into five vesicles. The prosencephalon is divided into the telencephalon and the diencephalon, which give rises to structures such as the thalamus, hypothalamus and the pair of optic vesicles. The mesencephalon remains as a single vesicle, while the rhombencephalon divides into the metencephalon and the myelencephalon, from which form the cerebellum and the medulla respectively.

The rhombencephalon is the most caudal region and it develops into the hindbrain. At some point in development, the rhomboencephalon is divided into segments known as rhombomeres. They are repeating units separated by distinct boundaries, controlled and specified by a specific set of genes known as homeobox genes (Hox). A specific set of genes control and specify the identity of each rhombomere[4].

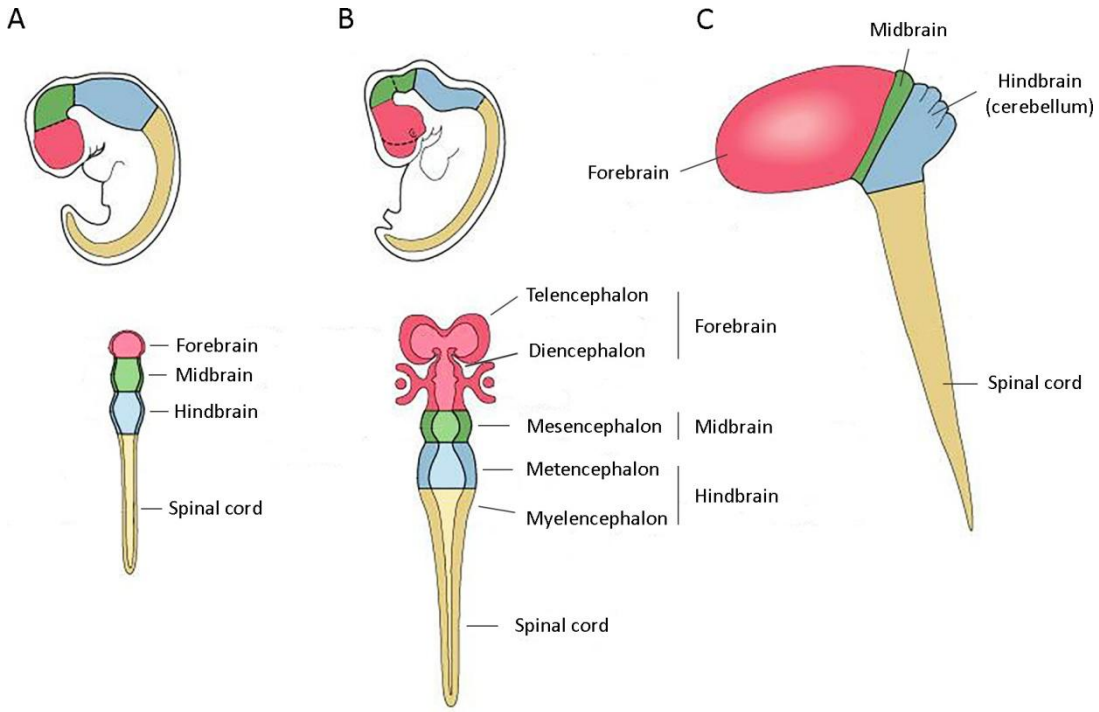

Figure 3 | Regionalization of the CNS. The vertebrate CNS develops from the neural tube. In this schema are shown lateral (upper) and dorsal (lower) views at successively older stages in embryonic development (**A**-**C**). At first stages, three brain vesicles are specified known as forebrain (prosencephalon) (red), midbrain (mesencephalon) (green), and hindbrain (rhombencephalon) (blue) (**A**). Next stages results in further subdivisions, with the forebrain vesicle becoming subdivided into the paired telencephalic vesicles and the diencephalon (red), and the rhombencephalon becoming subdivided into the metencephalon and the myelencephalon (blue) (**B**). These basic brain divisions can be related to the overall anatomical organization of the mature brain (**C**).

2. CEREBELLAR DEVELOPMENT

The cerebellum 'little brain' is a large and highly convoluted part of the brain. It represents one of the most architecturally elaborated regions of the central nervous system. In the cerebellum relies the control of our movements and particularly our balance, integration of several inputs from other areas of the central nervous system, as well as being important for cognitive processes, emotions and language processing. Although this will be described later in more detail, this thesis focuses on understanding axonal guidance processes of the granule cells (GCs), a key point for the proper cerebellar development.

2. 1. DEFINING BOUNDARIES (CEREBELLAR PRIMORDIUM)

The territory of the neural tube that generates the cerebellum is located between the midbrain and the hindbrain, which is called the isthmus. The anlage of the cerebellum is the product of several segmentation mechanisms that establish rhombomeric segmentation just after the neural tube closure. In fact, all the cells that build the cerebellum arise from the rhombomere 1 (r1), a region characterized by the absence of expression of Orthodenticle (Otx) and Hox genes[5]. Otx2 expression in the rostral part and Hoxa2 in the caudal part, define the midbrain/hindbrain boundary (MHB). MHB defines the expression of Gastrulation brain homeobox 2 (Gbx2) in r1 which is a requirement for the formation of the cerebellum[6]. On the other hand, FGF8 is the major signaling molecule at the MHB, which is expressed within the Gbx2-positive domain and repressing Otx2 expression[7].

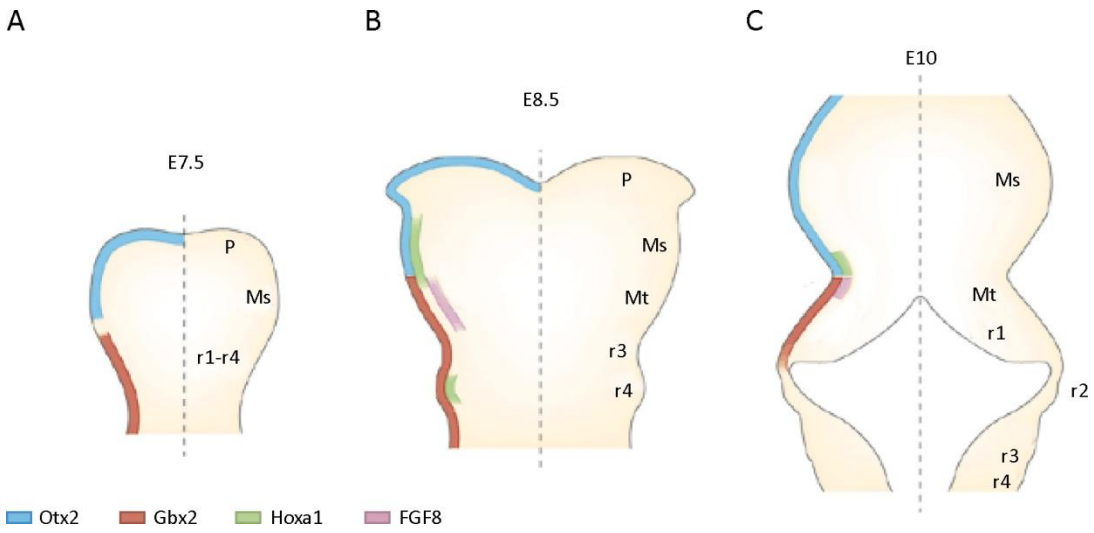

Figure 4 | The correct specification of the MHB is important for the correct cerebellar development. Schematic representation of coronal sections during MHB establishment. The neural plate at E7.5 is subdivided into an anterior domain that expresses Otx2 and a posterior domain that expresses Gbx2. The expression patterns of these genes meet at the MHB and form decreasing gradients in opposite directions (**A**). At E8.5 the expression of Otx2 and Gbx2 are sharpen and exclude each other. Hoxa1 expression is initiated in the mesencephalon and FGF8 expression starts to the caudal side of the Otx2-Gbx2 border (**B**). At E10, the Otx2-Gbx2 border identifies the MHB. The expression of Hoxa1 and FGF8 becomes restricted to narrow rings encircling the neural tube on either side of this boundary (**C**). P: Prosencephalon; Ms: Mesencephalon; Mt: Metencephalon.

2. 2. CEREBELLAR HISTOGENESIS

The cerebellum is a complex part of the brain, which requires a series of processes to build its intricate cytoarchitecture. The cerebellum is composed by the large Purkinje neurons, that are generated from the ventricular zone, near the fourth ventricle of the brain stem. Once they finish their final mitotic division, Purkinje cells migrate a short distance radially to accumulate irregularly in the cerebellar plate. As the cerebellum grows, Purkinje cells are finally arranged in a single cell layer. In addition to the Purkinje cells, from this ventricular zone also are generated other cerebellar interneurons such as stellate cells and basket cells.

Unlike these other type of cells, the most numerous type of neurons,the GCs, arise from another progenitor zone, called the rhombic lip[8]. The GC precursors migrate away from the ventricular zone, over the developing Purkinje cells to form a secondary zone of

neurogenesis, called the external granular layer (EGL). GCs ultimately migrate tangentially and are progressively placed beneath the Purkinje cell layer.

2. 3. CEREBELLAR CYTOARCHITECTURE AND CONNECTIVITY

2. 3. 1. STRUCTURE OF THE CEREBELLUM

The mammal cerebellum is a reproducible pattern of several anteroposterior folds called lobules. Mediolaterally, the cerebellum can be divided into three sections, the central part is called vermis, which is surrounded by the paravermis, to finally reach the hemispheres[9]. During embryonic development, the cerebellum is a smooth structure that, through a drastic cell movements during development, becomes a complex and folded structure that is completed at postnatal day (P) 20[10].

Each mediolateral region of the cerebellum contains all the cell types present in it, organized around a repeated anatomical plan[11]. It consists in a three layered cortex that surrounds an inner core of white matter and the cerebellar nuclei. The innermost layer of the cerebellar cortex is dominated by GCs, although, there are more cell types like Golgi cells, unipolar brush cells and mossy fiber terminals[11]. The outermost layer is the molecular layer, which contains parallel fibers from the GCs, climbing fiber terminals, Purkinje cell terminals, stellate cells and basket cells[11]. A monolayer of Purkinje cell somas is located between these two layers.

2. 3. 2. INTRINSIC CONNECTIVITY

Purkinje cells are monoinnervated by climbing fibers, which are the excitatory axons that project from the inferior olivary nucleus in the brainstem. Moreover, indirectly from GCs, Purkinje cells receive excitatory inputs from the mossy fibers, which originate from several nuclei in the brainstem and the spinal cord[12]. Excitatory parallel fibers from GCs in the molecular layer contact Purkinje dendrites, these excitatory inputs are mainly modulated by the stellate and basket cells. By integrating excitatory and inhibitory signals, Purkinje cells

respond to incoming sensory information by controlling the output to the vestibular and cerebellar nuclei, which ultimately communicate to the rest of the brain and spinal cord.

2. 3. 3. AFFERENT PROJECTIONS

The first afferent fibers to arrive in the developing mouse cerebellum are the mossy fibers at embryonic day (E) 12[13], followed by vestibular nuclei and spinal cord mossy fibers at E13[14], and climbing fibers at E15[15]. The rest of the mossy fibers arrive during later stages of development and early postnatal development[13]. Because Purkinje cells are arranged prior to the establishment of the afferent circuitry, it is thought that these cells regulate the circuit organization.

Mossy fibers contact unipolar brush cells and GCs in the adult cerebellum, but during development, they transiently contact Purkinje cells[16]. Mossy fibers are organized in a mediolateral pattern during the first postnatal week, just prior to definitely contact GCs. In the mature cerebellum, the major axonal input for the cerebellum are the climbing fibers from the inferior olivary nucleus that contact Purkinje cells. This works as an integration center where the information from the spinal cord is processed by the cerebellum to regulate motor coordination[17].

2. 3. 4. EFFERENT PROJECTIONS

Cerebellar and vestibular nuclei are the vehicle through which the cerebellar cortex communicates with the brain and the spinal cord. The Purkinje cell efferent projections to the cerebellar nuclei comprise the functional circuit of the cerebellum[18]. Purkinje cell axon elongation is initiated in mouse at E12[19], and these axons can be observed in the vestibular and cerebellar nuclei as early as E14 and E15 respectively[20]. The cerebellar nuclei projects to several major targets like thalamus, that ultimately contacts with the brain cortex[21].

2. 3. 5. GRANULE CELLS

Cerebellar GCs undergo rapid modifications while migrating from its birth place to the surface of the prospective cerebellum to the translocate to the deepest region of it. They represent good example of the two types of cell migration during CNS development, tangential and radial migration.

2. 3. 5. 1. FROM THE RHOMBIC LIP TO THE EXTERNAL GRANULAR LAYER (EGL)

As stated before, GCs precursors are originated from the dorsal portion of r1[8]. The specification of these cerebellar neurons is controlled by several transcription factors like Atonal BHLH Transcription Factor 1 (Atoh1)[22], and diffusible factors such as FGF and BMP[23].

GC precursors start their migration from the rhombic lip towards the cerebellum around E13 in mice[24] and migrate tangentially over the cerebellar surface to finally reach the EGL. Migrating GCs have a unipolar morphology and this migration is not glial-dependent[25]. GCs cover the totality of the EGL at E15 to birth date.

The molecules that control tangential migration of GCs are still largely unknown, but it is believed that in order to orientate GCs towards the EGL attractive and repulsive cues are crucial. For instance, stromal cell-derived factor-1 (SDF-1) is expressed by meninges and attracts embryonic GCs, which express the receptor Chemokine Receptor Type 4 (CXCR4), suggesting that SDF-1 maintains GC precursors within the pia surface of the cerebellum[26]. Phenotypic analysis of two spontaneous malformation in the cerebellum caused by the uncoordinated-5 homolog C (UNC5C) mutation[27, 28], revealed that UNC5C controls migration and axonal guidance of GCs. UNC5(A-D) mediate repulsive responses upon Netrin-1 binding. UNC5C is expressed by GCs precursors migrating from the rhombic lip. When UNC5C is knocked out, GCs invade the superior colliculus and the brainstem, suggesting that this cells are normally repelled from these territories[29]. UNC5 family receptors and their role in axonal guidance in GCs are the main topic in this thesis and will be deeply described in the following sections. Another guidance factor detected during this migration process is Slit, which signals

through their receptors Roundabout (Robo)[30]. Slit is expressed in the rhombic lip and Robo2 is expressed by the newly born GCs[31], which suggests that Slits steers the migration away from the rhombic lip through the Robo2 receptor.

2. 3. 5. 2. FROM PROLIFERATION TO DIFFERENTIATION

After reaching the final destination in the EGL, GCs stop migrating and become rounded cells[32]. In rodents, from the time of birth and after three weeks. Postmitotic GCs slide under precursor pool[32]. The EGL then, is differentiated into the upper EGL (uEGL), where GC precursors are dividing, and the lower EGL (lEGL) containing the newly specified GCs[33].

In granule neurons, both the trailing and leading processes, which are the structures that permit these cells to migrate and they respectively located at the rear and at the front of the cell, become axons with distinguishable growth cones. Therefore, from this point, granule neurons become bipolar, extending both axons in opposite directions and parallel to the cerebellar surface.

2. 3. 5. 3. EXITING THE EXTERNAL GRANULAR LAYER (EGL)

Ultimately, the GCs leave the EGL to translocate to the molecular layer (ML). At this time, GCs migration mode, changes from tangential to radial[34]. GCs extend a third process towards the EGL which becomes the leading edge during the radial migration[35].

Simultaneously, the 'T-shape' form of the parallel fibers are formed and stabilized. The cell soma starts migrating through the ML towards the internal granular layer (IGL), leaving an axonal trailing behind them that will permanently remain there[36]. This radial migration is the result of the association of the GCs to a specialized radial glia, called Bergmann glia[37].

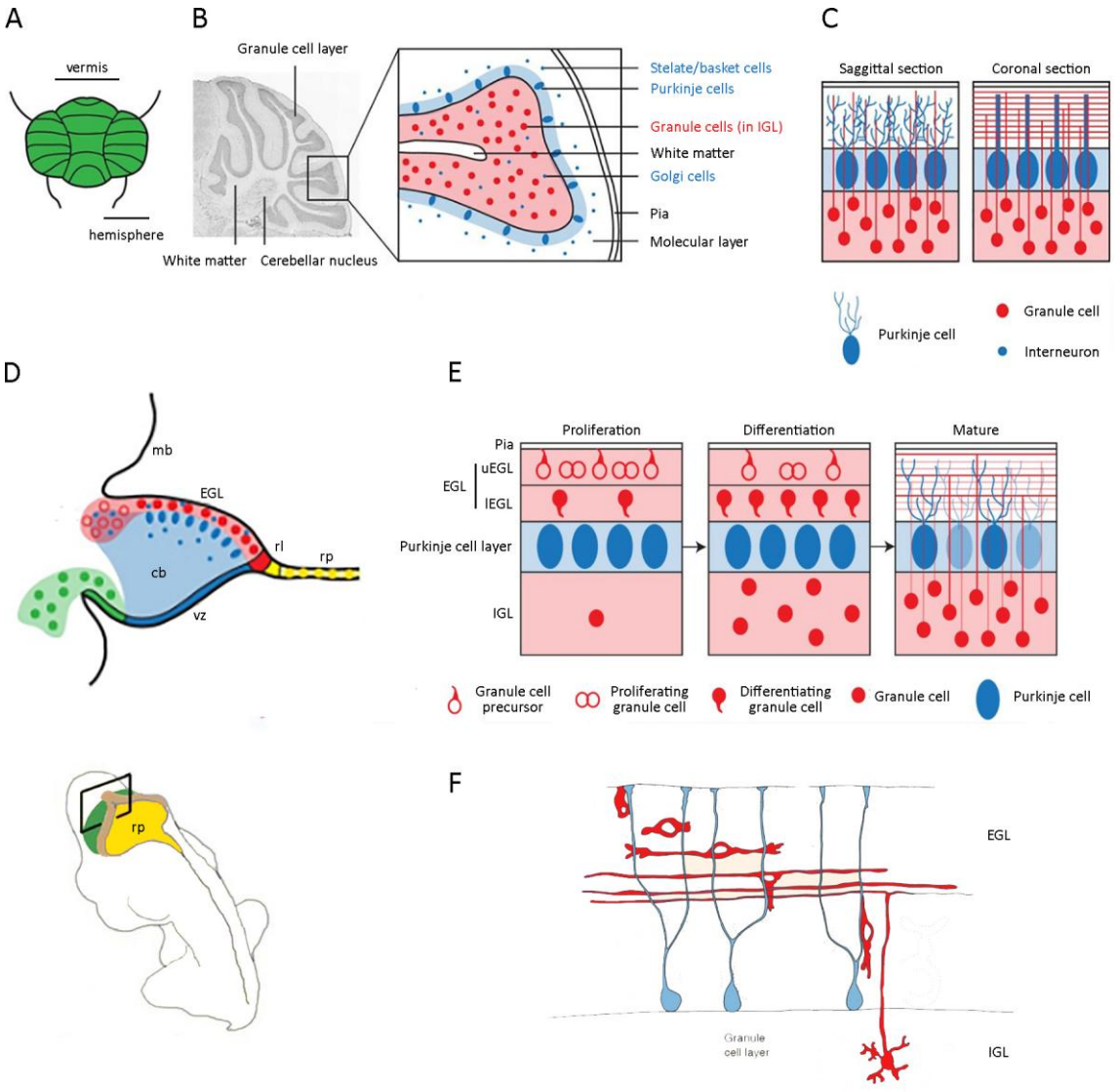

Figure 5 | Structure and development of the cerebellum. Viewed superficialy, the mammalian cerebellum is divided into the vermis, central folia, and the hemispheres, which are located flanking the vermis (**A**). From a sagittal view, the cerebellum can be subdivided into white matter, cerebellar nucleus and the granule cell layer laying beneath the Purkinje cell layer. In more detail, the cerebellum is a layered structure with specific cell types, Purkinje cell layer (blue), IGL (red) and a ML (not colored) in which Purkinje cell dendrites and granule cell axons interact. Each layer also contains characteristic interneuron subtypes (**B**). Schematic magnified views (sagittal and coronal sections) of the molecular layer of the cerebellum. Granule cell axons form parallel fibres arranged orthogonally to Purkinje cell dendritic arbors (**C**). Schematic sagittal section where different zones at the ventricular surface that contribute to different cerebellar cell subtypes following distinct migratory paths (**D**). Proliferation of the GCs takes place in the uEGL. GC precursors exit the cell cycle when they make the transition from the uEGL to the lEGL, where they are differentiated into GCs. GCs final position is beneath the Pukinje cell layer (**E**). GCs migrate inwards from the uEGL through the Bergmann glia to place beneath the Purkinje cell layer. During this migration GCs extent bipolar axons parallel to the cerebellar surface in th ML (**F**). mb: midbrain; cb: cerebellum; vz: ventricular zone; rl: rhombic lip; rp: roof plate.

3. AXON GUIDANCE

Newborn neurons send out axons that carry information to specific target cells and dendritic structures that receive inputs from these neurons. Projecting axons have to grow and reach their final destination that sometimes might be relatively away from the origin of the axon. To achieve that, axons need precise and specific cues, to finally build functional circuits. Axons navigate through pre-existing tissues, however, what may seem a relatively simple process, turns out to be very well tuned, considering that a human brain contains 80 billion neurons[38]. Elongating axons need proper guidance signals that integrate by expressing their receptors at the tip of the axon, a structure named growth cone.

3. 1. GROWTH CONE

The growth cone is the major motile structure at the tip of the axon that permits its elongation and senses the extracellular surrounding environment. The primary morphological characteristic of a growth cone is the sheet-like expansion that is found at the tip of the axon which is called lamellipodia. In a close look, numerous expansions from the lamellipodia are continuously forming and disappearing. These finger-like structures are known as filopodia. The morphology of the growth cone may acquire different shapes and structures depending on the presence of certain extracellular cues.. These morphological rearrangements are driven by cytoskeletal remodeling.

3. 2. CYTOSKELETAL DYNAMICS

The growth cone rearranges its cytoskeletal structures (microtubules and actin filaments) and associated proteins to lead the elongation and turning of the growing axon in response to guidance cues. Three phases involving the cytoskeleton can be detected in the growth cone while the axon is elongating: protrusion, actin from filopodia and lamellipodia are extended from the leading edge of the growth cone; engorgement, microtubules and transport vesicles

invade the periphery of the growth cone and consolidation, the axon shaft stabilizes through cortical actin depolymerization[39].

Growth cone motility depends on the actin cytoskeleton. Actin is a central part of axon elongation and growth cone exploration. By continuously turnover, filamentous actin (F-actin) provides the motor that keeps axon elongation and the ability to give proper responses to the molecular environment[40]. Nonetheless, actin is sufficient to power axon elongation. Without actin polymerization, the axon still can elongate, albeit the presence of growth cone abnormalities and substratum selectivity loss[41].

F-actin retrograde flow is driven by both contractility of the motor protein myosin II in the transition zone (T-zone), which is the region between the peripheral and central domains in the growth cone, and the push from F-actin polymerization in the peripheral domain (P-domain), the peripheral region of the growth cone that includes filopodia and lamellipodia structures[42]. Actin structures can be rapidly remodeled to give efficient responses based on the recognition of guidance cues by specific the receptors in the growth cone (see section 3.3).

Cell adhesion molecules (CAMs) bind to substrate in the growth cone, serving as anchoring points for F-actin and preventing cytoskeletal retrograde movements. Indeed, it has been shown that substrate adhesions are important for the correct growth cone motility[43], as well as the proper generation of traction through myosin II[44].

Microtubules have also significant roles in axon guidance processes[45]. Prior to growth cone protrusion, a population of individual and unstable microtubules explore the P-domain and interact with adhesion sites[46]. These microtubules are thought to serve as scaffolds for some key signaling components, needed for axon orientation like Src kinases or Ras homologous (Rho) family Guanosine-5'-triphosphate (GTP)ase regulators[47]. During the engorgement phase, stable bundled central domain (C-domain) microtubules determines the axonal direction that has been initially decided by actin remodeling[48].

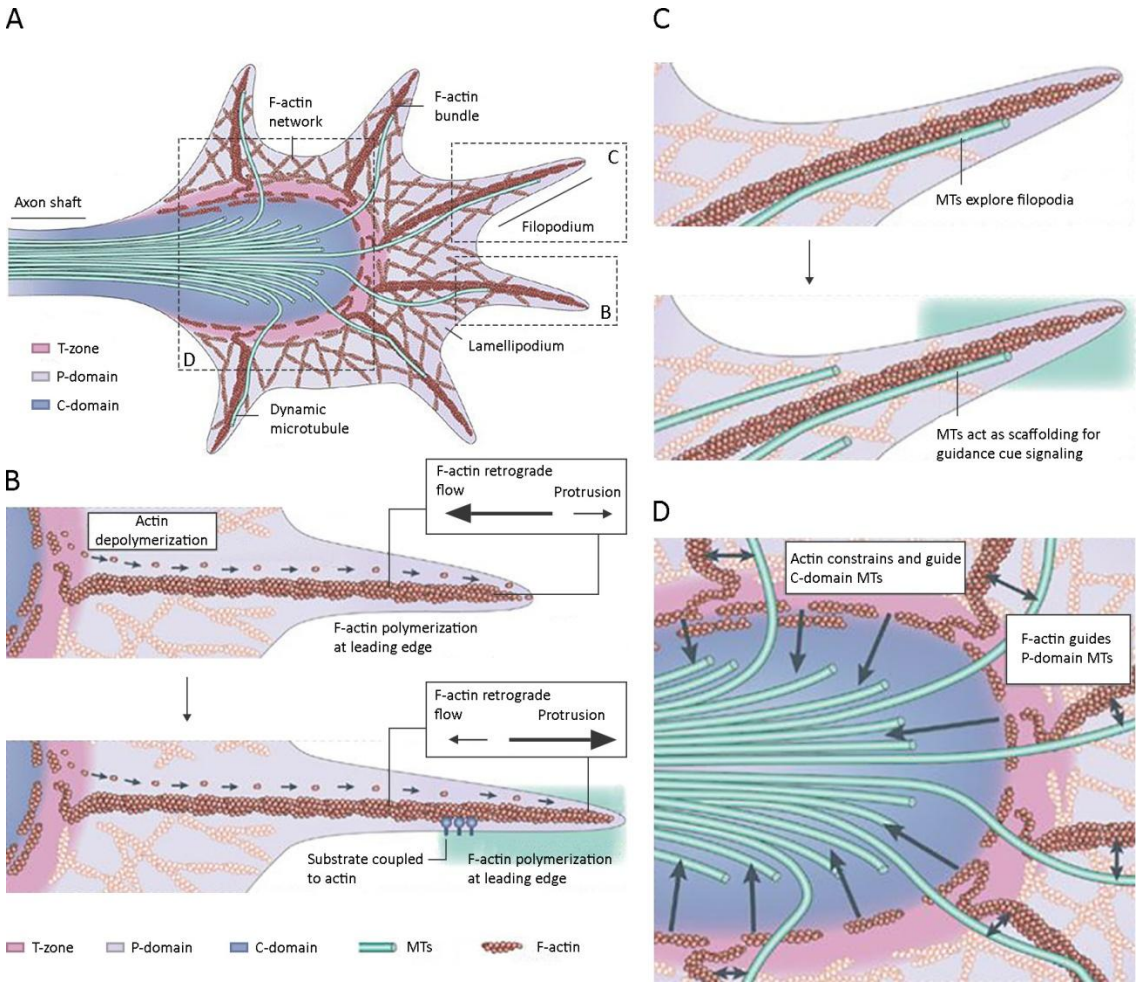

Figure 6 | Growth cone structure and cytoskeletal dynamics. Schematic representation of the growth cone. The growth cone is a motile structure located at the tip of the axon that senses chemotropic extracellular cues (**A**). The growth cone is composed by three differentiated areas with specific cytoskeletal components in each of them. F-actin polymerizes at the leading edge and severes at the T-zone with recycled subunits from the leading edge. When actin retrograde flow and polymerization are balanced, no protrusion occurs. When the growth cone receptors bind to a substrate, F-actin polymerization pushes the membrane forward, which results in growth cone protrusion (**B**). In the P-domain, microtubules explore filopodia along F-actin bundles. When filopodia encounters guidance cues, microtubules act as scaffolding for further signaling and recruitment of membrane receptors (**C**). The C-domain is mainly enriched in stable microtubules (**D**). MTs: microtubules.

3. 3. GUIDANCE CUES

Growth cone navigation is a dynamic process that involve pause, turning or collapsing of the axon. The growth cone requires a 'navigate system' that translate several guidance cues into

different integrated responses through specific receptors that ultimately remodel the cytoskeleton.

Guidance molecules interact with specific transmembrane receptors in the growth cone. These receptors initiate a signaling cascade upon ligand binding, that mainly translates into cytoskeletal changes. Guidance molecules can be enclosed into attractive or repulsive cues, depending on the effect in the elongating axon. Attractive cues, drive the axon towards the ligand source, while repulsive cues, cause an alienation of the axon from the source of it. There are several well known guidance molecules and receptors. Netrins are secretable molecules implicated in chemotropic signaling in axon guidance processes. Netrins signal mainly through their recognition by DCC and UNC5 receptors. Their effect depend on the receptor, resulting into attraction upon DCC binding and repulsion when binds to UNC5 receptors[49]. The erythropoietin-producing hepatocellular carcinoma (Eph) tyrosine kinase receptors and their ligands, Ephrins, are both membrane bound proteins. Eph receptors and Ephrin ligands are a vast family of proteins that mainly promote growth cone retraction[50]. Semaphorins are another family of diffusible guidance factors which mainly signal through the Neuropilin and Plexin family of receptors[51]. Slits mediate their activity through roundabout (Robo) receptors, promoting chemorepulsive responses that are involved in migration and axonal elongation during CNS development[52].

There are numerous signal transduction pathways that involve kinases, phosphatases and calcium ions (Ca^{2+}), but all these pathways converge into the Rho-family GTPases[53]. Rho-GTPases oscillate between the active (GTP-bound state) and the inactive form (Guanosine-5'-diphosphate (GDP-bound state)). The three best characterized members of this family include Rho, Rac and Cdc42, and their effects on actin cytoskeleton has been extensively studied during axon elongation and guidance[54]. Briefly, the activity of Rho-GTPases is modulated by two families of factors. GTPases activating proteins (GAPs) which favor the inactive form of Rho-GTPases by hydrolyzing GTP[55]; guanine nucleotide exchange factors (GEFs) that activate

GTPases[56]. Activation of Rho-GTPases leads to key cytoskeletal remodeling and their effects converge into three main outcomes: F-actin polymerization, F-actin disassembly and actomyosin contractility.

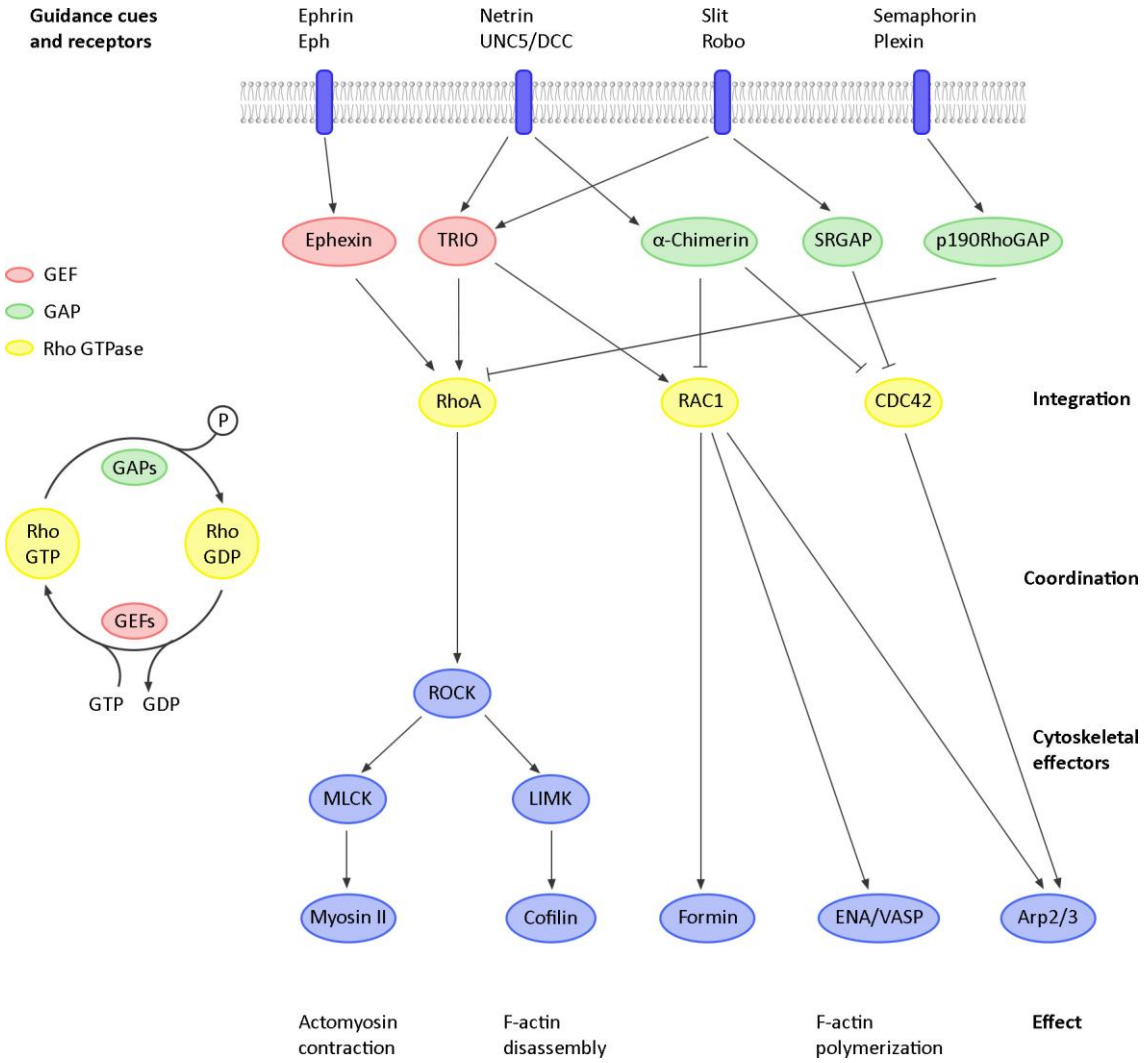

Figure 7 | Mechanisms to integrate extracellular signals in the growth cone. Transmembrane receptors at the growth cone sense different extracellular cues that are translated into different cytoskeletal dynamics (**A**). The activation of receptors leads to the activation of GTPase regulators (GEFs and GAPs) (**B**). Rho GTPases integrate responses of upstream pathways and coordinate downstream effects by influencing the function of cytoskeletal effectors (**C**). Activation or inactivation of the cytoskeletal effectors leads to a range of responses by the growth cone, actomyosin contraction, F-actin disassembly or F-actin polymerization affect the outcome of the growth cone turning response (**D**).

3. 3. 1. NETRINS

Netrins are highly conserved molecules throughout evolution. Vertebrates express the secreted Netrins, Netrin-1, Netrin-2, Netrin-3 and Netrin-4 and two related GPI-anchored membrane proteins, Netrin-G1 and Netrin-G2. All Netrins are composed of around 600 amino acids with a molecular weight of 70 kilodaltons (kD). They share two characteristic amino terminal laminin domains, the domains V and VI[57]. Mutations in the domain VI abrogate the ability of Netrins to attract or repel axons. The domain V contains three tandem arrays of cysteine rich epidermal growth factor (EGF) repeats named V-1, V-2 and V-3. Netrin-1 to 4 contain a conserved carboxyl terminal domain, named C domain. Mutational analysis have revealed no effects in axon guidance[58].

3. 3. 1. 1. NETRIN-1 RECEPTORS

Netrin-1 is a bifunctional guidance molecule, whose signal transduction depends on its receptor in the growth cone. Netrin-1 binding to deleted in colorectal cancer (DCC) results in attractive responses via homodimerization of the receptor[59]. Heterodimerization between DCC and UNC5 receptors converts the attraction into repulsion[60]. UNC5 is able to mediate repulsion to Netrin-1 in the absence of DCC[61] and sometimes interacting with down syndrome cell adhesion molecule (DSCAM) [62].

3. 3. 1. 1. 1. DELETED IN COLORECTAL CANCER (DCC)

DCC contains four Immunoglobulin (Ig) domains and six Fibronectin type III (FNIII) repeats in the extracellular region. The cytoplasmic domain contains three regions with high homology between other species, named P1, P2, P3[63]. Netrin-1 binding to the fifth and sixth FN3 repeats causes homodimerization of two molecules of DCC[64]. These homodimerization brings together the intracellular portions of two DCC, facilitating the interaction of the P3 domains[65]. This interaction forms a scaffold for the recruitment of downstream effectors involved in cytoskeleton remodeling, promoting axonal outgrowth[66].

3. 3. 1. 1. 2. UNCOORDINATED-5 (UNC5)

The UNC5 family receptors is composed by four members, namely, UNC5A, B, C and D. UNC5 receptors consist of two Ig domains where Netrin-1 binds and two thrombospondin type I (TSPI) repeats. The cytoplasmic domain is composed by a Zona ocludens/UNC5 (ZU5) domain, a DCC binding (DB) motif and a death domain (DD). UNC5 receptors function mediating the repulsive axon guidance to Netrin-1, through the heterodimerization with DCC for long-range repulsion[61], [67]. DCC-independent repulsion by UNC5 receptors require the ZU-5 motif of the intracellular domain[68]. The intracellular domain of UNC5 contains a binding site for the P1 domain of DCC, which is necessary for the Netrin-1 dependent axon repulsion[67].

3. 3. 1. 1. 3. NEOGENIN

It is known that Neogenin binds to Netrin-1, although many of the information about axon guidance comes from the comparison with DCC structure. Neogenin appears to facilitate spinal commissure formation in mice, along with DCC[69]. Expression studies of Neogenin in mice, show a broad distribution of this molecule in many types of maturing neurons, which suggests that Neogenin is not exclusively a Netrin-1 partner and it may be involved in a variety of processes regarding the development of the nervous system[70].

3. 3. 1. 1. 4. DOWN SYNDROME CELL ADHESION MOLECULE (DSCAM)

DSCAM is a transmembrane cell adhesion molecule that acts as a Netrin-1 receptor[71]. It has been described that DSCAM can also associates with UNC5 to mediate short-range repulsion[62]. Exogenously expressed DSCAM is able to mediate attraction upon Netrin-1 binding in collaboration with DCC[72]. It has been also shown that DSCAM interacts with UNC5C to promote growth cone collapse[73]. DSCAM is also involved in the regulation of the association of what??? with microtubules, and is also involved in axon fasciculation. Nevertheless, more studies are needed to address the precise mechanism of DSCAM in mediating Netrin-1 responses[74].

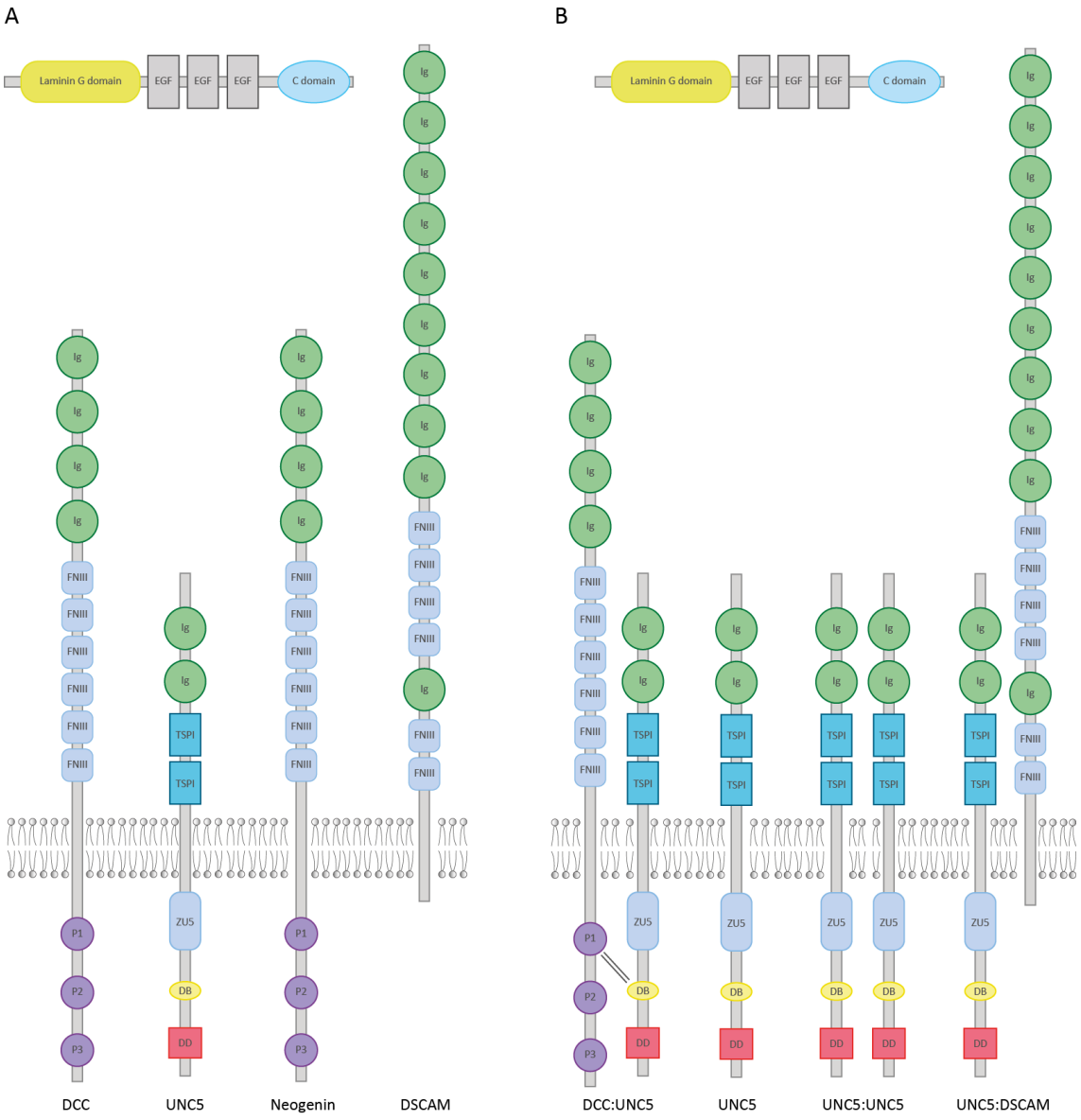

Figure 8 | Netrin-1 receptors and their interactions in axon repulsion responsiveness. Schematic representation of Netrin-1 receptors and their structural domains (**A**). From left to right, DCC, UNC5 family, Neogenin and DSCAM. Interaction between these receptors is often mediated through ligant binding (**B**) From left to right, DCC interacts with UNC5 through the P1 and DB domain. Short-range repulsion is mediated through single UNC5 protein. UNC5 receptors can homo- or heterodimerize upon Netrin-1 binding. DSCAM associates to UNC5 to induce axon repulsion.

3. 2. 1. 2. NETRIN-1 IN NERVOUS SYSTEM DEVELOPMENT

Netrin-1, -3, -4, G1 and G2 are expressed in mammals. Netrin-1 is expressed in the floor plate of the developing spinal cord in mice, where it directs the extension of commissural axons to the ventral midline of the developing spinal cord[75]. Netrin-1 deficiency also disrupts major axonal projections crossing the midline, including corpus callosum and the hippocampal commissure[76]. Acting as a repellent, Netrin-1 re-orientates the extension of axons from a subset of trochlear[77], cranial[78] and spinal accessory motoneurons[79].

Aside from guiding commissural axons towards the midline, Netrin-1 is expressed in the optic nerve and is necessary for the axons of retinal ganglion cells to exit the retina and enter the optic nerve[80]. Netrin-1 is also implicated in the guidance of dopaminergic axons in the ventral midbrain[81] and the formation of axon projections in the hippocampus[82].

During cerebellar development, Netrin-1 promotes the exit of post mitotic migrating neurons from the rhombic lip that reach the cerebellar primordium. Netrin-1 is expressed at P4 in the EGL and by basket and stellate cells of the cerebellar molecular layer[83]. Netrin-1 also repels parallel fibers and migrating GCs from explants obtained from the EGL[83].

4. CHOLESTEROL

4. 1. CHOLESTEROL IN THE CENTRAL NERVOUS SYSTEM

Unesterified cholesterol is a very important component of cellular membranes. Particularly, unestrified cholesterol accounts for the 25% of total lipidic composition of the plasma membrane, playing an essential role in determining the fluidity of this structure in every cell type[84]. A fraction of this pool of membrane cholesterol is constantly replaced and restored. Tightly regulated mechanisms are required to degrade and incorporate cholesterol molecules to the plasma membrane[85], maintaining the concentration of cholesterol in a steady state[85]. Most cells in the body synthesize cholesterol molecules from acetyl-Coenzyme A (CoA)[86], and only a small subset of cells can uptake it immersed in various apolipoproteins transported

through the interstitial fluid) . This selective uptake of cholesterol relies on processes such as receptor-mediated endocytosis, receptor-mediated selective uptake and bulk-phase endocytosis. Nonetheless, the importance of each of those processes vary from organ to organ.

Given its unique anatomy, structure and relative isolation, the metabolism of cholesterol in the CNS differs in a great extent to what can be observed in other organs in the body. Cells tend to accumulate cholesterol in the plasma membranes or in the cytosol, but it is not the case of cells in the CNS. Neurons need to increase the velocity of electrical currents and this is mainly achieved through increasing the thickness of the hydrophobic membranes surrounding axons. This is carried out by oligodendrocytes that synthetize vast sheets of dehydrated plasma membrane that wrap the neurons to form compact myelin[87]. Considering that these myelin sheets are enriched in cholesterol, the size of the pool of sterol in the CNS is higher than in other organs. In mice, the CNS pool of cholesterol represent 15% of the whole cholesterol content, whereas it only represents 1.7% of the body weight. This feature is even more dramatic in humans, where the CNS only represents 2.1% of the body weight but contains the 23% of all cholesterol.

This large bulk of cholesterol in the CNS should be acquired by *de novo* synthesis or by uptake of plasma lipoproteins across the blood-brain barrier. However, endothelial cells from brain capillaries are different from any other capillaries present in the body, containing tight junctions with high electrical resistance that prevent any vesicular transport[88]. Thus, the net movement of lipoproteins between plasma membrane and brain pericellular fluid requires protein-mediated transport. The identification of transporters such as Low-Density Lipoprotein Receptor (LDLR), Scavenger receptor class B type 1 (SR-BI) and ATP-binding cassette A1 (ABCA1)[89] suggested that CNS acquires part of its cholesterol from circulating plasma. However, measurements of net movement of cholesterol in the CNS failed to identify such transport. If there is no incorporation of cholesterol within lipoproteins from the plasma

to the CNS, then *de novo* synthesis must be responsible for most CNS cholesterol. In mice, the highest rates of cholesterol synthesis happens during the first four weeks after birth[90], decreasing later and stabilizing at constant lower levels during the whole life of the animal. the vast majority of cholesterol is synthesized by oligodendrocytes early in development during the formation of myelin. As CNS matures, myelin production decreases and cholesterol synthesis enters a steady state. Thus, although there is no direct evidence that lipoprotein cholesterol is used by the CNS, various studies seem to point that cholesterol is synthesized locally in different areas of the brain and the spinal cord[91].

While the majority of CNS cholesterol is synthesized during development, the sources that drive the turnover of cholesterol during adulthood are still unclear. Cholesterol synthesis has been described in glial cells and neurons *in vitro*. In neurons, the synthesis occurs in the cell body but not in the axon itself[92]. An additional source of cholesterol is required during synapse formation and axonal growth[93], being the astrocytes the cells that presumably provide this additional source of cholesterol[94].

4. 2. FROM THE CNS TO PLASMA

The CNS possesses enzymes capable of hydroxylating and further metabolizing cholesterol[95]. Such sterol hydroxylases are present in many tissues throughout the body. For instance, the sterol 27-hydroxylase (CYP27A1) is found in a number of tissues, facilitating the transport of cholesterol to the liver for its excretion[96]. One specific enzyme has been identified to be expressed exclusively in the CNS and specifically in a small subset of large neurons in the cortex and the cerebellum[97], the cholesterol 24-hydroxylase (CYP46A1)[97]. When the gene encoding the hydroxylase CYP46A1 is inactivated in mice, there is no change in cholesterol turnover in any organ except the brain, where it is decreased at approximately 40%[98]. these results suggest that the net flux of sterol released from the CNS is very small compared to other organs, and the majority of this sterol is hydrolyzed by CYP46A1 and excreted as oxysterol 24(*S*)-hydroxycholesterol.

5. CELL MEMBRANE

Like all other cellular membranes, the plasma membrane is mainly composed by lipids and proteins. The basic structure of the plasma membrane is the phospholipid bilayer, which serves the cell a natural barrier between two aqueous systems, intra- and extracellular. All cell types are limited by membranes which give them self identity and specific properties depending on the composition of lipids and proteins embedded in the phospholipid bilayer. Proteins present in the cell membrane carry out specific functions important for a vast range of cellular processes. The fact that hydrophobic moieties (non-polar ends) of lipids tend to associate, as well as hydrophilic moieties (polar ends) interact with aqueous environment and with each other is the basic principle of the spontaneous formation of lipidic bilayers of cell membranes. In this energetically favorable arrangement, polar groups face the aqueous system in the bilayer and non-polar groups are hidden in the interior of the membrane. This principle, is the chemical property that permits cells to segregate and isolate their internal constituents from the external environment. This same principle of amphipathy confers the intracellular organelles the same level of membrane organization.

5. 1. LIPID BILAYER

The model of the structure of biological membranes was first stablished in 1972 as the fluid mosaic membrane model. It is based on the composition and thermodynamically principles of organization of membrane lipids and proteins, and the evidence of asymetry between the inner and the outer leaflet, as well as the lateral mobility of cell membrane components[99]. Singer and Nicolson claimed that the cell membrane is a two dimensional fluid, where individual lipid molecules are able to freely diffuse within the bilayer. The fluidity of a lipid bilayer depends mainly on its composition. Cell membranes are mainly composed by four types of phospholipids, namely phosphatidylcholine, phosphatidylethanolamine, phosphatidylserine and sphingomyelin. These phospholipids are asymmetrically distributed

when comparing the inner and the outer leaflet of the cell membrane. The outer leaflet of the plasma membrane is mainly enriched in phosphatidylcholine and sphingomyelin, whereas the inner leaflet contains essentially phosphatidylethanolamine and phosphatidylserine. A less abundant phospholipid in the cell membrane is phosphatidylinositol. It also localizes in the inner leaflet of the lipid bilayer. Although being a minor component, phosphatidylinositol plays crucial roles during cell signaling and trafficking processes[100].

5. 2. MEMBRANE PROTEINS

While phospholipids are the fundamental structural elements of membranes, proteins are responsible of carrying out specific cellular processes. Total cell membrane weight is shared equitably by phospholipids and proteins. However, for every molecule of protein corresponds about 100 molecules of phospholipids, given the larger size of proteins compared to phospholipids[99].

Singer and Nicolson distinguished between two types of membrane proteins, integral and peripheral proteins. Integral proteins are tightly bound to membranes by hydrophobic forces and intercalated within the lipid bilayer. Integral proteins are crucial for maintaining the cellular membrane microstructure. Peripheral proteins are loosely bound by electrostatic or other non-hydrophobic interactions to hydrophilic portions of the cell membrane. These proteins are involved in performing enzymatic activities, scaffolding or membrane supporting structures[101]. Another type of membrane proteins proposed after Singer and Nicolson was termed membrane associated proteins[102]. These proteins are not transmembrane proteins *per se*, as they are cytoskeletal and associated signaling proteins located at the inner leaflet of the cell membrane, and glycoproteins and linked glycosaminoglycans located at the outer membrane surface. These membrane components are thought to be involved in stabilizing cell membranes, but do not participate in preserving the integral microstructure of the membrane. However, they are important in maintaining membrane functions and dynamics, being crucial for processes like cell-matrix and cell-cell adhesion, cell motility or endocytosis and exocytosis.

5. 3. MEMBRANE ASSOCIATIONS

5. 3. 1. MEMBRANE ASSOCIATED CYTOSKELETAL INTERACTIONS

There are a number of situations where trans-membrane regulation can alter the macrostructure of cell membranes. This type of regulation is often linked to a reduction or restriction in freedom of lateral movement or mobility of certain transmembrane proteins, as well as global movements of membrane proteins and lipid domains by tethering and clustering these complexes to cellular actin containing fibers or in some cases, direct movement through microtubular structures[103].

5. 3. 2. PROTEIN-PROTEIN INTERACTIONS

Most cell membrane proteins are not isolated elements, simply floating in a fluid lipid environment. They are normally assembled into macromolecular complexes, which can be part of a signaling system. Protein-protein interactions are involved in the dynamic formation of glycoprotein transmembrane signaling complexes at the cell surface. These interactions can be triggered by ligand binding to its receptors. Supramolecular structures competent for cell signaling can require the recruitment in *cis* of other transmembrane elements, and the *trans* recruitment of peripheral proteins at the inner surface of the cell membrane[104].

5. 3. 3. PROTEIN-LIPID INTERACTIONS

Membrane integral proteins must interact with membrane lipids in order to remain stably embedded in the plasma membrane. Membrane proteins interact with the acyl portions of the membrane phospholipids or hydrophobic portions of other membrane lipids to be stably embedded in the cell membrane[105]. In order to build an overall tensionless structure, additional considerations must be taken into account such as lateral pressure forces, lipid phase and composition, curvature or charge interactions[106]. For this reason in the cell membrane can be identified different lipid phases and domains[107]. This hydrophobic matching between membrane elements is essential for the maintenance of the lipid bilayer structure. If

such matching does not exist, it may result in an energy cost in the lipid-protein interaction that potentially can affect membrane protein function[108]. This can also result in the exclusion of certain membrane lipids, such as cholesterol, due to unfavorable membrane protein hydrophobic matching[109].

This lipid boundary effect can also affect protein-protein interaction and result in membrane integral protein clustering within the cell membrane. The hydrophobic mismatch is so unfavorable that interaction between lipids and proteins is reduced by transient formation of protein aggregates of protein-protein complexes in the cell membrane[110].

5. 3. 4. LIPID-LIPID INTERACTIONS

Membrane lipids are arranged asymmetrically throughout the cell membrane. They are unevenly distributed in the lipid bilayer which causes changes in the fluidity of the cell membrane. The main example is cholesterol, which is the only sterol present in the cell membrane and possesses the ability to form specific membrane domains[111].

Cholesterol has a very important role in regulating membrane organization. Cholesterol is able to change the membrane phase, turning it from a fluid phase to a liquid-ordered phase[112]. Cholesterol molecules are thought to play an important role in the sorting of membrane proteins into membrane microdomains. By modifying the thickness of the hydrophobic cores of membranes, integral membrane proteins might be excluded from certain regions and relegated to other domains where the hydrophobic matching is more favorable[113].

Not only cholesterol is important for the formation of cell membrane liquid-ordered phase microdomains. Sphingolipids like sphingomyelin and phosphatidylcholines, constitute more than 50% of membrane phospholipids and are the main interaction partners for cholesterol[114].

6. LIPID RAFTS

Lipid rafts are specialized structures in the plasma membranes that contain specific lipids, integral and peripheral proteins, forming compartmentalized signaling platforms. Lipid rafts are sterol and sphingolipid enriched nanoscale assemblies that associate and dissociate on a subsecond timescale[115]. The enrichment of these membrane portions, results in the separation of cell membranes in two phases: liquid ordered (L_o) and liquid disordered (L_d) phases. This compartmentalization of molecules causes lateral heterogeneity and modulation of the bioactivity of the raft components[116]. Specific protein localization to these microdomains are mainly driven by a glycosylphosphatidylinositol (GPI) anchor, certain post-translational modifications or discrete protein domains[117]. Lipid rafts provide cells with dynamic signaling and functional platforms within the lipid bilayer, being important for processes such as membrane trafficking, signal transduction or cell polarization[118].

The different lipid phases and their segregation appear to be important for membrane rafts formation in the cell membrane. The formation of these nanodomains is thought to be a dynamic and reversible process that is driven by hydrogen bonding, hydrophobic entropic forces, charge pairing and van der Waals forces.

Although there are still technical limitations in the study of lipid raft, they are thought to constitute functional and dynamic nano or submicro-sized domains (~10-200nm) but have the potential to aggregate and form microscopic domains (>300nm) upon clustering induced by protein-protein or lipid-protein interactions[119].

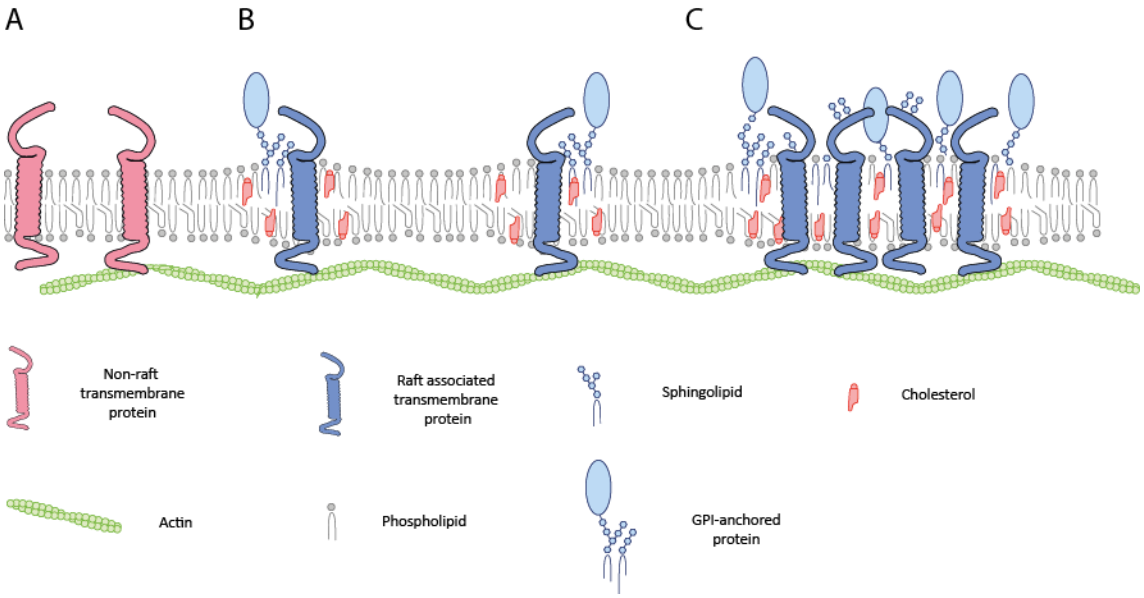

Figure 9 | Lipid raft-based heterogeneity in cell membranes. Diagram of a phospholipid bilayer. Enrichment of cholesterol and sphingolipids in the cell membrane seggregate proteins and bias its lateral composition. Some transmembrane proteins are excluded from these microdomains (red) (**A**). This cholesterol and sphingolipid assemblage can be accessed by GPI-anchored proteins or certain transmembrane proteins (blue) (**B**). These nanoscale assemblies are functional at larger levels by activation events such as multivalent ligand binding, synapse formation or protein oligomerization (**C**). This level of lateral sorting and protein clustering is often driven by cortical actin (green) interaction.

6. 1. GLYCOSYLPHOSPHATIDYLINOSITOL (GPI)-ANCHORED PROTEINS

GPI-anchored proteins are a class of membrane proteins containing a soluble protein attached to the outer leaflet of the plasma membrane by a conserved postranslational glycolipid modification, the GPI anchor[120]. GPI-anchored proteins play a wide variety of cellular roles such as enzymes, cell surface antigens, signaling receptors, cell adhesion or migration molecules[121]. The preformed GPI structure is assembled *en bloc* in the endoplasmatic reticulum (ER) by a transaminase to the C-terminal fraction of the nascent protein[122]. In the Golgi apparatus, GPI-anchored proteins are subjected to fatty acid remodeling, which replaces unsaturated fatty acids for saturated fatty acids. GPI- anchored molecules are found in detergent resistant membranes (DRMs), whose bioactivity is modified given its localization to membrane microdomains[123]. Thus, these postranslational modifications lead to a regulation of trafficking

to the cell surface and a determination of the subcellular localization of these proteins to lipid rafts[123].

6. 2. PALMITOYLATION

The addition of the fatty acid palmitate to membrane proteins promotes its stable localization in the plasma membrane. Protein S-palmitoylation is a covalent lipid modification that occurs in the side chain of cysteine residues with the 16-carbon fatty acid palmitate (C16:0), a reversible post-translational modification via thioester linkage[124]. These N-terminal acylations confer to transmembrane proteins hydrophobic characteristics thought to be important for membrane association and lipid raft localization[125].

6. 3. CAVEOLAE

Caveolae structures were first described in the 1950s[126]. Caveolae are flask-like invaginations of the plasma membranes of about 50-100nm, which are enriched in cholesterol and glycosphingolipids and provides floating anchors for some membrane proteins. Caveolae are specialized structures that contain high densities of the protein caveolin (cav), which is important to mold the invagination in the cell membrane. Lipid rafts and caveolae share a vast range of biochemical characteristics such as lipid composition and detergent insolubility[127]. Caveolae are sometimes considered as a subset of lipid rafts.

Cav proteins are composed of four structural domains. The caveolin scaffolding domain mediates the interaction with specific membrane proteins, sequestering them to caveolaes[128]. The oligomerization domain facilitates the aggregation between different cav proteins[129]. Cav contain a transmembrane domain, which is not important for the inclusion of Cav into membranes[130]. The C-terminal domain that contain three cysteine residues that are palmitoylated (Cys133, 144 and 156) and bind the protein to the inner leaflet of the membrane[131].

One important feature of caveolae is that it actively participate in certain types of internalization processes[132], like caveolae-mediated endocytosis.

6. 5. LIPID RAFTS IN THE NERVOUS SYSTEM

Lipid raft membrane microdomains are involved in protein and lipid sorting in polarized epithelial cells[118]. Neurons are one of most polarized cell types, with specific axonal and dendritic compartments, thus requiring a precise sorting and selective trafficking of certain proteins and membrane constituents. For example, it has been shown that dendritic spines are highly enriched in sphingolipids and many postsynaptic proteins[133], while axonal compartments contain specific molecules involved in motility and neurotransmitter release. Each mentioned regions contain proteins directly associated with membrane rafts[134]. It is, therefore, conceivable that lipid rafts play an important role in the segregation of certain molecules in neurons.

The idea that rafts are involved in signal transduction first came from the isolation of DRMs in which proteins like GPI-anchored proteins or src-family kinases tend to be concentrated[135]. Further studies showed that a plethora of other receptors and intracellular signaling components are associated with DRMs. Many different responses to extracellular signals are now thought to be dependent on the integrity of lipid rafts, including immune response, growth factor signaling, cell adhesion and chemotaxis.

One of the best examples of lipid raft signal transduction dependence is growth factor signaling cascade[136]. Membrane rafts are involved in the signaling induced by neurotrophins and glial cell line-derived neurotrophic factor (GDNF). These growth factors can influence in a variety of neuronal cell types and include different effects such as cell growth, proliferation, differentiation and survival. The signaling mechanisms that mediate the function of these two families involve the activation of receptor tyrosine kinases, which leads to the formation of intracellular complexes that have been shown to involve lipid rafts microdomains[136]. Neurotrophins, such as nerve growth factor (NGF), perform their effects by binding tyrosine

kinase receptors (TrkA, B and C) or the low affinity p75 neurotrophin receptor ($p75^{NTR}$). These receptors are lipid raft residents, whose signaling depends on the specific localization into membrane microdomains.which signals from membrane microdomains, that in turn, this signaling, appears to be enhanced from lipid rafts[137]. Similarly, but mechanistically different, GDNF signaling involves the recruitment of c-Ret, the receptor tyrosine kinase, to lipid rafts. Only when c-Ret is recruited to cholesterol enriched microdomains it associates with its downstream signaling partners residing in lipid rafts[138].

Synaptic transmission also rely on the structure of microdomains. Lipid rafts can influence synaptic transmission through controlling the exocytic processes of neurotransmitters release[139] and clustering post-synaptic neurotransmitter receptors[140].

6. 5. 1. MEMBRANE DOMAINS AND GROWTH CONE MOTILITY

Strikingly, many of the components that regulate actin cytoskeleton, cell motility and adhesion are associated with lipid rafts, those components include molecules like Rho GTPases or Src-family of tyrosine kinases[141]. Cell migration and axon elongation requires dynamic and spatial regulation of focal adhesion complexes. It has been shown, that asymmetrical distribution of these focal adhesions is due to lipid rafts involvement in the spatial regulation of cellular motile activities[142].

In developing neurons, axonal guidance processes rely on the growth and pathfinding of the growth cone. Proper orientation and directional motility of the axon in response of extracellular cues, depend on cytoskeletal dynamics, together with the adhesion and interactions with other cells or the extracellular matrix. Such interactions directly depend on cell adhesion molecules (CAMs) from both, the axon and the substratum. Some of these CAMs have been shown to be associated with DRMs, indicating that selective adhesion during growth cone motility may involve lipid rafts. As a consequence, disruption of lipid rafts affects the motility of the tip of the axon[143] and some proteins involved in cell adhesion and growth cone motility are associated to lipid rafts[134]. Therefore, lipid rafts play a key role in growth

cone motility. Since directed locomotion of growth cones requires proper functioning of cytoskeleton, membrane anchoring and cell adhesion, lipid rafts may serve as a platforms for spatial and temporal regulation of these events[144].

6. 5. 2. LIPID RAFTS IN AXON GUIDANCE

The formation of ligand-receptor binding is the first step in the signal transduction processes during axon guidance. Many guidance cues have the ability influence in the distribution of some receptors, causing for instance, clustering or oligomerization and complex formation with other membrane associated components[145]. The fact that these events occur at the plasma membrane level, suggests that the membrane lipid environment could be crucial for the signal transduction of these guidance cues. Certain lipid molecules, such as phosphatidylinositol-3, 4, 5-triphosphate (PIP_3) are known to play important roles in axon guidance processes[146].

To date, only few guidance molecules are known to reside in lipid rafts. For instance, ephrin ligands and the Eph receptor tyrosine kinases are well known molecules implicated in axon guidance. Ephrin A proteins are GPI-anchored ligands that reside in lipid rafts during the triggering of the signaling cascade[147]. Similarly, the Nogo receptor (NgR) and the coreceptor $p75^{NTR}$ have been shown to reside in lipid rafts[148]. The Netrin-1 receptor DCC also reside in lipid microdomains, whose localization is necessary for attraction and axonal outgrowth signaling[149].

The activation of downstream signaling molecules can be abolished after lipid raft destabilization, that in turn abrogates axon guidance responses to the brain derived neurotrophic factor (BDNF), Netrin-1 and Semaphorin3A (Sema3A) [150]. While receptors for these molecules are weakly associated to lipid rafts, upon ligand stimulation clustering and lipid raft localization of these molecules was strongly enhanced[150].

6. 6. STUDYING LIPID RAFTS

Since the term 'lipid raft' was first introduced by Kai Simons in 1988[151], the development of new techniques has vastly influenced the way to study and visualize these domains.

6. 6. 1. BIOCHEMICAL TOOLS

The first evidence of lateral heterogeneity in cell membranes was described in the 1970s upon the discovery of differences in detergent solubilization of lipids and membrane proteins[152]. Cellular membranes can be separated into different fractions, DRMs and detergent soluble membranes (DSMs), upon solubilization at low temperatures with non-ionic detergents. Cell lysates are ultra-centrifuged and forced to pass through a sucrose gradient column where DRMs and DSMs are separated. These fractions have different compositions. DRMs are enriched in cholesterol, sphingolipids and GPI-anchored proteins[153].

Differently to clathrin-coated pit vesicles, which also participate in cellular endocytosis, cav proteins reside in raft microdomains. Thus, cav proteins are widely used and accepted as lipid raft markers in membrane solubilization experiments, unlike clathrin marker, which is considered to be a non-raft marker.

When first discovered, DRMs extraction became the method of choice to identify lipid rafts associated proteins, however, this method not always reflect the native composition of the microdomains in live cells. Many factors can influence the final outcome of DRMs purification. For instance, the detergent used for solubilization or subtle variations in temperature represent variability factors that can modify the final composition of lipid rafts [154] . Although DRM assays have been proven to be informative tools to describe lipid rafts composition, more precise and quantitative assays are required to understand the association of certain proteins with lipid raft microdomains [155].

6. 6. 2. Selective probes for membrane domains (cholera toxin B-subunit)

On the use of selective probes to visualize membrane domains, cholera toxin B-subunit (CTxB), the membrane binding subunit of cholera toxin, is considered a *bona fide* lipid raft marker[156]. Cholera toxin itself consists of an enzymatically active A subunit and a homopentameric membrane binding B subunit. CTxB binds with high avidity up to five molecules of monosialotetrahexosylganglioside (GM_1)[157], which are heavily enriched in raft domains. CTxB can be easily added to cells or model membranes, and when appropriately labeled with fluorescent markers, can be observed with fluorescent microscopy.

Lipid rafts are nanoscopic domains which cannot be resolved by conventional optical microscopy, which has approximately 250nm of resolution limit that is set by Abbe law of diffraction. Although colocalization of certain molecules with putative raft markers have been widely used and detected by confocal microscopy to assess lipid raft association, the resolution of confocal microscopy is insufficient to directly identify raft domain structure and composition[158].

6. 6. 3. BIOPHYSICAL TOOLS

6. 6. 3. 1. ARTIFICIAL MODEL MEMBRANES

Artificial model membranes were developed in parallel with DRM assays to study the liquid-liquid phase that is thought to be the basic principle of lipid rafts assemblies[159]. Membranes that consist of relatively saturated lipids, unsaturated lipids and cholesterol can separate into two distinct compartments, L_o and L_d phases. Given its tight molecular packing and cholesterol enrichment, the L_o phase is considered as a model for lipid rafts. Biomimetic monolayers, supported lipid bilayers, nanoscopic bilayer vesicles and giant unilamellar vesicles (GUVs), have all been used to understand, at a the molecular level, the basis of this phase separation[160]. Although this is a very useful tool to study lipid phase separation, there is a huge difference

between artificial membranes and biological membranes. Do to the simplicity of the artificial membrane model, it does not reflect protein/lipid ratio present in cell membranes.

6. 6. 3. 2. BIOPHYSICS OF CELL MEMBRANES

Several optical and biophysical tools have been recently developed and have been applied to study nanoscopic structures and their dynamics in cells. Techniques such as fluorescence recovery after photobleaching (FRAP) or single particle tracking photoactivated localization microscopy (sptPALM) are microscopy based techniques with a great potential in membrane microdomains study[161, 162].

6. 6. 3. 2. 1. FLUORESCENCE RECOVERY AFTER PHOTOBLEACHING (FRAP)

FRAP is a microscope-based technique that was developed three decades ago, in 1976[163]. FRAP is a biophysical methodology designed to study the mobility of fluorescently labeled molecules, proteins or small organelles in a living cell[164]. A sub-region of a biological sample, i. e. a small region of the cellular membrane, containing mobile fluorescent elements (proteins or lipids) is rapidly and irreversibly photobleached by irradiating with an intense source of light[165]. The selective photobleaching only in a region of interest (ROI) produces a transient distinction between bleached molecules inside the ROI and non-bleached molecules flanking it. Immediately after the photobleaching, non-bleached molecules outside the irradiated area move into the bleached region (influx), and simultaneously bleached molecules from the irradiated area move out (efflux). Most proteins in a cell undergo continuous turnover or are permanently moving, allowing the bleached pool of molecules to be replaced by intact fluorescent proteins. The consequence is the recovery of the fluorescence in the bleached ROI. The initial recovery of the fluorescence usually happens at a relatively fast pace, and is followed by a slow recovery, until the fluorescent intensity finally reaches a *plateau*. The fraction of molecules below the reached *plateau* is known as the mobile fraction (Mf) and

represents those proteins that freely diffuse in the bleached area. The fraction of molecules above the *plateau* represents what is known as the immobile fraction[166].

6. 6. 3. 2. 2. SINGLE-PARTICLE TRACKING PHOTOACTIVATED LOCALIZATION MICROSCOPY (SPTPALM)

sptPALM is a microscope based technique[167], which combines two different techniques, the method of single-particle tracking and the method of single-molecule localization using photoactivated localization microscopy (PALM)[168]. The technological basis of sptPALM is the localization of proteins at near molecular spatial resolution and in an environment of living cells where proteins coexist in high density[168]. This method takes advantage of photoactivable fluorescent proteins (PA-FP)[169], although antibody targeted photoswitchable synthetic labels are also commonly used[170]. In PALM, photoswitchable molecules are continuously activated, imaged and bleached in order to temporally separate molecules that would be spatially undistinguishable. Because PA-FPs are stochastically activated, distinguishable molecules are sparse enough, a single molecule is activated within a given diffraction-limited region. This is achieved by using a very low intensity illumination at the activation wavelenght, while excitation intensity is adjusted to photobleach and maintain a low density of photoactivated molecules. The position of each molecule is calculated by fitting the measured photon distribution with the point spread function of the microscope itself[171].

6. 6. 3. 2. 3. DIFFERENT FORMS OF MOBILITY RESTRICTION IN MEMBRANES

The original lipid bilayer model proposed that integral membrane proteins are intercalated in a fluid lipid matrix and can move freely along it[99]. However, we know now that membrane proteins usually find restrictions to lateral movements.

Restrictions in the lateral mobility have been attributed to several elements like binding to extracellular matrix, association to membrane nanodomains (i. e lipid rafts)

association to cortical actin cytoskeleton or formation of large supramolecular complexes where high protein concentration decrease the lateral mobility[172].

Based on their mobility, transmembrane proteins can be classified into different general groups where diffusion rates and covered membrane area are taken into account; (a) trapped proteins due to association to certain membrane clusters or domains, (b) transient confinement by the cytoskeleton, where proteins can move freely into restricted "corrals", (c) directed motion by direct or indirect attachment to the cytoskeleton, (d) free and random diffusion in the membrane plane[173].

6. 6. 4. LIPID RAFTS TARGETING DRUGS

A common tool for the study of lipid rafts have been the use of drugs to impair or affect the structure of these microdomains.

6. 6. 4. 1. METHYL-B-CYCLODEXTRIN (MBCD)

Cyclodextrins are water soluble oligosaccharides containing hydrophobic cavities[174]. Depending on the dimensions of these cavities, cyclodextrins form inclusion complexes only with low molecular weight molecules from the cell membranes. Methyl-β-cyclodextrin (MβCD) can accommodate a wide variety of organic molecules such as macrocycles and sterols, but has a great affinity to cholesterol[175]. As lipid rafts are membrane regions enriched in cholesterol, the most common raft disrupting agent MβCD[176]. MβCD is a widely used method to acutely extract cholesterol from cell membranes. MβCD has a central cavity in its structure able to form complexes with cholesterol[177]. MβCD has a faster action mechanism compared to other cholesterol depleting drugs, it does not produce degradation products and if used appropriately, it is compatible with live cell and *in vivo* experiments. However, some undesired effects must be considered when using MβCD as it is not specific for cholesterol and its action may extend beyond lipid raft disruption[178]. Moreover it increases membrane permeability which causes a disruption of membrane potential and it is potentially cytotoxic[179].

6. 6. 4. 2. CHOLESTEROL OXIDASE (CHOA)

Drugs like cholesterol oxidase (ChoA)[180], act as cholesterol modifying enzymes. ChoA is a monomeric enzyme that catalyzes the two step conversion of cholesterol into cholest-4-en-3-one. The first step of the reaction is the oxidation of cholesterol through a tightly bound flavin adenine dinucleotide (FAD) molecule, resulting in H_2O_2 and cholest-5-en-3-one. The second step is the isomerization of this cholest-5-en-3-one into cholest-4-en-3-one[180]. This enzyme is used by nonpathogenic bacteria as part of their metabolic pathway, to use cholesterol as a source of carbon. In pathogenic bacteria, the enzyme is used to destabilize cell membrane and is required to infect the host macrophages[181]. The fact that ChoA has the ability to alter the structure of lipid rafts has emerged as a powerful tool to study the functionality of these microstructures[182].

ChoA is a water soluble molecule and cholesterol is integrated in the lipid bilayer of the cell membrane. For this reason, the enzyme must associate with the membrane before binding cholesterol in its active site[183], providing a hydrophobic binding cavity that will allow favorable translocation of cholesterol from the membrane to the enzyme[180].

6. 6. 4. 3. STATINS (NYSTATIN)

Statins are drugs used to destabilize lipid rafts[184], affecting cholesterol synthesis pathway. Nystatin is a polyene antibiotic used clinically as a potent antifungal agent. It has higher affinity for ergosterol than for cholesterol[185]. Nystatin exerts its antifungal activity when interacting with ergosterol in the fungal cell membrane, which results in the formation of barrel-like membrane spanning ion channels[186] that will cause changes in cell permeability and, eventually, cell lysis. Nystatin influences cellular functions through its interaction with cholesterol in the cell membrane, reducing the ability of cholesterol to interact with other membrane components[187].

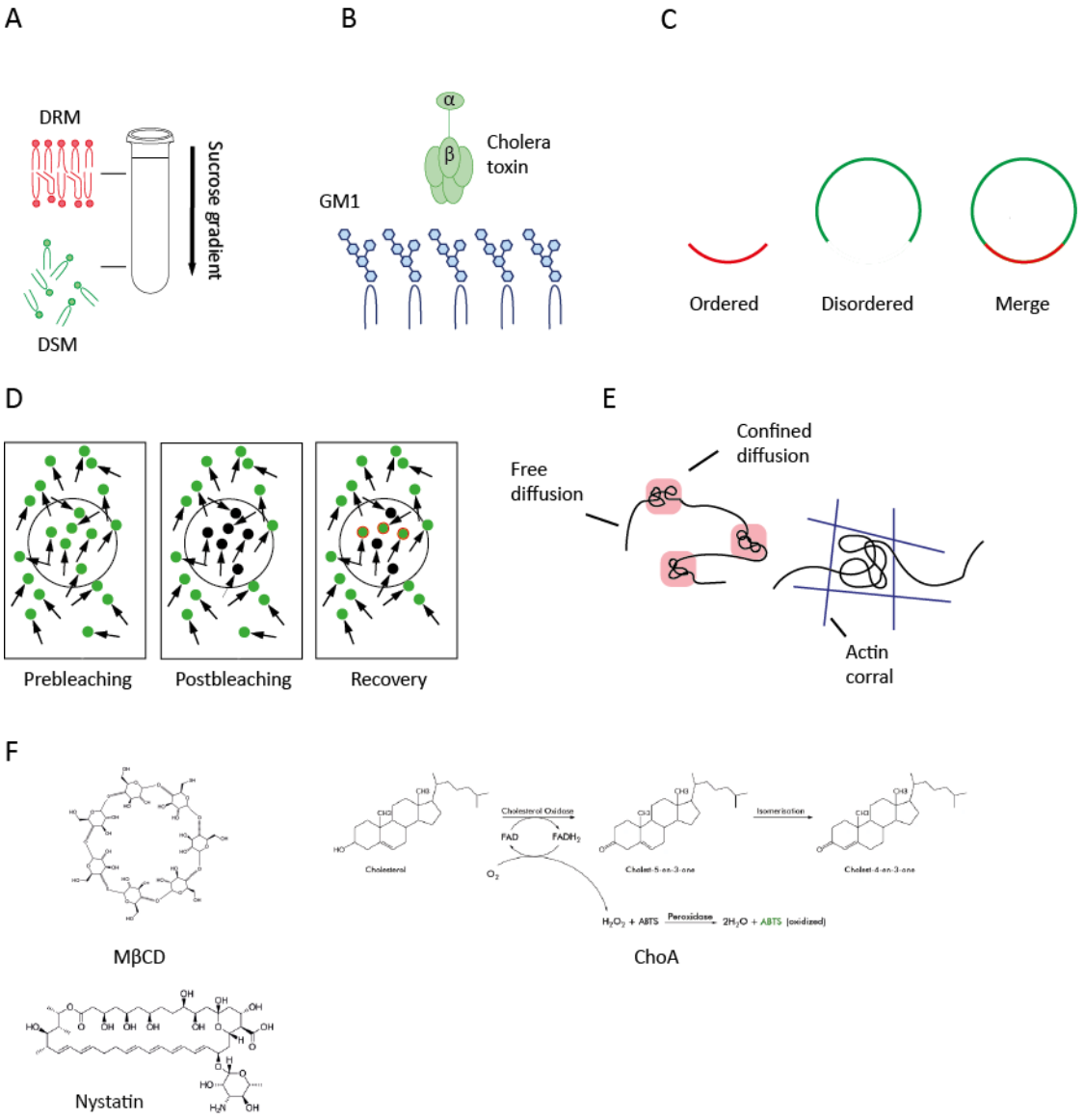

Figure 10 | Raft microdomains under scope. Schematic representation of some of the most useful methodologies to study lipid rafts. Cholesterol-enriched microdomains can be isolated thanks to their properties of insolubility in cold detergent solubilization. After sucrose gradient centrifugation, buoyant fractions are enriched in raft microdomains (DRM). In lower fractions DSMs can be detected. Thanks to this methodology protein associations to these domains can be identified (**A**). CTxB is a very useful lipid raft marker, it binds up to 5 molecules of GM1, a ganglioside abundantly present in raft microdomains (**B**). In GUVs, L_o and L_d phases can be easily separated. These fractions have different lipidic composition and therefore it is a simplified and easier methodology to study membrane fractions enriched in certain lipids (**C**). FRAP is a microscope-based technique to study lateral diffusion of proteins in living cells. Fluorescently labeled proteins move within a cellular compartment (prebleaching), after targeting a subregion of the sample, fluorescence is irreversibly switched off (postbleaching) where the fluorescence is recovered due to molecules movement after a certain period of time (recovery) (**D**). sptPALM takes advantage of super-resolution microscopy to stochastically activate a small amount of fluorescently labeled proteins in a living system, and track them over a short period of time. Single molecules can be imaged and therefore, calculate their dynamics (**E**). Drugs like MBCD, ChoA or nystatin are able to destabilize lipid raft by modifying cholesterol levels in the cell membrane (**F**).

7. PROGRAMMED CELL DEATH

Programmed cell death is an evolutionary conserved event in the development of the CNS. Control of cell number and programmed cell death during neural development is crucial for the proper embryonic and early postnatal brain development. It is an important event to achieve the desired number of cells in a given region of the central nervous system. For instance, mice lacking pro-apoptotic genes are lethal and show defects in multiple organs, including CNS. Apoptotic signals can be exogenous or endogenous. The susceptibility of cells to undergo apoptosis may differ among regions or developmental stages.

How apoptosis is regulated in the CNS remains unclear, however, it is thought to work in combination of trophic factors, pro- and anti-apoptotic. Key regulators of apoptosis in the CNS are the B-cell lymphoma 2 (Bcl-2) family of proteins, which contain multiple pro-apoptotic and anti-apoptotic proteins[188]. The Bcl-x gene is known to play an important role controlling programmed cell death during CNS development[189]. Importantly, it produces two different splice variants: Bcl-x_L (long form) and Bcl-x_S (short form). While the long form has anti-apoptotic effects, the short form is known for its pro-apoptotic activity[190]. The alternative splicing of Bcl-x during the development of CNS is reciprocally regulated by expression of each spliceoform (Bcl-x_L and Bcl-x_S)[189]. Therefore, a ratio between those two isoforms is crucial to maintain cell survival[189].

7. 1. NEURONS TARGETING TO INAPPROPRIATE REGIONS

Programmed cell death plays an important role during embryo morphogenesis and wiring of the CNS. Proper organ and tissue size demands a finely regulation of cell proliferation, cell size and cell death. The determination of cell viability versus death is mainly regulated by the availability of trophic factors. Building a complex neuronal circuit demands fine tuning many processes simultaneously. By programmed cell death, neurons projecting to incorrect brain regions (areas that are not supposed to be innervated in the adult) are eliminated. This

regulation is mainly carried by the action of dependence receptors that senses the lack of certain ligands during aberrant axonal outgrowth, and trigger the apoptosis signal.

7. 2. DEPENDENCE RECEPTORS

The triggering of cell death during the development of the CNS can be classified into different mechanistically events: induction of death ligands and/or pro-apoptotic proteins, loss of survival signals, growth factor signaling, cell-cell interaction, and intrinsic transcription factor expression. In this chapter we will focus in the ability of Netrin-1 receptors, DCC and UNC5, to induce cell death when survival signals are lacking.

There is a vast range of membrane receptors that play important roles in the development of the CNS. Key events such as angiogenesis, neural migration, axonal guidance or cell survival are crucial for the correct development of the CNS. Some of these events rely on the ability of transmembrane receptors to sense and integrate extracellular signals to finally give an accurate response. DCC and UNC5 family members (UNC5(A-D)) are transmembrane receptors for Netrin-1, known for its role in axon guidance among many other processes. DCC and UNC5 receptors have also the ability to trigger cell death signaling when uncoupled to its ligand, similar to what can be observed in $p75^{NTR}$ receptor (neurotrophin receptor)[191] or the androgen receptor[192]. Therefore, when Netrin-1 is not present, unbound receptors expressed at the cell surface, actively initiates apoptosis. Thus, DCC and UNC5 receptors belong to the growing family of dependence receptors.

DCC receptor is well known for its pro-apoptotic activity when uncoupled to Netrin-1 and mechanisms involving cell death initiation have been deeply studied. Cell death induction by DCC, requires the cleavage of an intracellular domain in the aspartic acid residue 1290 by the cysteine aspartic protease caspases[193]. This cleavage drives to the release of the inhibitory domain of DCC and exposes an upstream domain to the cleavage site, named addiction/dependence domain (ADD), which is sufficient to induce cell death and caspase activation[193]. A Protein kinase B (PKB)-like molecule named DCC interacting protein 13 (DIP13),

was identified as a interactor of the ADD domain and is required for the initiation of DCC-induced apoptosis[194]. The ADD of DCC is known to interact with caspase-9 in the absence of Netrin-1. When the ligand is bound to DCC, this interaction is markedly reduced[195]. Hence, initiation of apoptosis by DCC is caspase-dependent and requires a cleavage in the intracellular domain and the presence of the adaptor protein DIP13.

UNC5 receptors display a death domain cassette in their intracellular sequence, a domain that is usually found in other dependence receptors such as $p75^{NTR}$. It has been described that the initiation of apoptosis by UNC5B receptor starts (1) upon physical interaction with the serine/threonine kinase death-associated protein kinase (DAPK) and the DD cassette of UNC5B receptors[196,] and (2) after cleavage of caspase-3 in the DXXD (where X is any amino acid) intracellular sequence[197], conserved among all UNC5 members. Both mechanisms are known to be important for the regulation of apoptosis through UNC5B, but it is still unclear which is the first event in the apoptosis cascade. Determination of the crystal structure of UNC5B, shed light on how UNC5 proteins work as dependence receptors. Upon Netrin-1 binding, UNC5B intracellular domain adopts a closed conformation that hides the caspase cleavage domain, preventing the triggering of apoptosis[198].

Interestingly, UNC5A is the only member of the UNC5 family with the ability to interact with the neurotrophin receptor-interacting MAGE homolog (NRAGE) protein through its intracellular ZU-5 domain[199]. When comparing the apoptosis exerted by UNC5 members, UNC5A is by far the receptor with a stronger capacity to induce cell death *in vitro*[199]. Moreover, experiments *in vivo* showed that UNC5A is able to trigger cell death, in collaboration with NRAGE, independently of Netrin-1, during spinal cord development.

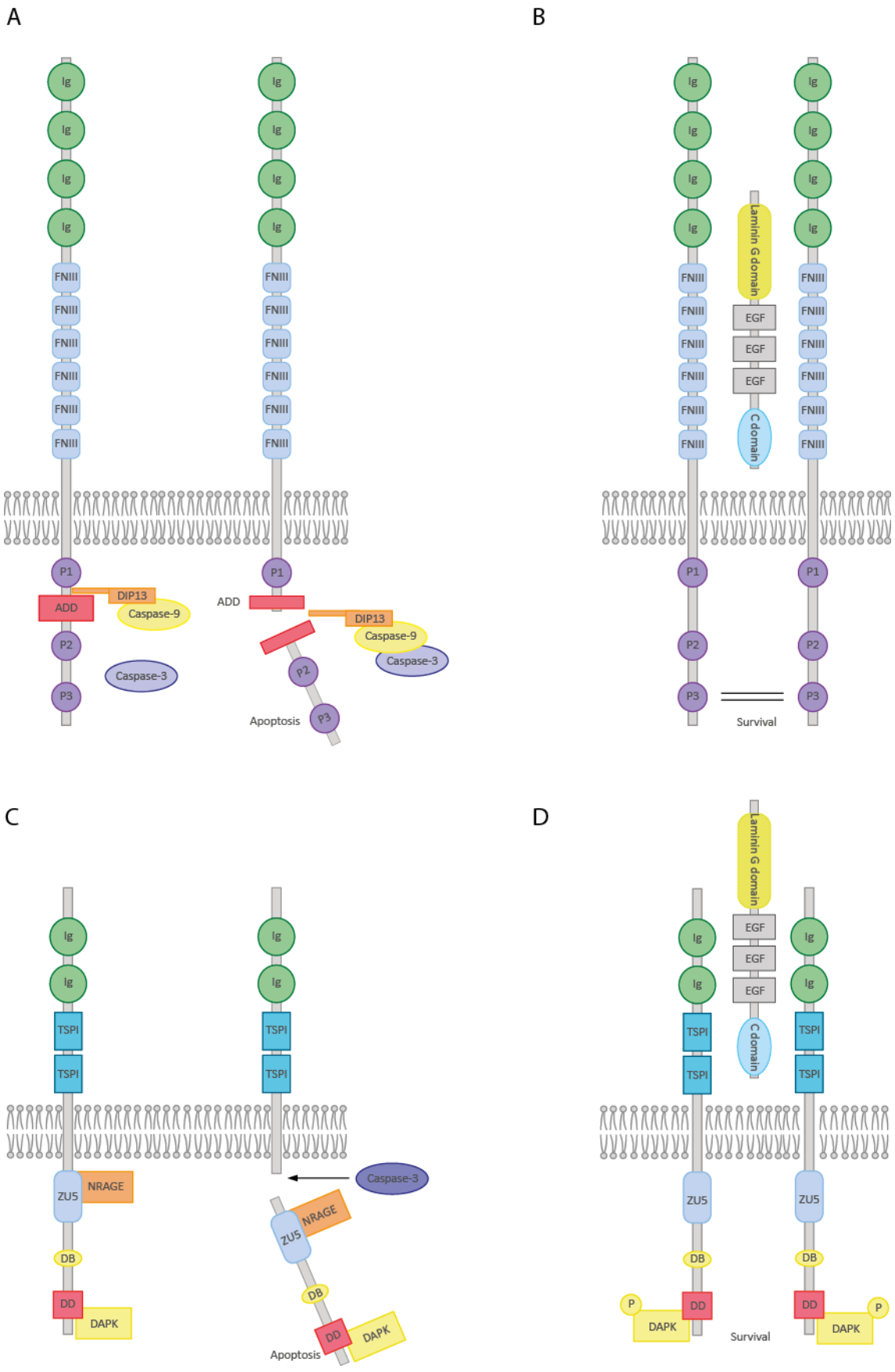
A
Ig
FNIII
P1
P2
P3
ADD
DIP13
Caspase-9
Caspase-3
Apoptosis
B
Laminin G domain
EGF
C domain
Survival
C
TSPI
ZU5
NRAGE
DB
DD
DAPK
Caspase-3
Apoptosis
D
Laminin G domain
EGF
C domain
P
DAPK
Survival

Figure 11 | Cell death induction by DCC and UNC5 Netrin-1 receptors. Caspase-3 interacts with the cytoplasmic domain of DCC in the presence of Netrin-1 (**B**). Upon Netrin-1 withdrawal, caspase-9 is recruited to form a complex with caspase-3 and DCC. This interaction results in activation of caspases and cleavage of the ADD. DIP13 has also been reported to interact with ADD and cause apoptosis (**A**). UNC5 receptors are also caspase substrates that mediate apoptosis upon Netrin-1 withdrawal. Apoptosis induction is blocked in presence of Netrin-1 (**D**). In this processes also participates NRAGE, which directly interacts with the ZU5 domain of UNC5. DAPK is also recruited to the DD (**C**).

7. 3. NETRIN-1 IN TUMORIGENESIS

Many genes involved in axon guidance show genetic and epigenetic alterations in a number of cancers: Netrin-1, DCC, the UNC5 family members, Semaphorin3B (Sema3B), Semaphorin3F (Sema3F), Roundabout1 (Robo1) and EphB2. In this direction, Netrin-1 has not only been shown to be a key molecule for neuronal survival and axon guidance during CNS development. Netrin-1 has arisen as a regulator of tumorigenesis, mainly acting through its receptors DCC and UNC5.

Several studies have addressed the implication of Netrin-1 loss in some human cancers. For instance, expression of Netrin-1 is markedly reduced or absent in brain tumors and neuroblastomas, where it frequently carries missense mutations[200]. Therefore, Netrin-1 is a molecule that would be of major interest when developing therapies for the treatment of some cancers.

The gene encoding the Netrin-1 receptor DCC was originally isolated as a candidate tumor-suppressor gene, which was frequently deleted in colorectal cancer[201]. Many genetic and epigenetic aberrations in the DCC gene have been observed in numerous human cancers. In colorectal cancers, it is commonly found a 120-300bp expansion in the intron region immediately downstream of exon 7 of the DCC gene [201]. This leads to a reduced expression of DCC. An aberrant splicing leading to the generation of transcripts encoding defective DCC protein, has been observed in a number of brain tumours[202]. Introduction of an intact copy of DCC in nude mice resulted in the suppression of tumorigenicity[203]; and inhibition of DCC

expression in cancer cell lines led to an anchorage-independent growth *in vitro* and tumor formation *in vivo*[204]. These observations support the idea of DCC as a tumor-suppressor gene.

Similarly, UNC5 receptors expression is altered in a number of human cancers, including brain cancers[205]. More precisely, UNC5C is the most downregulated receptor in cancers, found in the 75% of cancers, followed by UNC5A and UNC5B (48% and 27%, respectively). Furthermore, UNC5C loss of function is associated with tumor progression in mice. As well as DCC receptor, many evidences lead to the hypothesis that UNC5 receptors are putative tumor suppressors, given frequent alterations observed in a number of human cancers[205].

8. ALTERNATIVE SPLICING

The finding of viral sequences can be removed from the mRNA and exons can be joined back together, led the discovery of a fundamental principle in biology. In humans have been identified 25000 protein-coding genes and, to date, more than 90000 different proteins have been identified[206]. Led Gilbert[207] proposed for the first time in 1978 the concept of alternative splicing which made the statement "one gene, one protein" obsolete. About 95% of genes are susceptible to undergo alternative splicing in a dependent and highly regulated manner. Alternative splicing may occur in a tissue- or developmental-specific manner or in response to different cellular responses, being a key role in many cellular processes[208].

Most eukaryotic genes are expressed as precursor mRNAs (pre-mRNA) that are ultimately converted to mature mRNA by alternative splicing, a step in which non-coding sequences known as introns are skipped, while exons, which are coding sequences, are ligated together. Constitutive splicing is known as the process of intron removal and exon ligation for the majority of exons that are found in a gene. Contrarily, alternative splicing consists in a shift of this canonical sequence, resulting in the skipping of certain exons ,that ultimately should compose the mature mRNA. A highly dynamic machinery, called spliceosome, mediates this

process. Alternative spliced proteins may result in isoforms with different or even antagonistic functions, with altered stability or different subcellular localization.

Alternative splicing events are largely controlled by the recruitment of RNA-binding proteins (RBPs) that recognize specific sequences in the pre-mRNA. Some RBPs are specifically detected in neuronal cell types, such as Nova, Rbfox or Ptbp2 among others[209, 210]. Pre-mRNA splicing is catalyzed by the spliceosome, a multi-megadalton ribonucleoprotein (RNP) complex. The conformation and composition of the spliceosome are highly dynamic, giving the complex accuracy and flexibility at the same time. The first assembled subunits of the spliceosome are the pre-catalytic B complex, in which the 5-splice site (5'ss) and the branch point sequence of a intron are recognized by U6 and U2 small nuclear ribonucleoproteins (snRNP). RNP remodelling by the B complex results in the dissociation of U1 and U4 snRNP and the recruitment of about 20 proteins that will form the activated spliceosome (B^{act} complex)[211]. At this point, the B^{act} complex still cannot catalyze the branching reaction. The catalytically activated B complex (B* complex) by ATPase/helicase Prp2 allows the branching reaction to occur, generating a loop between 5'-exon and 3'-intron. The resulting catalytic step (C complex) is converted by Prp16 into the activated spliceosome (C* complex) which will finally catalyze the ligation of the 5'-exon with the 3'-exon[212].

Alternative splicing events are classified into four main groups: (1) exon skipping, the exon is skipped out together with flanking introns, (2) alternative 5'ss and (3) 3'ss selection, which consists in the recognition of one or more splicing sites at one end of an exon, and (4) intron retention, in which an intron remains in the mRNA sequence[213].

8. 1. ALTERNATIVE SPLICING IN THE CNS

Alternative splicing occurs at high frequency in tissues during central nervous system development. Alternative splicing has been demonstrated to be a key event in processes such as cell-fate decisions, neuronal migration, axon guidance and synaptogenesis. Temporal

control of alternative splicing is crucial for the transition embryo-to-adult during development, being a hallmark in the study of some genetic diseases during development.

Some axonal guidance processes rely in this phenomenon, regarding the establishment of proper neuronal circuits and pathfinding of some axons. It is the case of the Netrin-1 receptor DCC, a crucial receptor for axonal navigation during spinal cord formation, which has been shown to be alternatively spliced[214]. One of the isoforms is able to bind Netrin-1 with higher specificity[214]. Nova splicing factors are known to participate in the splicing of DCC receptor and Nova1/2 knockout mice resembles the phenotype of DCC knockout mice[214], which shows aberrant neuronal migration and axonal pathfinding in commissural neurons of the spinal cord[214].

OBJECTIVES

Axon guidance is a key mechanism during CNS development. Guidance cues and their receptors coordinate their responses in order to properly guide axons towards their final destinations, to ultimately establish functional circuits within the brain and spinal cord. Subcellular localization of axon guidance receptors is crucial to give appropriate responses to the extracellular environment. Netrin-1 UNC5 receptors are necessary for axon repulsion events. In this thesis we have tackled the importance of the association of UNC5 receptors to lipid rafts microdomains and the implication in axon repulsion mediated by these receptors. Therefore, the main objectives of this thesis are:

1. To investigate differences in biophysical properties of UNC5 receptors with quantifiable techniques such as FRAP and sptPALM, beyond biochemical approaches.

Subcellular distribution, dynamics and association to membrane microdomains are a key aspect in the functionality of cell membrane receptors. Beyond biochemical fractionation of cell membranes, we wanted to examine UNC5 receptors mobility and biophysical properties with confocal live imaging techniques.

2. To determine biophysical properties of UNC5B and UNC5C under different conditions: cholesterol removal and death domain deletion.

UNC5B and UNC5C are Netrin-1 receptors involved in axon repulsion events during outgrowth of the parallel fibers in the cerebellum. It has been reported by biochemical fractionation that both DCC and UNC5 are lipid rafts residents. For this reason, we wanted to assess biophysical properties of these receptors upon cell membrane cholesterol, a key element in rafts composition, disturbance and the intracellular DD ablation of UNC5B and UNC5C.

3. To investigate biophysical properties of the observed UNC5C clusters in the cell membrane with FRAP technique.

After examination, we observed differential distribution between UNC5B and UNC5C within the cell membrane. Thus, in this objective we studied in more detail the clusterized distribution of the UNC5C receptor.

4. To assess the relevance of cholesterol-enriched microdomains in axon guidance events where UNC5 receptors participate.

UNC5B and UNC5C are expressed in GCs during postnatal cerebellar development. Alongside with Netrin-1, they prevent parallel fibers to elongate in undisered territories. In this objective, we wanted to assess the importance of the integrity of lipid rafts in Netrin-1 mediated repulsion by UNC5 receptors in GCs.

Alternative splicing is an important process during developmental and postnatal stages in which one gene can produce a plethora of different proteins with different structures and functions. During the elaboration of this thesis we observed a spliced form of the Netrin-1 receptor UNC5A, whose localization and function differs dramatically from that described for the canonical form of UNC5A:

5. To Understand subcellular localization and functionality of the short isoform of UNC5A receptor.

UNC5A suffers alternative splicing which results in a shorter form compared to the canonical sequence. Here, we assess the implication of the missing extracellular domain in subcellular localization and functionality of this isoform.

RESULTS

1. IMPLICATIONS OF THE ASSOCIATION TO LIPID RAFTS IN AXON GUIDANCE OF UNC5 RECEPTORS

1. 1. LOCALIZATION OF UNC5(A-D) YFP-TAGGED RECEPTORS

To investigate the membrane distribution and dynamics of the UNC5 receptors involved in the repulsion associated with the recognition of the Netrin-1 ligand, we fused the fluorescent protein YFP to the C-terminus of all members of the UNC5 family of proteins, UNC5A, UNC5B, UNC5C, UNC5D. We first expressed the DNAs encoding each YFP-tagged UNC5 receptor (UNC5-YFP) in Human Embryonic Kidney 293T (HEK293T) cells, and examined under confocal microscope their subcellular spatial distribution. To determine the proper targeting of all UNC5 receptors to the cell membrane, we specifically labeled the cytoplasmic membranes incubating the cells with a fluorescently tagged wheat germ agglutinin (WGA) and we evaluated the co-distribution of the membrane marker with the receptors. We observed that the four UNC5(A-D) constructs co-localized with the cell membrane marker (Fig. 1A, C, E, G). We plotted the signal intensity of both, receptors and the membrane marker along specific regions of the cells by drawing a straight region of interest (ROI) crossing twice the cell membrane and analyzing the intensities. As expected, two peaks in the WGA signal were detected in each analyzed cell. The two WGA intensity peaks overlapped with peaks corresponding to the UNC5 channels (Fig. 1B, D, F, H). Although all four YFP-tagged UNC5 constructs traffic efficiently to the cell membrane, we observed higher intracellular retention of the UNC5D construct compared with the other UNC5 partners.

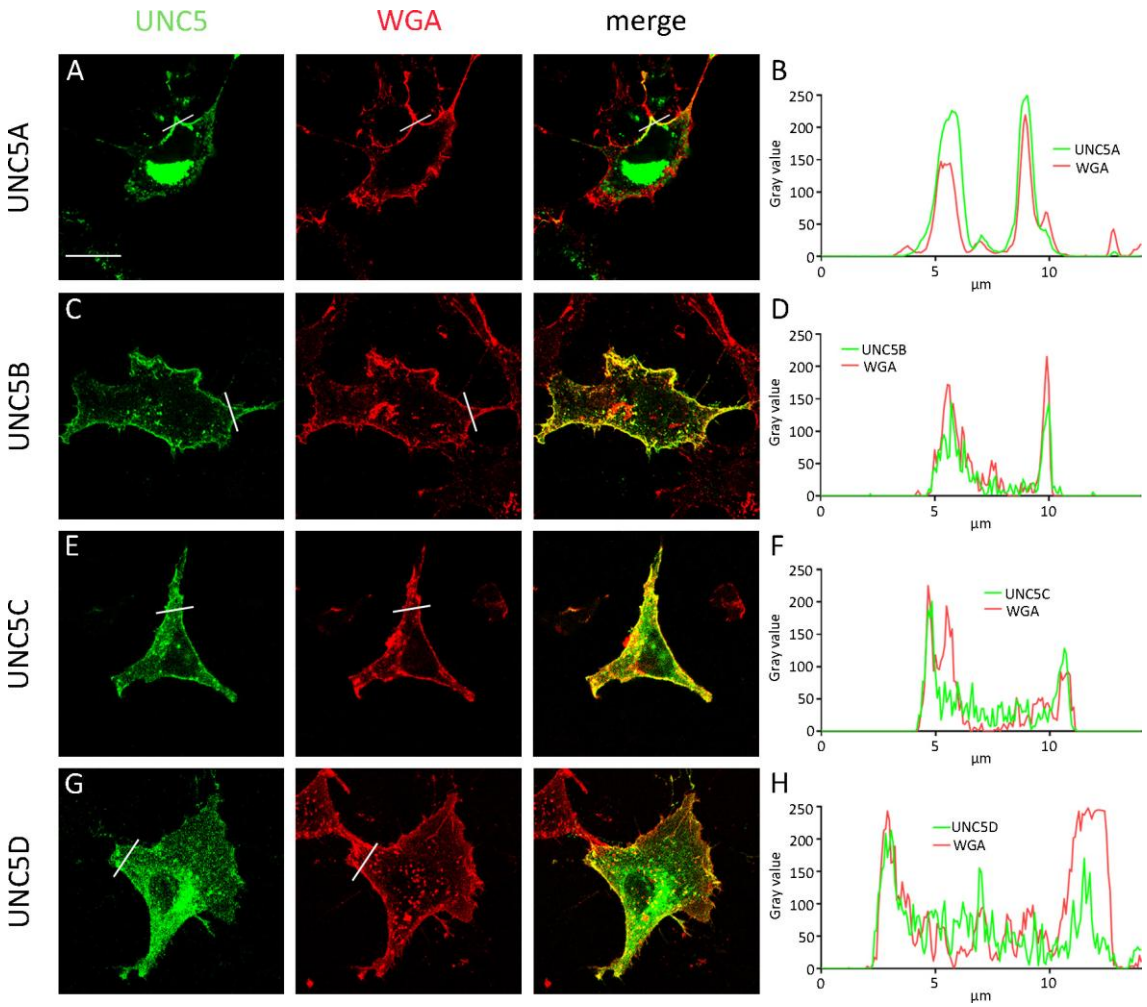

Figure 12 | Expression and localization of YFP-tagged UNC5 receptors in HEK293T cells. Confocal images of HEK293T cells expressing UNC5A-YFP (**A**), UNC5B-YFP (**C**), UNC5C-YFP (**E**) and UNC5D-YFP (**G**) receptors. Cells were labeled with WGA, a plasma membrane marker. WGA labeling was performed before fixation and at 4ºC to avoid internalization of the marker (**A**, **C**, **E**, **G**). Optical sections correspond to the relative middle of each cell. Intensities for each channel were plotted in a xy graph, illustrating intensities where the drawn line was placed, UNC5(**A**-**D**) (green line) and WGA (red line) (**B**, **D**, **F**, **H**). Note that WGA peaks correspond to peaks found in UNC5 receptors, meaning that all constructs reach the cell surface. Scale bar: 20µm.

To better examine the intracellular distribution of UNC5 receptors, we acquired Z-stacks and composed an x-z representation of each UNC5 in HEK293T (Fig. 2A-1D). The distribution of all UNC5 receptors along the cell membrane was further verified. Interestingly, here we observed a differential pattern of membrane distribution among the receptors. Whereas UNC5A and UNC5C were distributed predominantly forming clusters along the cell membrane (Fig. 2A, 1C, bottom panels, arrows), UNC5B was evenly distributed within the plasma membrane (Fig. 2B).

We also verified that UNC5D was the construct that evidenced a more cytoplasmic retention (Fig. 1D).

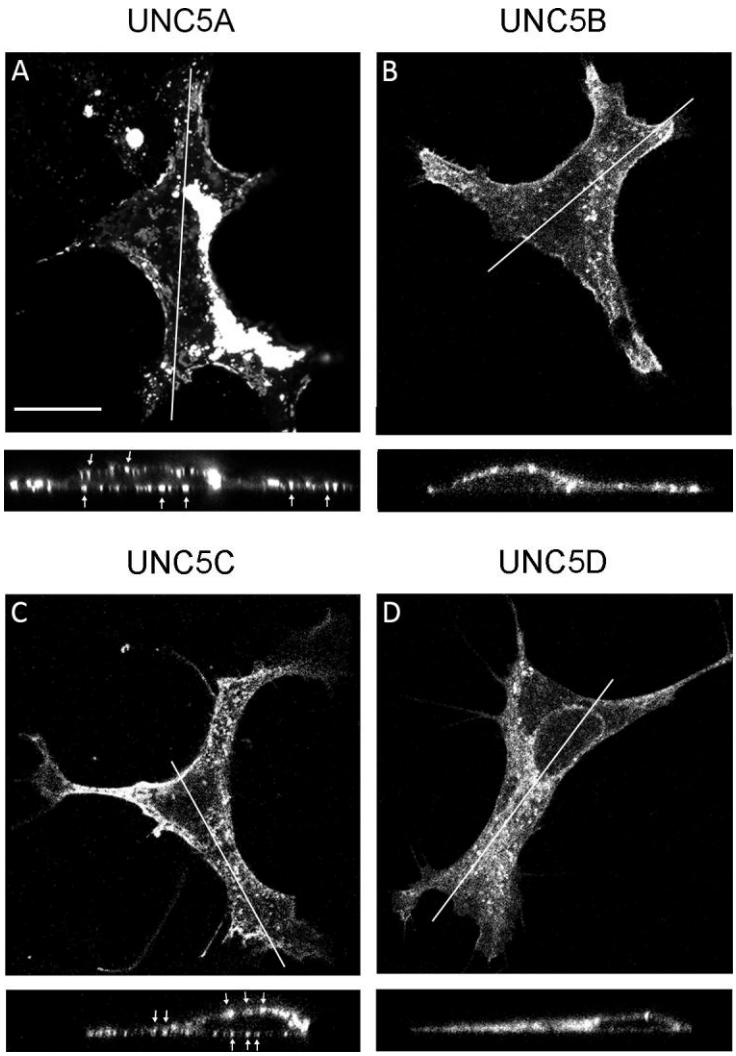

Figure 13 | Differential distribution of YFP-tagged UNC5 receptors into macro-domains. Series of confocal images were taken from HEK293T cells expressing each YFP tagged receptor. Three-dimensional confocal stacks were used to generate x-z reconstructions of each cell expressing YFP tagged receptors, UNC5A-D (**A**-**D**). Line illustrates xy axis in which stack level is observed (**A**-**D** bottom panels). UNC5A (**A**) and UNC5C (**C**) are distributed into macroclusters within the cell membrane. Arrows point to clusters of UNC5A (**A**) and UNC5C (**C**). UNC5B is evenly distributed along the cell membrane (**B**), while UNC5D can be observed inracellularly to a greater extent (**D**). Scale bar: 20μm.

Alignment of the aminoacidic sequences, revealed that structural domains analyzed, Ig, TSPI, transmembrane domain and DD, of UNC5 family members are conserved when examining the four receptors (Fig. 3A). UNC5A shares 54% and 56% in homology when compared to UNC5B and UNC5C, respectively (Fig. 3B UNC5). The homology between UNC5B and UNC5C is 65%, which is the highest homology among all UNC5 members (Fig. 3B UNC5). Contrarily, UNC5D is the most distant member in sequence homology of the UNC5 family (Fig.

3B UNC5). It is known that DD is a key domain for UNC5B to target into cholesterol enriched plasma membrane domains[215], for this reason we also wanted to analyze particularly the sequence homology of DDs of the UNC5 members. UNC5B and UNC5C are the closest members, sharing a 67% of homology (Fig. 3B DD). The DD of UNC5A shares 49% homology with UNC5B and 48% with UNC5C (Fig. 3B DD). UNC5D shares 43% of homology with UNC5A, and 55% and 50% of homology in the aminoacidic sequence with UNC5B and UNC5C respectively (Fig. 3B DD). Therefore, unlike the comparison of the whole sequence of UNC5 members, when comparing sequence homology of only DDs, UNC5A results the more distant member of the entire UNC5 family.

A


UNC5A_MOUSE
UNC5B_MOUSE
UNC5C_MOUSE
UNC5D_MOUSE

B


UNC5
UNC5D
UNC5A
UNC5B
UNC5C
DD
UNC5A
UNC5D
UNC5B
UNC5C

Figure 14 | Structural domains are conserved across all UNC5 family members. Alignment of mouse UNC5A, UNC5B, UNC5C and UNC5D protein sequences. Similar aminoacid residues are shaded, ranging from white, different aminoacid residues, to dark gray, identical aminoacid residues (**A**). Signal peptide is shaded in pink at the beginning of each sequence (**A**). Structural domains are boxed, Ig domains (yellow), TSPI repeats (red), transmembrane domain (blue) and DD (green) (**A**). Phylogenetic trees comparing known sequences of UNC5 members (UNC5) and their respective DDs (DD) (**B**). Accession numbers are: NP_694771, UNC5A; NP_084046, UNC5B; NP_001280490, UNC5C; NP_694775, UNC5D.

1. 2. DYNAMICS OF UNC5(A-D) RECEPTORS IN THE PLASMA MEMBRANE

Most UNC5 receptors are organized within raft microdomains[215]. Qualitatively and as mentioned in the Introduction, lipid raft association can be determined by assessing co-localization with Cholera toxin B-subunit[156] (CTxB). Here, we first wanted to verify whether all UNC5 members are localized into cholesterol-enriched lipid rafts. By performing immunocytochemistry analysis of the membrane co-localization of all UNC5 receptors with the raft marker CTxB, tagged with the fluorophore Alexa fluor 555, in previously transfected HEK293T cells with the YFP-tagged UNC5 receptors, we found that all four members of the UNC5 family partially co-localize with lipid raft membrane regions (Fig. 4A-D). Distribution into patches of UNC5C receptor co-localize with membrane domains enriched in CTxB labeling (Fig. 4C arrowheads).

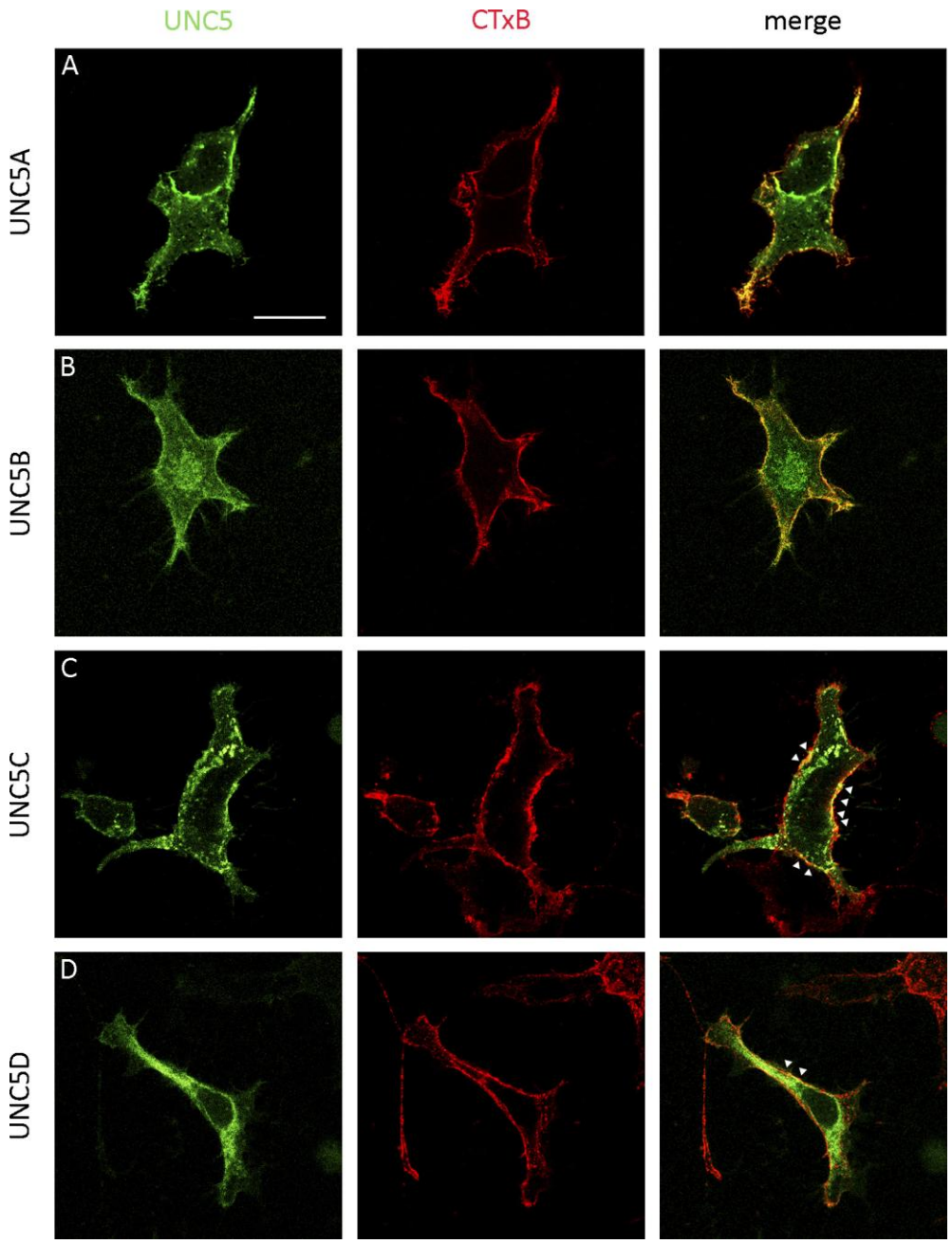

Figure 15 | Colocalization of UNC5(A-D) receptors with the lipid raft membrane marker CTxB. Confocal images of HEK293T cells expressing UNC5A-YFP (**A**), UNC5B-YFP (**B**), UNC5C-YFP (**C**) and UNC5D-YFP (**D**) receptors. Cells were labeled with CTxB, a lipid raft marker in the plasma membrane. CTxB labeling was performed before fixation and at 4ºC to avoid internalization of the marker (**A-D**). Optical sections correspond to the relative middle of each cell. Arrowheads in A and C indicates the clustered organization ofUNC5A and UNC5C. Scale bar: 20µm.

To quantify the retention of UNC5 receptors in specific membrane microdomains, we performed FRAP assays, elucidating the different dynamics of each receptor (Fig. 5). In HEK293T cells expressing each of all the UNC5 (A-D) receptors, a small region of interest (ROI) along the cell surface was bleached using the 488 nm laser line. The recovery of the fluorescence within the bleached area was monitored by acquiring images in different sections (see Materials and Methods) during 240 s. The fluorescence values were normalized to the prebleach intensity and corrected with the background intensity and the cumulative unspecific photobleaching due to the scanning protocol. When comparing the membrane dynamics between the four receptors, UNC5A showed the slowest fluorescence recovery rate, with an average mobile fraction (Mf) of 0.22±0.003 (Fig. 5A, B). UNC5B exhibited a Mf of 0.65±0.007 (Fig. 5C, D). UNC5C, which showed with UNC5A a marked clustered distribution, displayed a Mf of 0.31±0.0081 (Fig. 5E, F). UNC5D exhibited the fastest fluorescence recovery rate, with a Mf of 0.7±0.012 (Fig. 5G, H). Interestingly, whereas all UNC5 receptors localize in lipid raft domains, our results using FRAP analysis suggest that the two receptors (UNC5A and UNC5C) that distribute in distinct surface puncta along the cell membranes and share a similar low lateral membrane mobility. The receptors (UNC5B and UNC5D) which are evenly distributed in the cell membrane exhibit a faster lateral mobility.

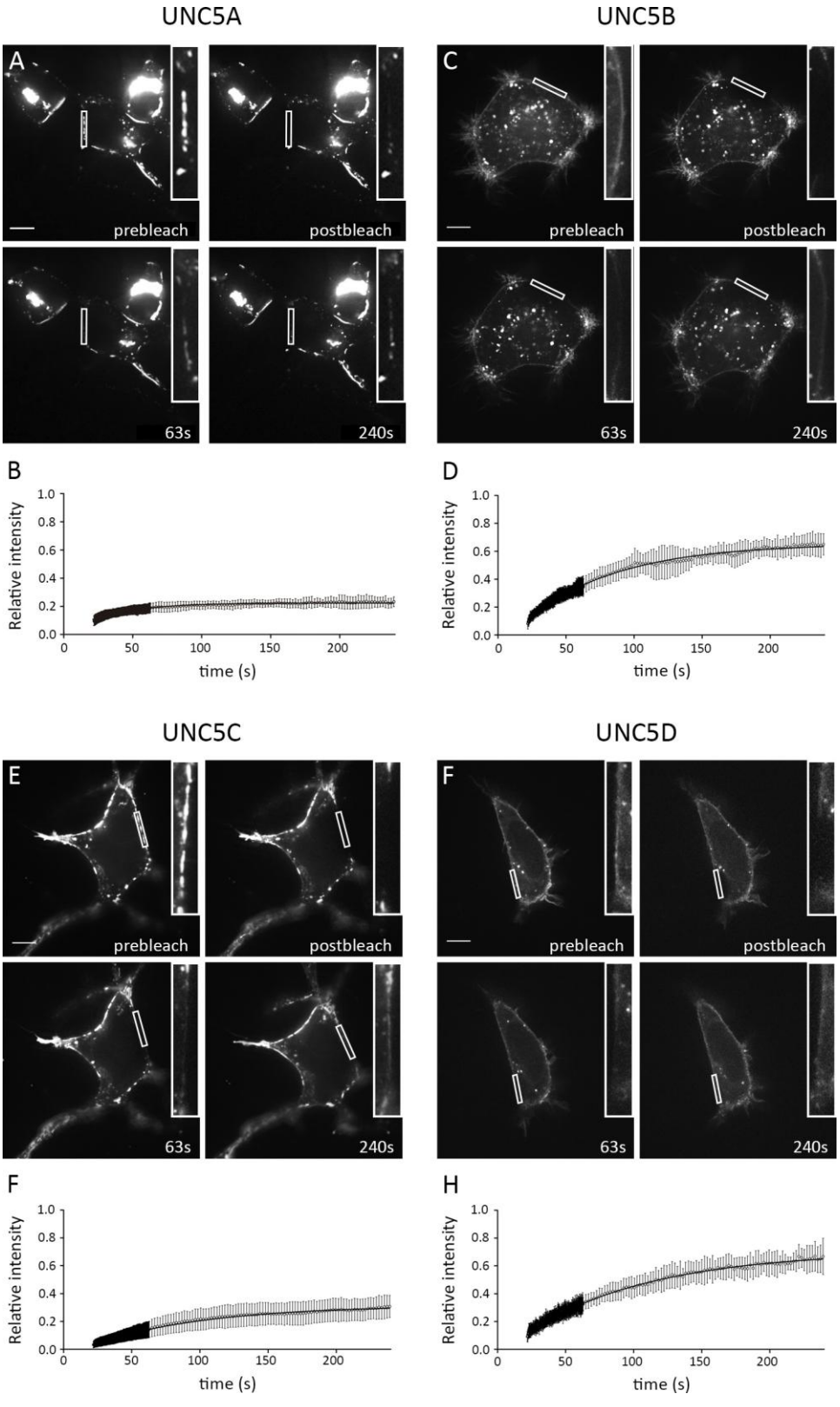
UNC5A
UNC5B
A
C
prebleach
postbleach
63s
240s
B
D
Relative intensity
time (s)
UNC5C
UNC5D
E
F
H

Figure 16 | Differences in the lateral mobility of the four UNC5(A-D) receptors. Images from FRAP experiments at different time points (prebleach, postbleach, 63 and 240 seconds) of cells expressing each receptor, UNC5(A-D) (**A**, **C**, **E**, **G**). The highlighted box indicates where the photobleaching was targeted followed by the scanning of the recovery after photobleaching for every UNC5 receptor (see Materials and Methods). Fluorescence at each time point was normalized to the prebleach intensities (bleach=time 20 seconds) and averaged for all cells (UNC5A-YFP n=8, UNC5B-YFP n=13, UNC5C-YFP n=15, UNC5D-YFP n=13). Standard deviation is shown for each averaged point. The solid lines through the averaged points are single exponential fitted to the data (**B**, **D**, **F**, **H**). UNC5A-YFP Mf=0.71±0.005 (**B**); UNC5B-YFP Mf=0.65±0.007 (**D**); UNC5C-YFP Mf=0.31±0.0081 (**F**); UNC5D-YFP Mf=0.7±0.012 (**H**). Scale bar: 20μm.

Among the different UNC5 receptors, their role during axonal guidance processes have been widely characterized in UNC5B and UNC5C. Both receptors participate in the correct elongation of axons during the development of the cerebellum[83] and are responsible for the repulsion to Netrin-1 observed in this neuronal system[83]. To better determine whether mobility ratios found in HEK293T cells are consistent with the membrane dynamics of the receptors in neurons, we performed FRAP experiments in transfected hippocampal neurons with UNC5B and UNC5C constructs (Fig. 6). As EGL cerebellar granule cells are one of the smallest neurons in the brain, a proper FRAP analysis of transfected UNC5 receptors was not possible in this neuronal type. By using the same FRAP protocol as in HEK293T cells experiments, the obtained Mf of UNC5B (Fig. 6A, B Mf=0.64±0.009) and UNC5C (Fig. 6C, D Mf=0.3±0.005) in hippocampal neurons were similar to those obtained in HEK293T cells (Mf UNC5B=0.65±0.007; Mf UNC5C=0.31±0.0081).

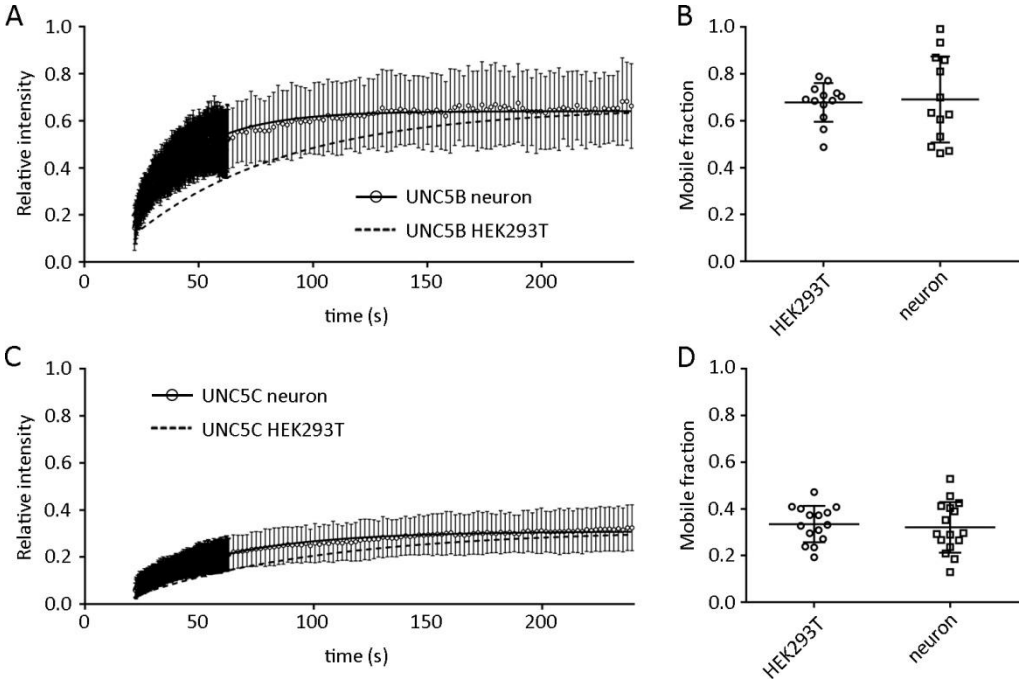

Figure 17 | UNC5B and UNC5C lateral mobility in transfected hippocampal neurons. Average recovery after photobleaching of hippocampal neurons expressing UNC5B-YFP (n=13) (**A**) or UNC5C-YFP (n=16) (**C**). Solid line represents calculated average recovery curve of hippocampal neurons. Dashed line represents calculated average recovery curve of HEK293T cells expressing UNC5B-YFP (**A**) or UNC5C-YFP (**C**). Calculated Mf from both, HEK293T and hippocampal neurons are represented in a graph (**B**, **D**). No differences are found when comparing HEK29T or hippocampal neurons, expressing UNC5B-YFP (**B**) or UNC5C-YFP (**D**). Data represents means ± SD ($^{ns}p > 0.05$).

As a comparison, we also analyzed the membrane dynamics of the Netrin-1 receptor DCC. The evenly distribution observed in HEK293T cells, matched with its Mf is 0.59±0.007, similar to the one obtained by UNC5B (Fig. 7A). The Mf exhibited by DCC receptor in hippocampal neurons was 0.4±0.01, slightly lower than the obtained in HEK293T cells (Mf=0.59±0.007) (Fig. 7B, C).

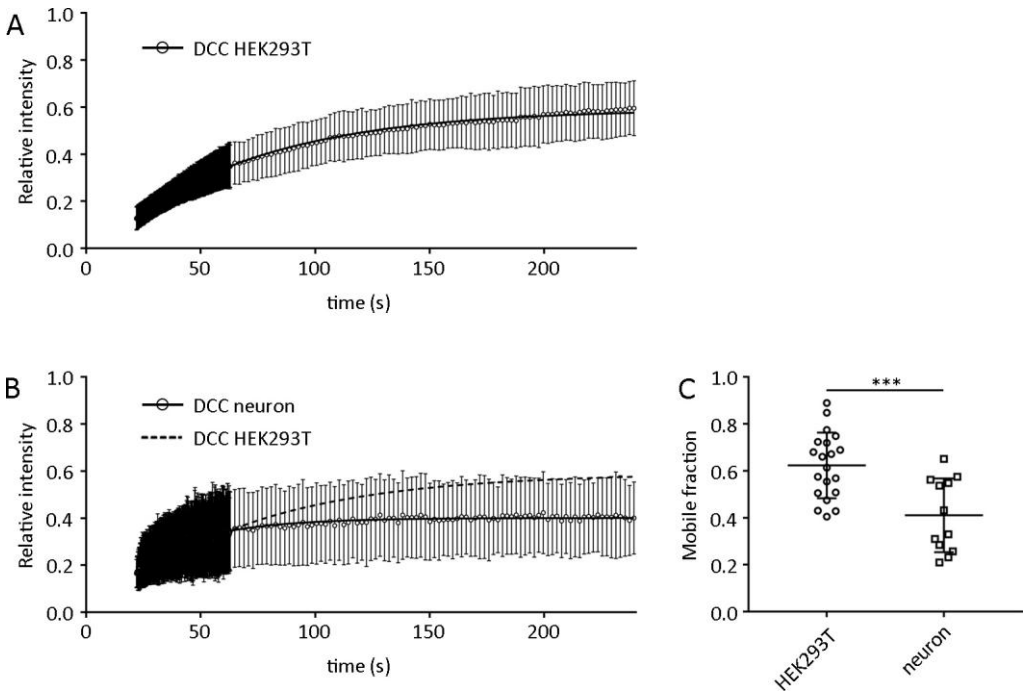

Figure 18 | DCC Netrin-1 receptor dynamics in HEK293T and hippocampal neurons. Average recovery after photobleaching in transfected HEK293T cells expressing DCC-YFP (**A**) (n=20) and in transfected hippocampal neurons with DCC-YFP (n=12), solid line represents average recovery for hippocampal neurons and dashed line illustrates recovery calculated with HEK293T (**B**). Mf from both, HEK293T cells and hippocampal neurons expressing DCC-YFP, is represented in the graph. After comparing both Mf, HEK293T cells exhibited a higher Mf rather than hippocampal neurons (**C**). Data represents means ± SD ($^{***}p \leq 0.001$).

1. 3. UNC5B AND UNC5C ARE PRESENT IN DRM FRACTIONS

In these experiments we analyzed whether UNC5B and UNC5C receptrs are associated to lipid rafts microdomains. Lipid rafts can be isolated due to their insolubility properties in cold detergent solubilization, and separated from disordered membrane fractions by a sucrose gradient centrifugation.

YFP-tagged UNC5B and UNC5C were transfected into HEK293T cells, 1 day after transfection, cells were harvested and performed lipid raft isolation. After immunoblotting detection, a significant fraction of both, UNC5B and UNC5C were found in DRM. DRM fractions can be identified thankful to their enrichment in Cav proteins. In control media, a proportion of UNC5B and UNC5C were found in DRM fractions (Fig. 8A, C). Conversely, the non-raft marker clathrin, was preferentially found in fractions 9-12, which represent DSMs. A

substantial proportion of UNC5B and UNC5C was also found in DSM fractions (Fig. 8A, C). To further assess the cholesterol implication in the association of these receptors to the buoyant fractions, we treated HEK293T cell cultures with MβCD, which removes membrane cholesterol by forming inclusion complexes in the cell membrane[216], and therefore destabilized cholesterol enriched membrane microdomains. Pre-incubation of MβCD resulted in the partial loss of the lipid raft marker (Fig. 8B) or reorganization of Cav proteins into non-buoyant fractions (Fig. 8D). Detection of the UNC5B receptor was completely lost in the DRM fractions (Fig. 8B), while UNC5C was found to be redistributed, with the raft marker, closer to DSM fractions (Fig. 8D).

This assay was also performed with native tissue, by using isolated cortex and cerebellum from P4 mice, we performed membrane biochemical fractionation and assessed the efficiency by detecting clathrin, for the non-raft fractions and Cav and Flotillin for DRM fractions. DSMs were preferentially found in the heavy fractions (9-12) and DRMs, cholesterol enriched membranes, were isolated in 4-5 fractions for both raft markers. Next, we tried to assess the localization of UNC5B and UNC5C with specific antibodies. Nevertheless, we were unable to detect these receptors nor in DRMs nor in DSMs (Fig. 8E). These results will be further discussed in the Discussion section.

Together, these results evidence that UNC5B and UNC5C receptors partly are associated with lipid rafts. This association is membrane cholesterol-dependent, as after MβCD treatment, receptors were reorganized into non-raft or DSM fractions. Nonetheless, results from biochemical membrane separation must be taken carefully as they may exhibit some variability, this limitations will be further discussed in this thesis. Ultimately, we were able to isolate membrane raft from mice native tissue, however, we could not detect the receptors of interest.

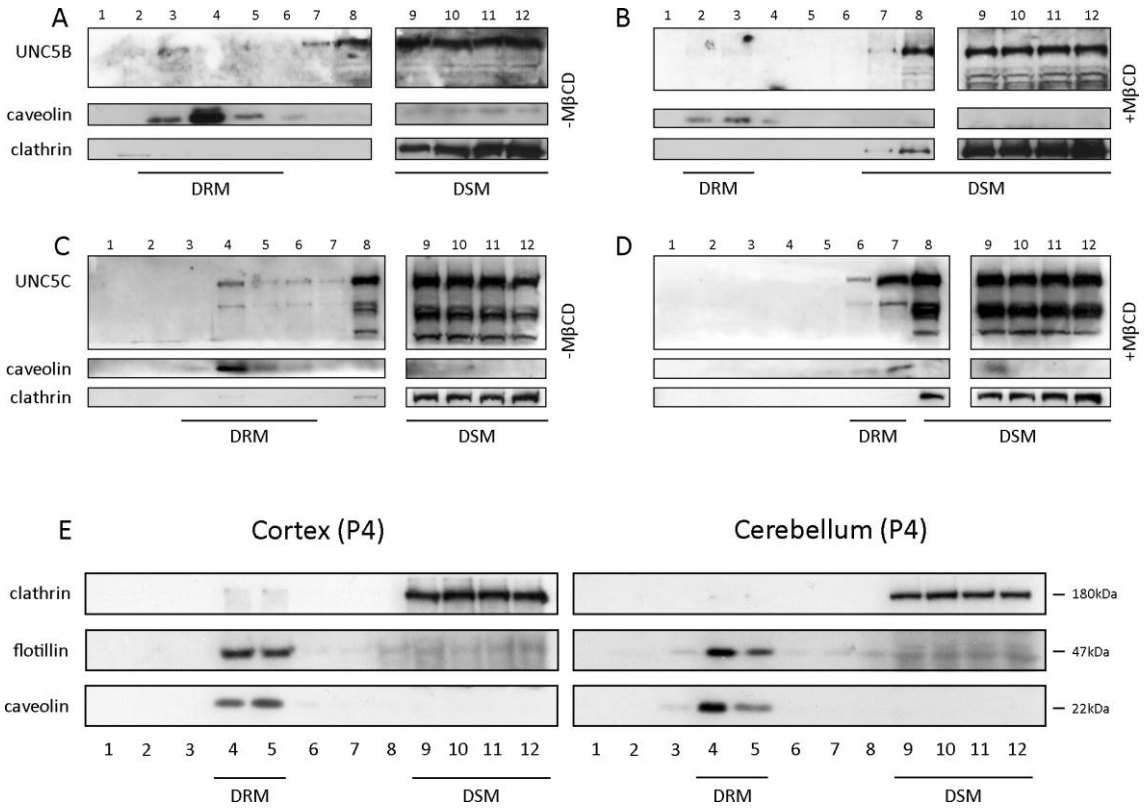

Figure 19 | Cell membrane biochemical fractionation and lipid raft isolation of HEK293T cells expressing UNC5B and UNC5C receptors and mouse nervous tissue. HEK293T cells were transiently transfected with UNC5B (**A**, **B**), UNC5C (**C**, **D**), YFP tagged plasmids. After 24 hours of transfection cells were incubated with control media (**A**, **C**) or MβCD containing media (**B**, **D**). Detection of immunoblots were performed against GFP; caveolin, a lipid raft marker; clathrin, a non-raft marker. Note that detergent resistant membranes (DRM) are detected in 3-5 fractions as evidenced by caveolin detection that in time partly corresponds with YFP tagged receptors detection. Cells treated with MβCD shift localization of cavelin to 6-8 fractions and receptors are not found in this fractions. Clathrin, the non-raft marker is typically found in 8-12 fractions, termed detergent soluble membranes (DSM). Biochemical fractionation performed with mouse tissue, in cortex and cerebellum from P4 mice (**E**). Caveolin and flotillin are used as lipid raft markers (DRM), found in fractions 4 and 5. Clathrin presence in fractions 9-12 indicate DSM (**E**).

1. 4. UNC5B AND UNC5C MEMBRANE DYNAMICS ARE MODIFIED AFTER CHOLESTEROL DEPLETION AND DEATH DOMAIN (DD) DELETION

We then performed FRAP experiments on UNC5B and UNC5C after disruption of lipid rafts with different types of cholesterol-depleting reagents, MβCD and cholesterol oxidase (ChoA). ChoA is an enzyme that catalyzes the oxidation and isomerization of cholesterol into oxysterol[217]. UNC5B exhibited an increment of its Mf after the treatment with MβCD

(Mf=0.75±0.008) (Fig. 9A, 4G) or ChoA (Mf=0.77±0.013) (Fig. 9C, 4G). Similarly, UNC5C showed increased lateral mobility after treatment with MβCD (Mf=0.45±0.017) (Fig. 9B, 4H) or ChoA (Mf=0.39±0.016) (Fig. 4D, 4H). Taking together, this data suggests that depletion of cell membrane cholesterol with MβCD and ChoA increases the amount of UNC5B and UNC5C that can freely diffuse within the membrane.

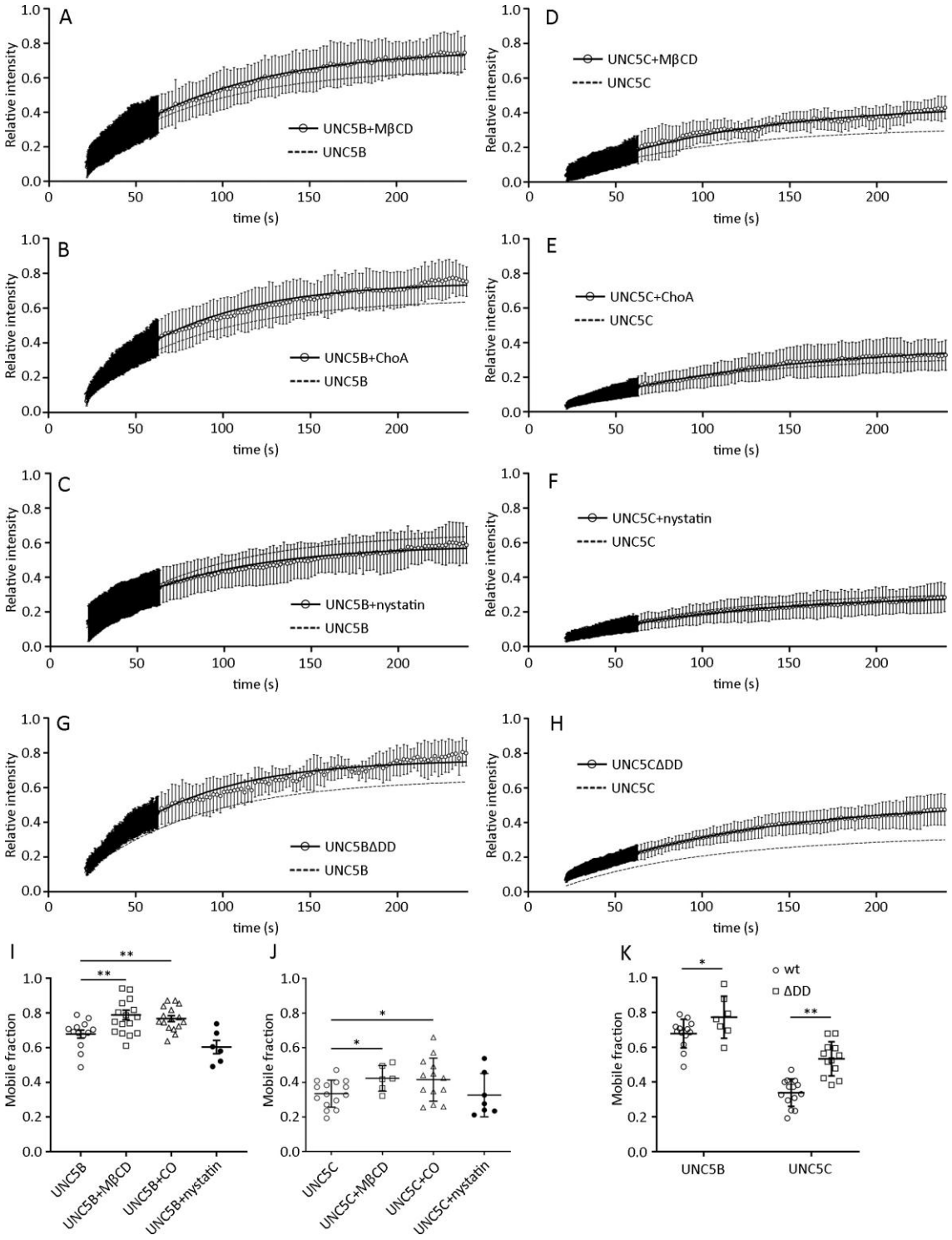

Figure 20 | UNC5B and UNC5C membrane dynamics after cholesterol depletion and DD deletion. Average recovery after photobleaching of HEK293T cells expressing UNC5B-YFP (n=16; MβCD) (n=16; ChoA) (n=6; nystatin) (**A**, **B**, **C**) and UNC5C-YFP (n=6; MβCD) (n=13; ChoA) (n=7; nystatin) (**B**, **D**, **E**) after treatment with MβCD, ChoA and nystatin (described in Materials and Methods) (**A**-**F**). Average recovery after photobleaching of UNC5BΔDD-YFP (n=7) (**G**) and UNC5CΔDD-YFP (n=12) (**H**). Fluorescence at each time point was normalized to prebleach intensities. The dashed line in each plot represents dynamics of each receptor under control conditions, whereas, without treatment or wild type receptor. All curves were fitted to a single exponential. The Mf for each drug treatment was compared to basal dynamics of the corresponding receptor, UNC5B-YFP (**I**), UNC5C-YFP (**J**). Mf of the wild type receptors were also compared to that exhibited by the forms lacking DD (**K**). Data represents means ± SD ($^{ns}p > 0.05$, $^{*}p \leq 0.05$, $^{**}p \leq 0.01$).

It has been reported by biochemical fractionation that the DD of UNC5B is necessary for this specific localization to lipid rafts[215]. Regarding that, we investigated whether the deletion of the DD in UNC5B and UNC5C affects the dynamics of these receptors in the cell membrane. We expressed in HEK293T cells YFP-tagged truncated forms of UNC5B and UNC5C receptors lacking the DD (UNC5BΔDD and UNC5CΔDD), and performed FRAP experiments to assess the dynamics of both truncated forms (Fig. 9E, 9F). The deletion of the DD resulted in the increase of the Mf of the receptors (Mf=0.76±0.01 for UNC5BΔDD, Mf=0.52±0.011 for UNC5CΔDD). This increase was higher in the case of UNC5CΔDD (40.3% of increment) than for UNC5B-ΔDD (14.4% of increment) (Fig. 9I). Our results suggest that the DD is a key element for the UNC5 receptors to maintain their biophysical properties in the cell membrane.

1. 5. BIOPHYSICAL PROPERTIES OF UNC5C CLUSTERS

We used FRAP experiments to examine the stability of individual UNC5C clusters located along the plasma membrane. We performed the same FRAP protocol as described previously and photobleached an area of the membrane containing clustered and non-clustered receptors. As UNC5C is unevenly distributed across the bleached ROI, we measured the recovery by selecting smaller sub-ROIs containing exclusively bleached clusters (Fig. 10D “cluster”) or bleached non-clusters (Fig. 10D “non-cluster”). Strikingly, the Mf of the clustered proteins was 0.25±0.025, while the Mf in a non-clustered region was 0.79±0.014. These results suggest that

UNC5C shows two distinguishable dynamics along the cell membrane, immobilized and freely diffusive.

We next wanted to assess whether the localization of the clusters of receptors remained immobile along time. Using the same FRAP protocol, we photobleached an area with distinguishable clusters (ROI in Fig. 10A) and followed the fluorescence recovery at four different time points, prebleach (immediately before the photobleaching), postbleach (immediately after the photobleaching), 63 seconds and 240 seconds after photobleaching (Fig. 10B). The fluorescence intensities were normalized to their prebleach values and plotted against their specific localizations (Fig. 10C). The 6 intensity peaks observed in the graphic (arrows in Fig. 10C) correspond to each of the 6 clusters of UNC5C located along the plasma membrane (arrowheads in Fig. 10B). The fluorescence recovery 62 seconds after photobleaching was almost null and undistinguishable from the postbleach instant. However, 240 seconds after photobleaching, the intensities of all 6 UNC5C signals were partially recovered in the same spatial position as the original photobleached clusters. These results suggest that UNC5C-containing clusters represent stable and well defined regions of the cell surface where the receptor exchange occurs. Non- bleached molecules can move in and out of the clustered regions.

We then investigated whether these clusters are enriched in the lipid raft marker CTx. UNC5C-RFP was transfected into HEK293T cells and incubated with CTxB Alexa-488. UNC5C cluster regions were enriched in CTxB labeling, suggesting that the receptor clusters occupy lipid rafts microdomains (Fig. 10G). We then performed FRAP on a clustered area using a 568 laser beam to specifically photobleach the intensity corresponding to UNC5C receptor without affecting the raft marker (Fig. 10H). After 420s of photobleaching, UNC5C preferentially redistributes back and reconstitutes its clusters within the preexisting cholesterol enriched regions (Fig. 10I). These results reinforce the idea that UNC5C receptors accumulate into membrane raft microdomains forming a temporally stable structure.

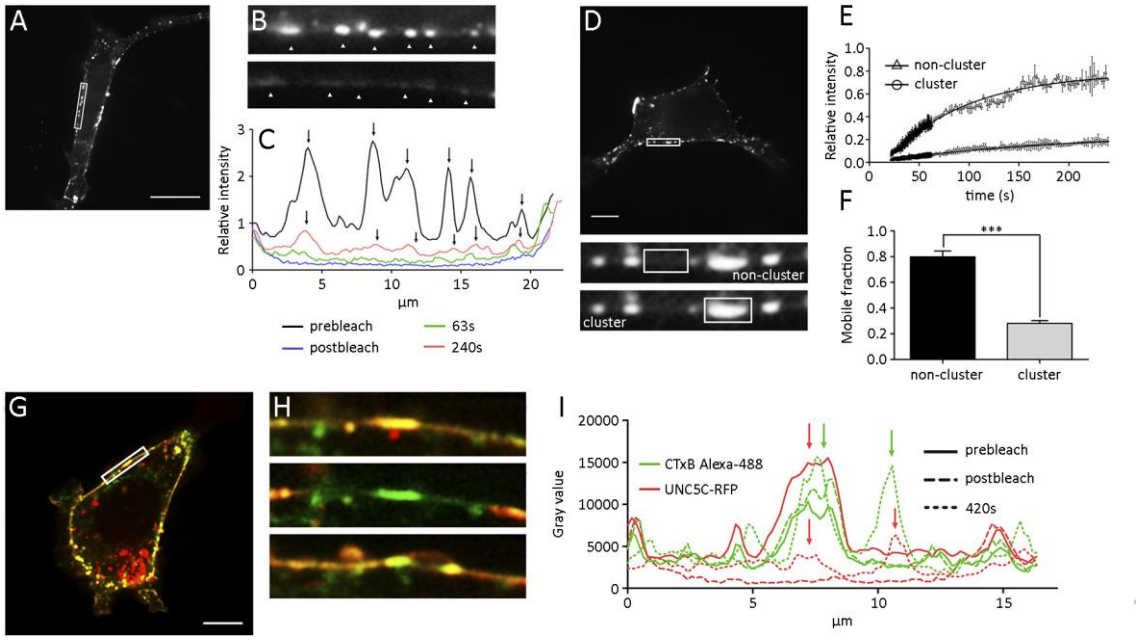

Figure 21 | Study of dynamics of UNC5C clusters. HEK293T cells expressing UNC5C-YFP, distributed into clusters, were photobleached in the area highlighted in a box (**A**). Magnification of the photobleached area showing two different time points, prebleach and after 240 seconds of bleaching (**B**). Arrowheads indicate UNC5C clusters distributed in the plasma membrane (**B**). Note that intact UNC5C has preference to occupy and reorganize in the same clusterized areas it was before photobleaching. Relative intensities of the magnified area plotted in the graph. Arrows indicate UNC5C clusters in prebleach and 240s time points, intensity peaks after 240s of photobleaching coincide with those shown in the prebleach (**C**). A HEK293T cell expressing UNC5C-YFP was photobleached in the highlighted area (**D**). Two measurements were taken from the same cell of 3 different cells (highlighted regions), inside and outside of the clusterized areas. Fluorescence recoveries were normalized to prebleach intensities, averaged for all cells (n=3) and fitted to a single exponential. Error bars are shown for each time point. Mf in the cluster region was 0.25±0.025 and 0.79±0.023 in non-cluster areas (**E**). Mf plotted in a bar graph and compared each other. Data represent means ± SD (n=3). ($^{***}p \leq 0.001$) (**F**). HEK293T cell labeled with CTx (green) and expressing UNC5C-RFP (**G**). The boxed area indicates where the photobleaching was performed. Magnifications of the photobleached region during prebleaching, postbleaching and after 420s of bleaching (**H**). The cell was excited simultaneously with a 488 and a 568 nm diode laser and photobleaching was only performed using a 568 nm diode laser. Intensity values plotted in a graph, showing that UNC5C has preference to organize into clusters and that this receptor clustering is enriched in CTx labeling (arrows) (**I**). Scale bars: 20µm.

1. 6. Single particle tracking photoactivation localization microscopy (sptPALM) reveals different dynamics and subpopulations in UNC5B and UNC5C receptors

sptPALM is a super-resolution microscopy technique that allows investigation of the mobility of single molecules *in vitro* and *in vivo*[218]. Receptors were fluorescently tagged with mEos2, a

photoswitchable fluorescent protein. Because these molecules are photoconverted stochastically, we could ensure that activated molecules are sparse enough to get single molecule trajectories within a given diffraction-limited region.

In order to assess the behavior of single molecules of UNC5B and UNC5C receptors, we took advantage of total internal reflection fluorescence microscopy (TIRF) to photoconvert and image single molecules of the receptors that are present in the plasma membrane. Analysis of single molecules of mEos2-tagged receptors, allows quantification in the cell membrane of mean square displacement (MSD) curves, diffusion coefficients and classification of trajectories considering their mobility (trapped, confined and free). To quantify receptor dynamics we combined data from multiple trajectories (>1000 trajectories per cell, 12-15 cells) to calculate MSD and diffusion coefficient distribution, as well as relative frequencies of different mobility types.

As we could see in FRAP experiments, whereas UNC5C is organized into macroclusters, UNC5B is evenly distributed within the cell membrane, and the Mf corresponding to UNC5B proteins are higher than the Mf of UNC5C. UNC5B-mEos2 and UNC5C-mEos2 were transfected into HEK293AD cells. Low-resolution TIRF images of UNC5B and UNC5C receptors are shown (Fig. 11Ai, Bi). Obtained single-moleculer trajectory tracks are arbitrary colored (Fig. 11Aii, Bii). Depicted UNC5B trajectories regarding considering mobility and diffusion coefficients are heterogeneous (Fig. 11Aiii, Aiv), and we detected both mobile and immobile populations. UNC5C trajectories showed a higher proportion of immobile molecules with low diffusion coefficients (Fig. 11Biii, Biv). MSD is a measure of the deviation of a particle over time and with a reference position. MSD calculated curves show that UNC5B (red) has a high displacement compared to that showed for UNC5C (blue). Calculated area under the curve for UNC5B is 0.01875$\mu m^2 s$, a value significantly higher than UNC5C area, being 0.01143$\mu m^2 s$ (Fig. 11C). Distribution of diffusion coefficients showed two distinguished populations of UNC5B receptor, immobile and mobile, and the major population of UNC5C receptor is found in the immobile

fraction. Relative frequencies for the distribution of both immobile and mobile fractions for each receptor were plotted. When compared, immobile and mobile fractions for both receptors resulted significantly different. UNC5C has a high frequency of diffusion coefficients with low values compared to UNC5B, while the frequency of values in the mobile fraction is higher for UNC5B (Fig. 11E). We classified each trajectory based on the diffusion coefficient and the area occupied by the molecule, into four different categories: trapped (Fig. 11Gi), confined (Fig. 11Gii), free (Fig. 11Giii) and mixed (Fig. 11Giv). We calculated the frequencies of approximately 4000 trajectories for each receptor. UNC5C exhibited more trapped trajectories and very few free when compared to UNC5B trajectories, nonetheless, the proportion of confined trajectories were similar for both receptors (Fig. 11F).

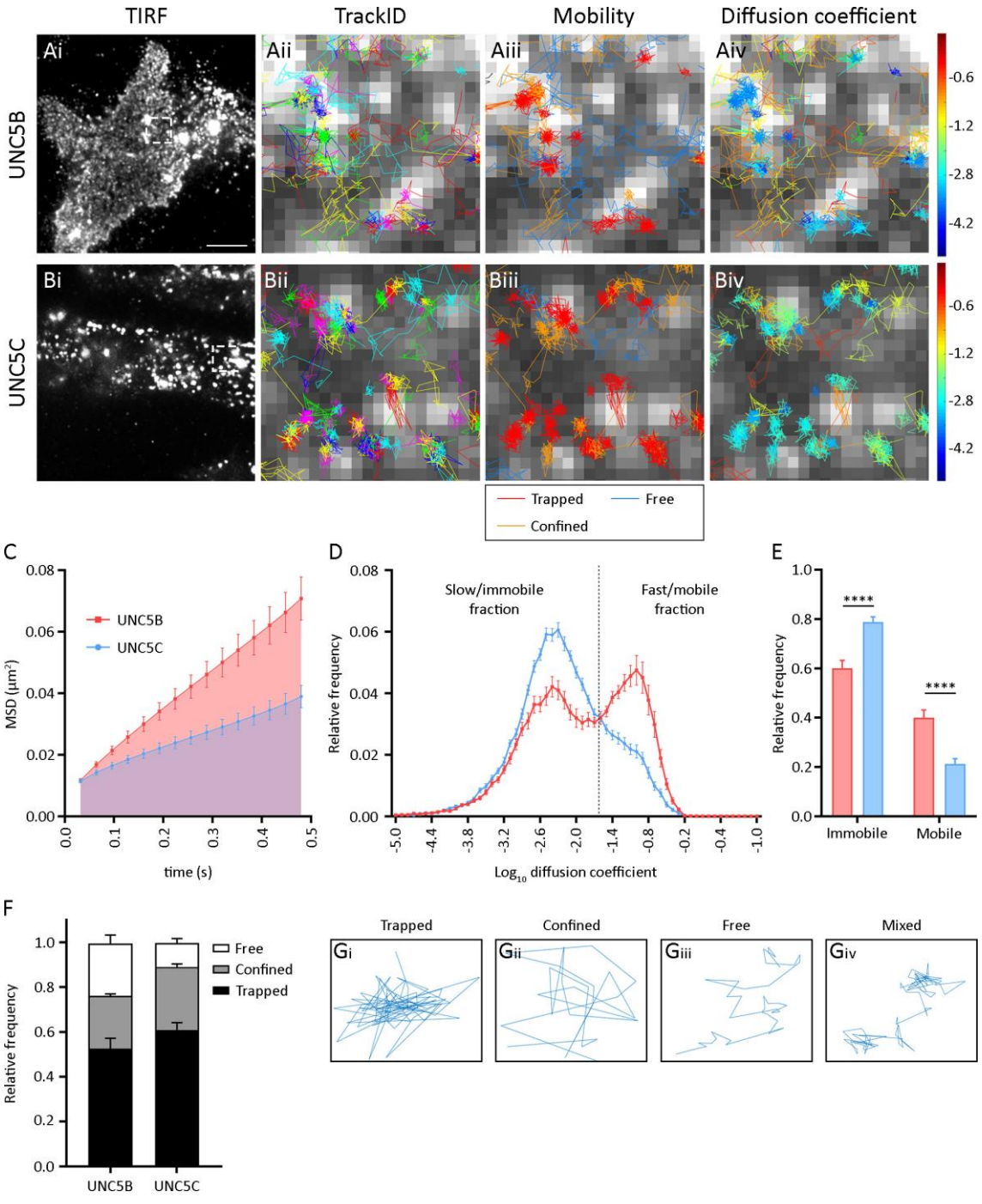
TIRF
TrackID
Mobility
Diffusion coefficient
UNC5B
UNC5C
Ai
Aii
Aiii
Aiv
Bi
Bii
Biii
Biv
-0.6
-1.2
-2.8
-4.2
Trapped
Free
Confined
C
MSD (μm²)
time (s)
UNC5B
UNC5C
D
Relative frequency
Slow/immobile fraction
Fast/mobile fraction
Log10 diffusion coefficient
E
Relative frequency
****
****
Immobile
Mobile
F
Relative frequency
Free
Confined
Trapped
UNC5B
UNC5C
Trapped
Confined
Free
Mixed
Gi
Gii
Giii
Giv

Figure 22 | sptPALM experiments reveal new insights in UNC5B and UNC5C mobility and diffusion constants. Low-resolution TIRF images of the bottom membrane of HEK293T cells transfected with both UNC5B-mEos2 (**Ai**) and UNC5C-mEos2 (**Bi**). Magnifications are illustrated with a dashed line box. Cells were imaged before the single-particle experiments that are shown. sptPALM trajectories of single receptors are shown in arbitrary color coded for UNC5B (**Aii**) and UNC5C (**Bii**) receptors. Mobilities of single trajectories calculated in MatLab are shown for each receptor (n=12-15 cells from 4 independent experiments). Considering diffusion coefficients and the occupied radius of a single molecule (**Aiii**, **Biii**), trajectories are classified into trapped (red), confined (orange) and free (blue) (bottom panel). Single trajectories colored regarding its Log_{10} diffusion constants, ranging from blue to red, being blue low diffusion constants and red high diffusion constants (**Aiv**, **Biv**). Averaged (±SEM) mean-squared displacement (MSD) vs. time plots for UNC5B (blue) and UNC5C (red) receptors recorded at 36.0 ± 1.5°C (**C**). Relative distributions of Log_{10} diffusion coefficients for both UNC5B (blue) and UNC5C (red) (**D**). Note that distributions of UNC5C plotting results in one peak in the immobile fraction (Log_{10} [D] < -1.6) while UNC5B distributions outline two peaks, one in the immobile and the other in the mobile fraction. Comparison of immobile and mobile populations calculated from the relative frequencies for both UNC5B (blue) and UNC5C (red) receptors (**E**). Plotting of relative frequencies of the sptPALM trajectories considering classification mentioned above, trapped, confined and free (**F**). UNC5B has more proportion of free molecules and less of trapped ones compared to that observed in UNC5C trajectories (n>4000 trajectories). Arbitrary taken trajectories to exemplify classification regarding mobility, trapped (**Gi**), confined (**Gii**), free (**Giii**) and mixed (**Giv**) trajectories. All data represents means ± SEM ($^{****}p \leq 0.0001$). Scale bar: 30μm.

1. 7. CHOLESTEROL REMOVAL BLOCKS NETRIN-1-DEPENDENT AXON COLLAPSE AND REPULSION IN EGL NEURONS

The role of the UNC5/Netrin-1 pair has been mainly studied in the distribution of external granular layer (EGL) neurons during the early post-natal development of the cerebellum by controlling the Netrin-1 chemorepulsion of growing parallel fibers[83, 28, 62]. These types of neurons co-express DCC, neogenin, DSCAM, UNC5B and UNC5C that sense Netrin-1 expressed in the EGL and interneurons of the molecular layer of the cerebellum[83]. We isolated mouse EGL neurons from postnatal mice at day 4 (P4), grown them during 3 days *in vitro* (3DIV) and performed immunostaining against UNC5B and UNC5C receptors, detecting their presence within growth cones (Fig. 12A and 12B). To investigate whether the differential distribution of UNC5B and UNC5C in transfected HEK293T cells and hippocampal neurons was also observed in EGL neurons, we used the raft marker CTx and found that both receptors partially colocalize

with CTx (Fig. 12C and 12D). CTxB colocalization disappeared after incubating the neurons with MβCD (1mM, 10 minutes) (Fig. 12E and 12F).

After demonstrating the distribution of UNC5 receptors into specific raft microdomains, we wanted to evaluate the functional relevance of that membrane organization into the neuronal repulsion to Netrin-1. EGL neurons at 3DIV were treated with MβCD (1mM, 10 minutes) or CO (2U, 2 hours) to dissociate the rafts microdomains before inducing growth cone repulsion and collapse by incubating with Netrin-1 (300ng/mL) during 45 minutes. Phalloidin was used to label the growth cone actin cytoskeleton and provide *bona fide* information of the growth cone organization. Collapsed growth cones, recognized by the typical shriveled, pencil-like shape were counted and expressed in relative numbers against EGL treated with no Netrin-1 supplemented media. Our results show that, whereas Netrin-1 increases growth cone collapse in EGL neurons (Fig. 13A, D), this process is inhibited after preincubation with lipid raft disrupting agents (Fig. 13B, C, D), suggesting that cholesterol levels are important for Netrin-1 mediated growth cone collapse.

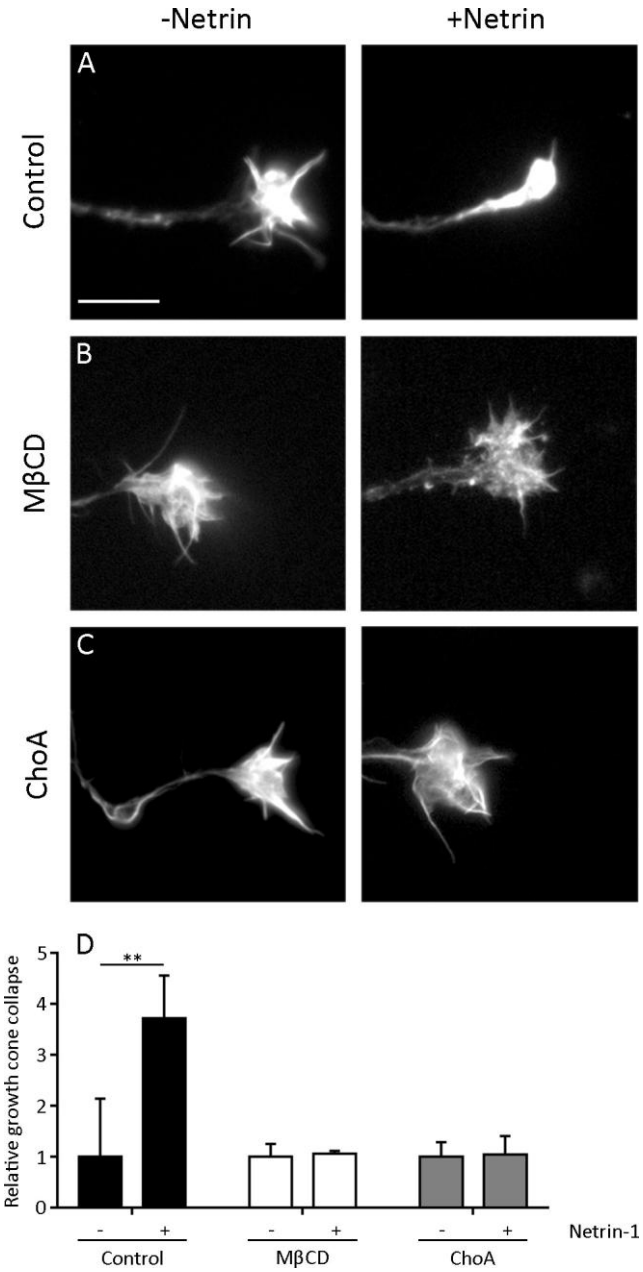

Figure 23 | Depleting membrane cholesterol abolishes Netrin-1-induced collapse in EGL neurons. EGL neurons were dissected from a P4 mice cerebellum. After 3DIV neurons were treated with either control media or Netrin-1 supplemented media (300ng/mL) (**A**-**C**). Previous Netrin-1 treatment, cells were treated with control media (**A**), MβCD (**B**) or ChoA (**C**). Percentage of collapsed growth cones was calculated and plotted in a graph (**D**). Data represents means ± SD ($^{**}p \leq 0.05$). Scale bar: 10µm.

We next analyzed the extension of axonal guidance processes from cerebellar EGL explants grown embedded in a type I collagen 3D hydrogel, and confronted with aggregates of either control HEK293T cells or HEK293T cells expressing Netrin-1[219]. The formed gradient of secreted Netrin-1 along the hydrogel causes a marked axonal repulsion on the EGL processes[83]. Some EGL explants were treated with MβCD (1mM, 30 minutes) after being embedded in the collagen matrix. After 2DIV, explants were fixed and labeled with tubulin-βIII to better identify axonal projections (Fig. 14A-7F). In the absence of MβCD, the explants confronted with control

cells showed a radial outgrow (Fig. 14A, 7D), and the explants confronted with Netrin-1 expressing cells showed a markedly repulsion (Fig. 14B, C, F). Whereas treatment of explants with MβCD did not affected the normal radial extension of axons in control conditions (Fig. 14D), MβCD reduced the chemorepulsive response to Netrin-1 (Fig. 14E). The results were analyzed by measuring the % of repelled explants (Fig. 14G) and the P/D ratio (Fig. 14H). To corroborate the specificity and reversibility of MβCD-mediated cholesterol depletion, endogenous cholesterol was restored by incubating with exogenous cholesterol immediately after MβCD treatment. The Netrin-1-dependent axon chemorepulsion was restored by adding cholesterol in the media (Fig. 14F). The loss of Netrin-1-induced growth cone collapse and repulsion of EGL axons, after incubation with drugs that decrease cholesterol membrane levels, indicates the importance of this lipid in the process of axon guidance in EGL neurons driven by Netrin-1.

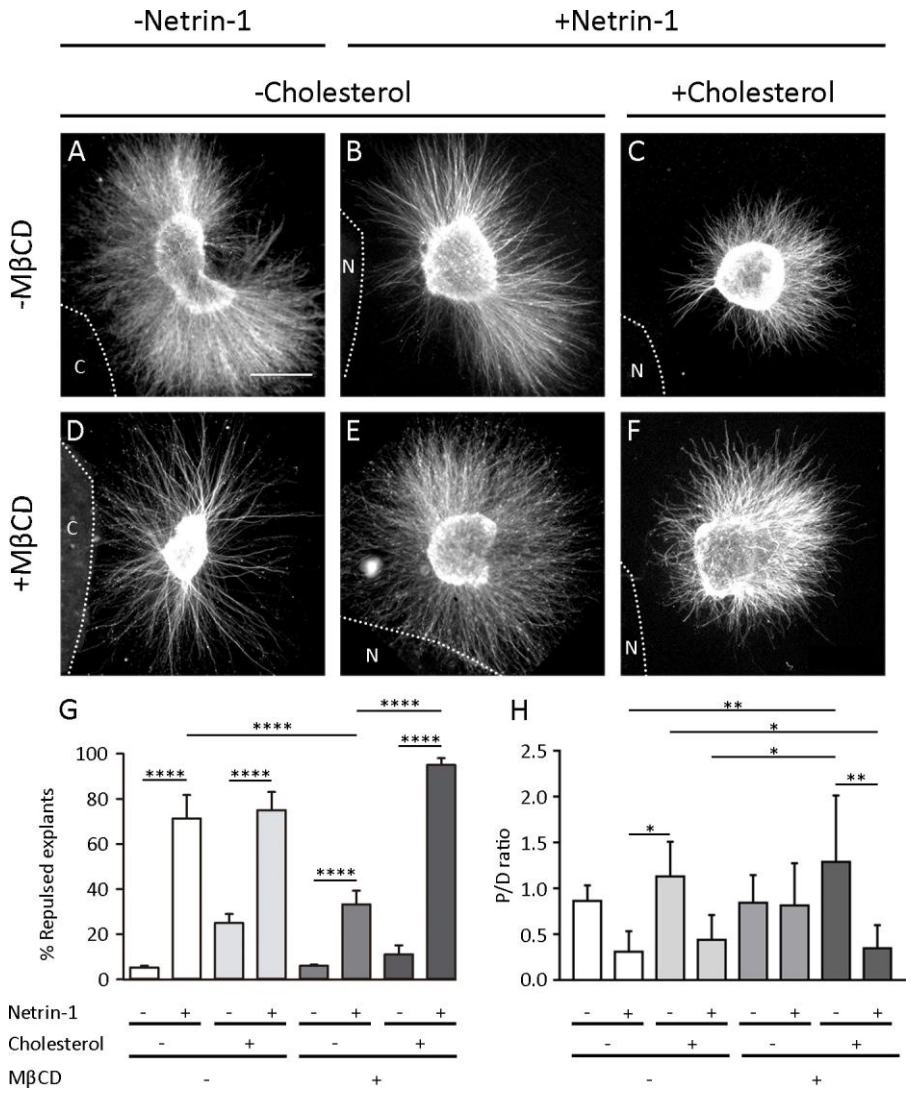

Figure 24 | Cholesterol depletion blocks Netrin-1 induced repulsion in EGL explants. Representative images of EGL explants dissected from P4 mice (**A**-**F**). Axonal outgrowth shows radial distribution when confronted with HEK293T control cell aggregates (**A**, **D**), outlined with a dashed line. Explants that were not treated with lipid raft disrupting drug MβCD showed a marked repulsion axonal grow (**B**, **C**). Explants treated with MβCD showed a radial distribution (**E**) that is reverted into repulsion after loading cholesterol (**F**). Graphs show % of repelled explants (**G**) and calculated P/D ratio (**H**). Data represents means ± SD ($^{ns}p > 0.05$, $^{*}p \leq 0.05$, $^{**}p \leq 0.01$, $^{****}p \leq 0.0001$). Scale bar: 100µm.

EGL neurons express both DCC and UNC5 Netrin-1-receptors, and we have demonstrated that both proteins are located into raft microdomains. To evaluate the importance of DCC in the EGL chemorepulsion to Netrin-1, we specifically blocked DCC by incubating EGL explants in the presence of specific anti-DCC monoclonal antibody[220]. The presence of anti-DCC antibodies did not affected the observed chemorepulsion, suggesting that DCC receptors are not functionally relevant during the Netrin-1-dependent repulsion of EGL axons (Fig. 15A-E).

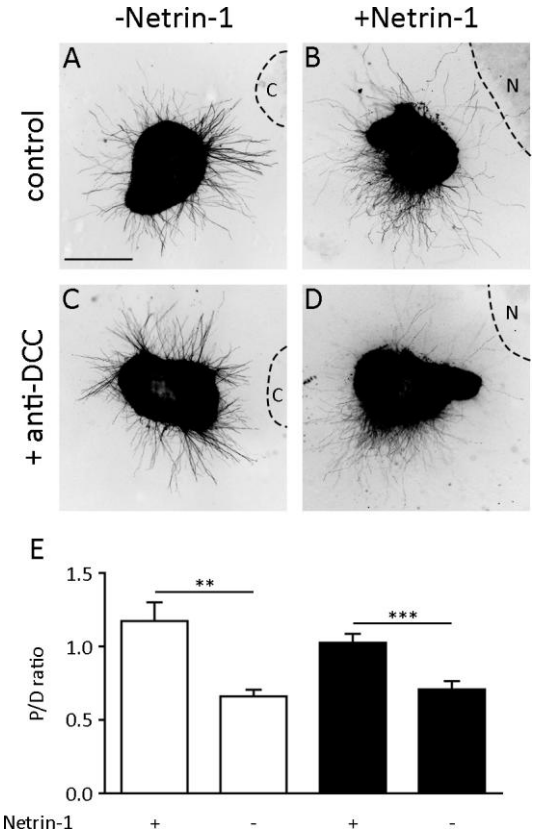

Figure 25 | UNC5 mediated repulsion in EGL explants is independent to DCC association. Representative images of EGL explants, dissected from P4 mice and immunodetected with anti-tubulin beta-III (**A**-**D**). Explants were incubated in absence (**A**, **B**) or in presence (**C**, **D**) of anti-DCC antibody, shown to block DCC ability to bind Netrin-1, and confronted to either control HEK293T cell aggregates (**A**, **C**), or Netrin-1 expressing HEK293T cell aggregates (**B**, **D**). Cell aggregates are outlined with a dashed line showing where cell aggregates were placed, C for control aggregates and N for Netrin-1 expressing aggregates. Radial axonal outgrowth can be detected when opposing explants to control cells (**A**, **C**), while repelled outgrowth pattern is evidenced in Netrin-1 conditions, both, by blocking (**D**) or not (**B**) DCC receptor. P/D ratios were calculated and plotted in a bar graph (**E**). Data represents means ± SD ($^{ns}p > 0.05$, $^{**}p \leq 0.01$, $^{***}p \leq 0.001$). Scale bar: 100µm.

1. 8. REPULSION MEDIATED BY NETRIN-1 IS ABOLISHED AFTER CYP46A1 DEPLETION

To further characterize the importance of cholesterol dependent raft microdomains in the repulsion against Netrin-1, we genetically modulated the levels of cholesterol in neurons by altering the expression of the enzyme 24S-cholesterol hydroxylase (Cyp46A1). Cyp46A1 is a cholesterol-catabolic enzyme that converts cholesterol to (24S)-24-hydroxycholesterol[97]. Cyp46A1 is abundantly expressed in the brain where it controls the cholesterol efflux because it transforms the impermeant cholesterol to (24S)-24-hydroxycholesterol that can efficiently

pass the blood–brain barrier to be secreted into the circulation[98]. Downregulation the expression of Cyp46A1 in hippocampal neurons increases the neuronal concentration of cholesterol[221, 222]. By using a short hairpin RNA directed against the mouse Cyp46A1 mRNA we evaluated the effect of increasing the levels of cholesterol on the Netrin-1 chemorepulsion. The modulation of Cyp46A1 in EGL explants did not affected the degree of axonal repulsion against a source of Netrin-1 (Fig. 16A-D, I). Contrarily, overexpressing Cyp46A1 decreases the levels of cholesterol in neurons[221]. We transfected EGL explants with plasmids expressing Cyp46A1 or an empty vector. While non-transfected neurons exhibited a normal repulsive response to Netrin-1, the specific analysis of neurons overexpressing Cyp46 revealed that the repulsiveness against Netrin-1 is now decreased (Fig. 16E-H, J). Overall, the results presented suggest that decreasing cholesterol levels has major consequences for axonal responsiveness against Netrin-1.

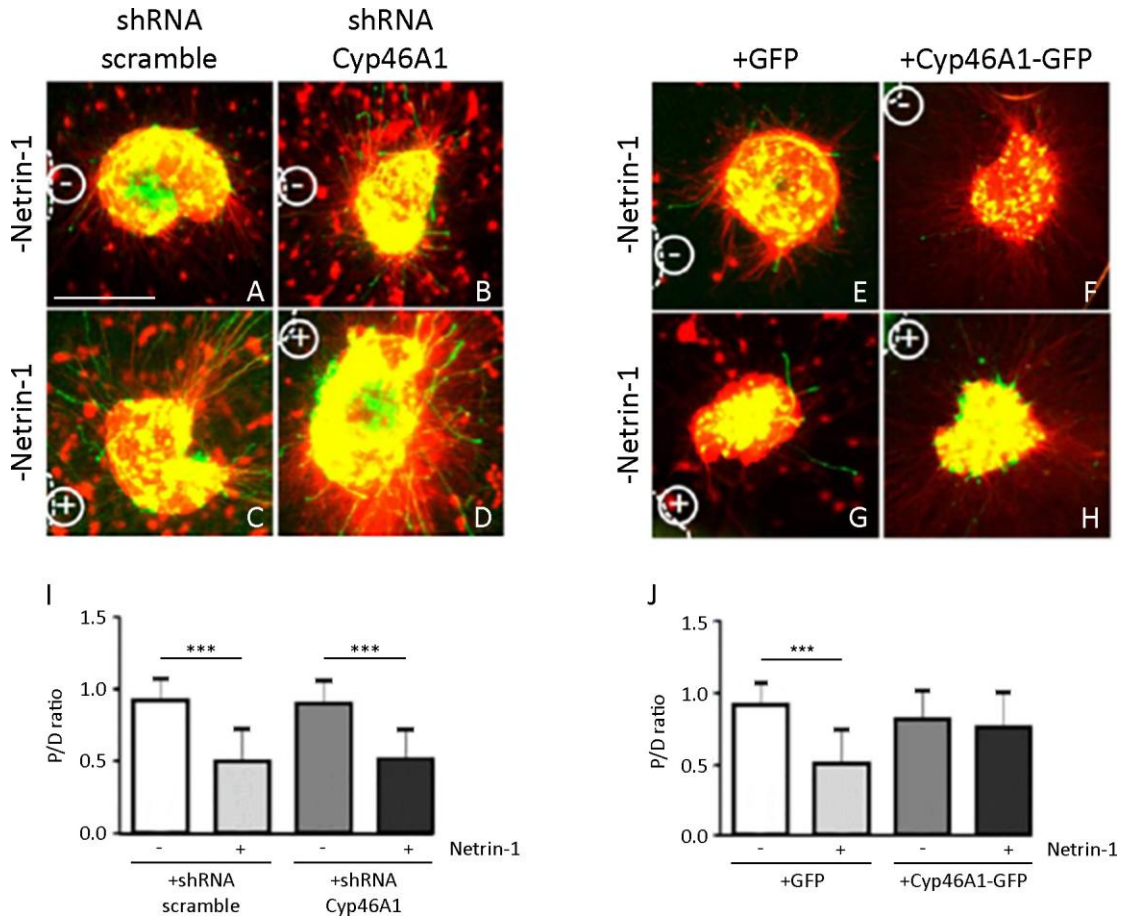

Figure 26 | Genetically modified levels of cholesterol shifts repulsion into radial axonal outgrowth in EGL explants. Images from EGL explants dissected from P4 mice (**A**-**H**). Explants were electroporated with shRNA scrambled (**A**, **C**); shRNA against Cyp46A1 (**B**, **D**); control plasmid GFP (**E**, **G**) or Cyp46A1 overexpression plasmid (**F**, **H**). EGL explants were confronted against HEK293T control cell aggregates (**A**, **B**, **E**, **F**) or HEK293T Netrin-1 expressing cell aggregates (**C**, **D**, **G**, **H**), aggregates are remarked with a dashed line. Axonal repulsion can be detected after transfecting EGL explants with either shRNA scrambled or shRNACyp46A1 and confronted with Netrin-1 cell aggregates (**C**, **D**), but not with control cell aggregates (**A**, **B**). Calculated P/D ratio shows differences between the two conditions (**I**). Cyp46A1 overexpression causes a loss of Netrin-1 induced repulsion (**H**). Neither control GFP plasmid (**E**, **G**) or Cyp46A1 transfected explants (**F**) causes a change in Netrin-1 responsiveness. Calculated P/D ratios are shown in the graph (**J**). Data represents means ± SD ($^{***}p \leq 0.001$). Scale bar: 100μm.

2. ALTERNATIVE SPLICING OF UNC5A. SUBCELLULAR LOCALIZATION AND FUNCTIONALITY OF THE SHORT SPLICE VARIANT

2. 1. EXPRESSION PATTERN OF UNC5A AND UNC5AΔTSPI_1 IN MOUSE CNS

It is known that UNC5A is alternatively spliced in rat. This alternative splicing consist in skipping exon 6 which corresponds to the conserved first repetition of the two extracellular TSPI domains[223], which from now on will be termed TSPI_1 to distinguish it from the second TSPI repetition (TSPI_2). Nonetheless, to date, nothing is known about the implications of lacking TSPI_1.

We first wanted to know whether UNC5A and the alternative spliced form of UNC5A (UNC5AΔTSPI_1) have different expression patterns, regarding tissues within the CNS and developmental and adulthood stages. For this reason, we isolated the brain and the spinal cord (SC) of developing mice (E12 and E18) and cortex (Ctx), cerebellum (Cb) and spinal cord (SC) from postnatal (P7) and adult mice (3 months old). By reverse transcription polymerase chain reaction (RT-PCR) we extracted the RNA and retrotranscripted into cDNA (see Materials and Methods). Primers were designed to amplify a region of UNC5A that comprised the TSPI_1, targeting nucleotides 482-1371, expecting to amplify a 889bp product in the UNC5A form and

a 727bp product in the case of UNC5AΔTSPI_1 considering that the TSPI_1 is 162bp length, in order to differentiate between UNC5A and UNC5AΔTSPI_1. We also designed primers targeting the same region of UNC5B to ensure that the alternative splicing is a specific feature of UNC5A. For both, UNC5A and UNC5B, we detected expression in all the tissues and stages analyzed. Expression of UNC5A (upper band) could be detected in the spinal cord of both E12 and E18 mice, that co-expressed with UNC5AΔTSPI_1 (lower band). However, in the brain of E12 and E18 mice we only detected expression of UNC5AΔTSPI_1. In the cortex of P7 mice we only detected the UNC5AΔTSPI_1 form, while in the cerebellum both forms are co-expressed. Accordingly to the results obtained in developmental stages, in the spinal cord both forms are co-expressed but with a significantly increment of the UNC5A form. Same results were obtained in adult mice with a slightly increment of UNC5AΔTSPI_1 in the cerebellum, in detriment of the UNC5A full length isoform. On the other hand, using a primer pair targeting the TSPI_1 of UNC5B, expecting to amplify nucleotides 467-1348, we detected a single band, which considering its size (881bp), we assumed that exon 6 is not skipped.

At this point, we sequenced the upper and lower band detected when amplifying UNC5A gene to ensure that the upper band corresponded to the UNC5A with the TSPI_1 and the lower band was due to the alternative splicing in UNC5A lacking the TSPI_1. By using the same pair of primers to amplify the region in the RT-PCR, sequencing resulted as expected, the longest amplified product corresponds to UNC5A while the shorter amplified region is UNC5AΔTSPI_1.

UNC5A undergoes alternative splicing in mice, as observed in rats. The result product of the alternative splicing of the canonical form of UNC5A is a shorter form that lacks the first extracellular repetition of the TSPI. This alternative splicing follows different patterns regarding different areas in the CNS and different stages like development, postnatal and adulthood. Another UNC5 family member, UNC5B, does not suffer this kind of alternative splicing.

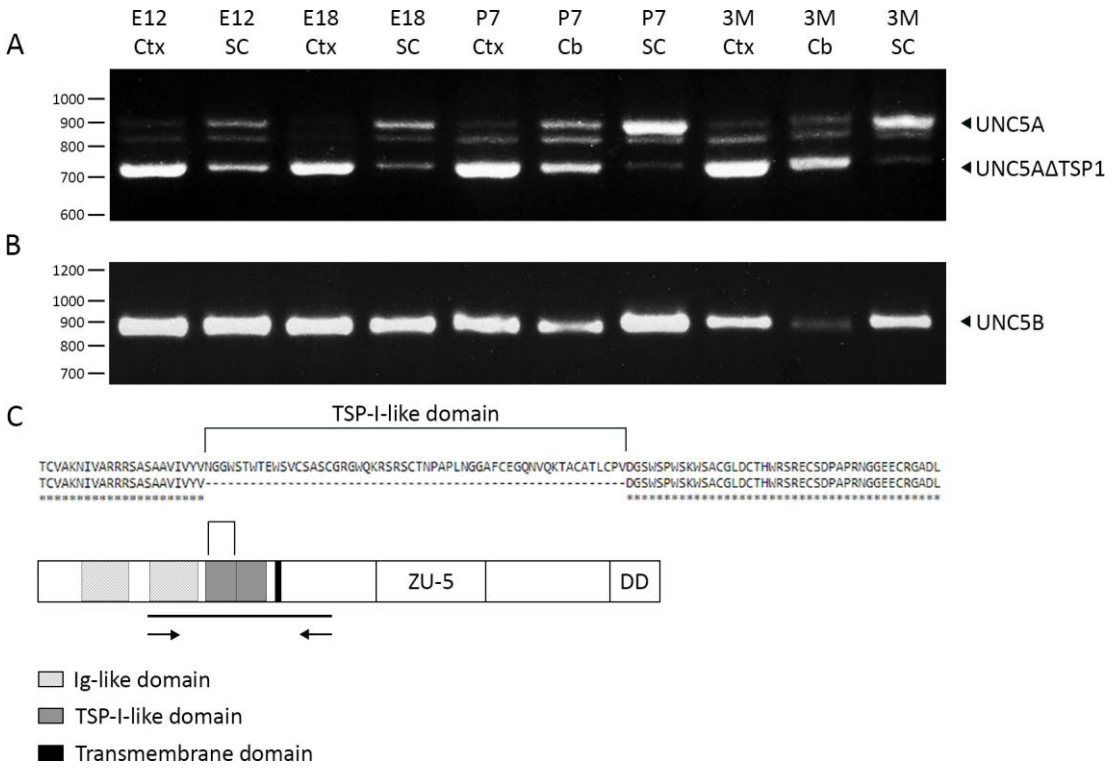

Figure 27 | UNC5A mRNA suffers alternative splicing and the expression shift is time- and tissue-specific. RT-PCR performed at different time points during development and adulthood and in different tissues in the CNS (**A**, **B**). Products resulted to amplify UNC5A cDNA with primers comprising the TSPI_1 repeat and resolved with an agarose gel. Upper band represents full lenght form of UNC5A, while detected lower band represents the spliced form of UNC5A, UNC5AΔTSPI_1 (**A**). Products resulted to amplify UNC5B cDNA with primers comprising the TSPI_1 repeat and resolved with an agarose gel. Note that unlike UNC5A, when using specific primers for UNC5B a single band was detected (**B**). Nucleotidic sequences resulted from sequencing the lower and upper bands detected in UNC5A RT-PCR. The fragment that lacks in the lower band corresponds to the TSPI_1 repeat. Diagram representing amplified section of UNC5A and UNC5B gene. Primers are represented with arrows and the straight line represents the expected amplified fragment. Amplification comprises the TSPI_1 (**C**). Cortex (Ctx), Cerebellum (Cb), Spinal cord (SC), Embryonic day 12 (E12), Embryonic day 18 (E18), Postnatal day 7 (P7), 3 months old (3M).

2. 2. SUBCELLULAR DISTRIBUTION OF UNC5A AND UNC5AΔTSPI_1 IN HELA CELLS.

Nothing is known about the implications of lacking the TSPI_1 of UNC5A regarding its function and subcellular distribution. We next wanted to assess whether there was a significal change of the subcellular distribution between those two isoforms. By directed mutagenesis we created restriction sites (EcoRI) flanking the TSPI_1 of the UNC5A full length isoform YFP-

tagged construct and digested with the mentioned enzyme to finally create the UNC5AΔTSPI_1 form. After ensuring the correct sequence of the newly engineered form, we transfected both, UNC5A and UNC5AΔTSPI_1, into HeLa cells. Cells were labeled with the fluorescently tagged membrane marker wheat germ agglutinin (WGA) to assess the membrane targeting of the UNC5AΔTSPI_1. Strikingly, confocal images revealed that UNC5AΔTSPI_1 did not co-localize with the membrane marker WGA and exhibited a dramatic intracellular retention, contrarily to what was previously observed for UNC5A, here, the appropriate targeting to the cell membrane was corroborated.

Despite UNC5C does not suffer the same alternative splicing as UNC5A we wanted to assess the implications for another UNC5 family member of losing the TSPI_1. We created, by directed mutagenesis, restriction sites (AscI) in the UNC5C YFP-tagged construct, flanking both ends of the TSPI_1. Following the same protocol as with UNC5A, we transfected UNC5C and UNC5CΔTSPI_1 into HeLa cells. Distribution of UNC5CΔTSPI_1 changed from membrane localization to intracellular retention, which was the same phenotype as observed for UNC5AΔTSPI_1. On the other hand, we followed the same procedures to eliminate the TSPI_2 repetition, when UNC5AΔTSPI_2 was transfected into HeLa cells, we detected partial overlapping with the WGA label and intracellular signal detected differed from that exhibited by UNC5AΔTSPI_1.

A recent publication[224] showed that three Tryptophan residues (245, 248 and 251) in the TSPI_1 domain of UNC5A are mannosylated in the consensus sequence (WxxWxxWxxC). When two distinct *C*-mannosyltransferases are knocked-out, the mannosylation does not occur and causes an intracellular redistribution of UNC5A, suggesting that this post-translational modification is necessary for the cell membrane targeting. Because we wanted to analyze whether the phenotype observed in this investigation resembled our findings of the localization of UNC5AΔTSPI_1, we point mutated the nucleotidic sequence by directed mutagenesis to change these three Tryptophan residues by Phenylalanine residues. Upon

transfecting this form (UNC5A_W>F) into HeLa cells we observed the same intracellular retention as detected for UNC5AΔTSPI_1 and UNC5CΔTSPI_1.

For every representative image, we plotted signal intensities by drawing a line ROI crossing twice the cell membrane. Two peaks can be observed in the WGA labeling which corresponds to the cell membrane. Intensities of the constructs transfected in the HeLa cells that target to the cell membrane overlap with these two WGA peaks, while intensities of those exhibiting intracellular retention are detected between these two peaks. Moreover, a magnification is shown to better appreciate membrane targeting or intracellular distribution.

The intracellular retention that we observed in the UNC5 forms lacking the TSPI_1, followed a similar distribution as the ER. We next wanted to analyze co-localization of a ER tracker and the UNC5 constructs previously analyzed. Thus, we co-transfected each UNC5 form mentioned above, along with red fluorescent protein (RFP)-tagged ER tracker and observed transfected HeLa cells under a confocal microscope. As we expected, UNC5AΔTSPI_1, UNC5CΔTSPI_1 and UNC5_W>F constructs, completely co-localized with the ER marker, while full length forms only partially co-localized with the ER labeling, probably due to membrane trafficking. Again, we plotted signal intensities by drawing a line ROI in representative images, to better illustrate co-localization of both intensity signals.

The integrity of the TSPI_1 repeat, and not the TSPI_2, is necessary for the proper targeting to the cell membrane of at least two UNC5 family members (UNC5A and UNC5C). Specifically, three Tryptophan residues within the TSPI_1 are necessary for UNC5A to reach the cell membrane. UNC5 forms that are retained cannot progress beyond the ER, suggesting that these proteins may be lacking some sort of post-translational modification.

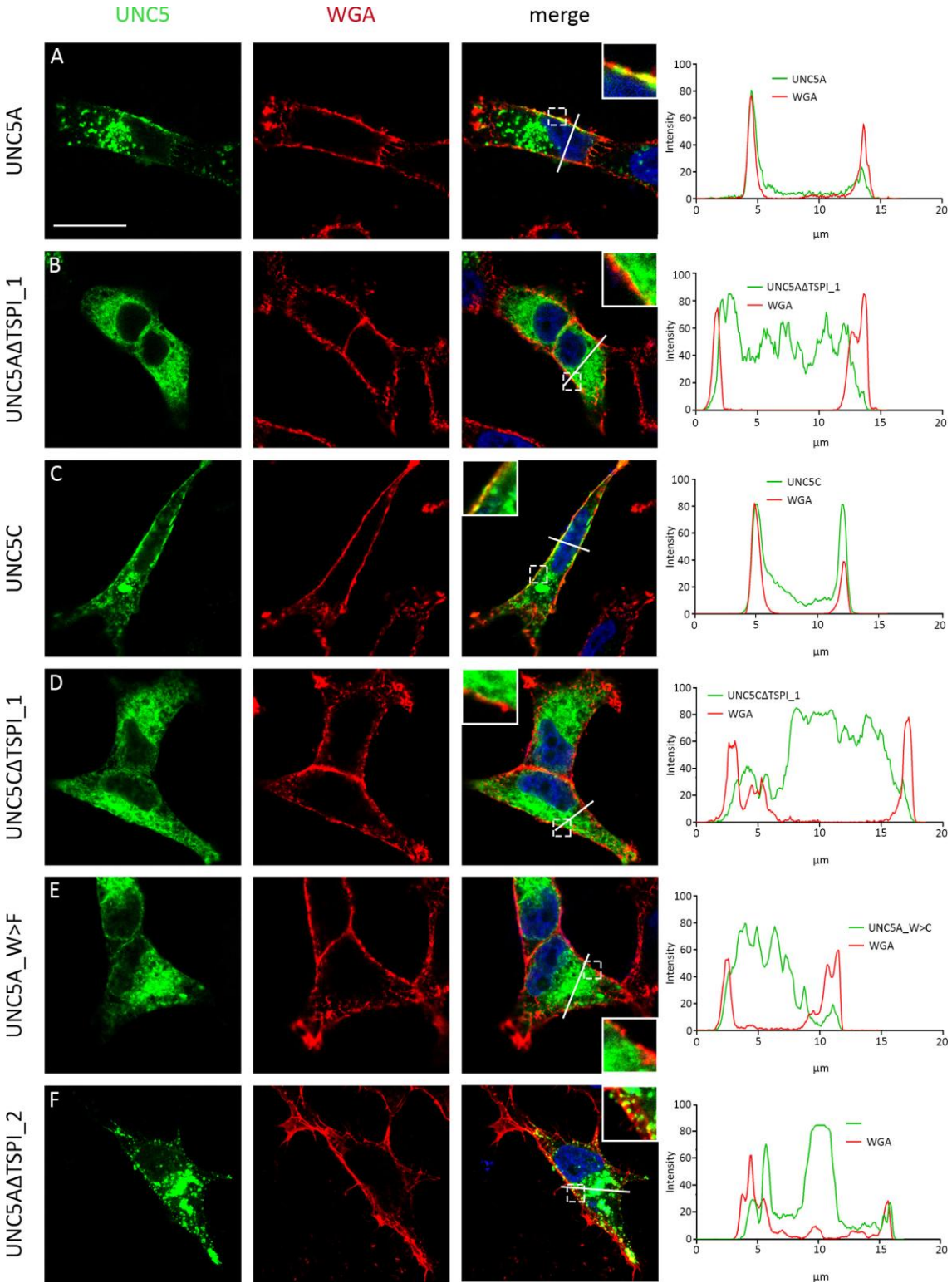

Figure 28 | Cell membrane targeting of UNC5 constructs involving integrity of TSPI_1. Confocal images of HEK293T cells expressing UNC5A (**A**), UNC5AΔTSPI_1 (**B**), UNC5C (**C**) and UNC5CΔTSPI_1 (**D**), UNC5A_W>F (**E**), UNC5AΔTSPI_2 (**F**) YFP-labeled constructs. Cells were labeled with WGA, a plasma membrane marker (**A**-**F** central panels). Images were merged with both channels and with nuclei labeling (blue). A detailed magnification is shown of a membrane region indicated with dashed line square. Optical sections correspond to the relative middle of each cell. Intensities for each channel were plotted in a xy graph, illustrating intensities where the drawn line was placed, UNC5 constructs (green line) and WGA (red line) (**A**-**F**). Scale bar: 20µm.

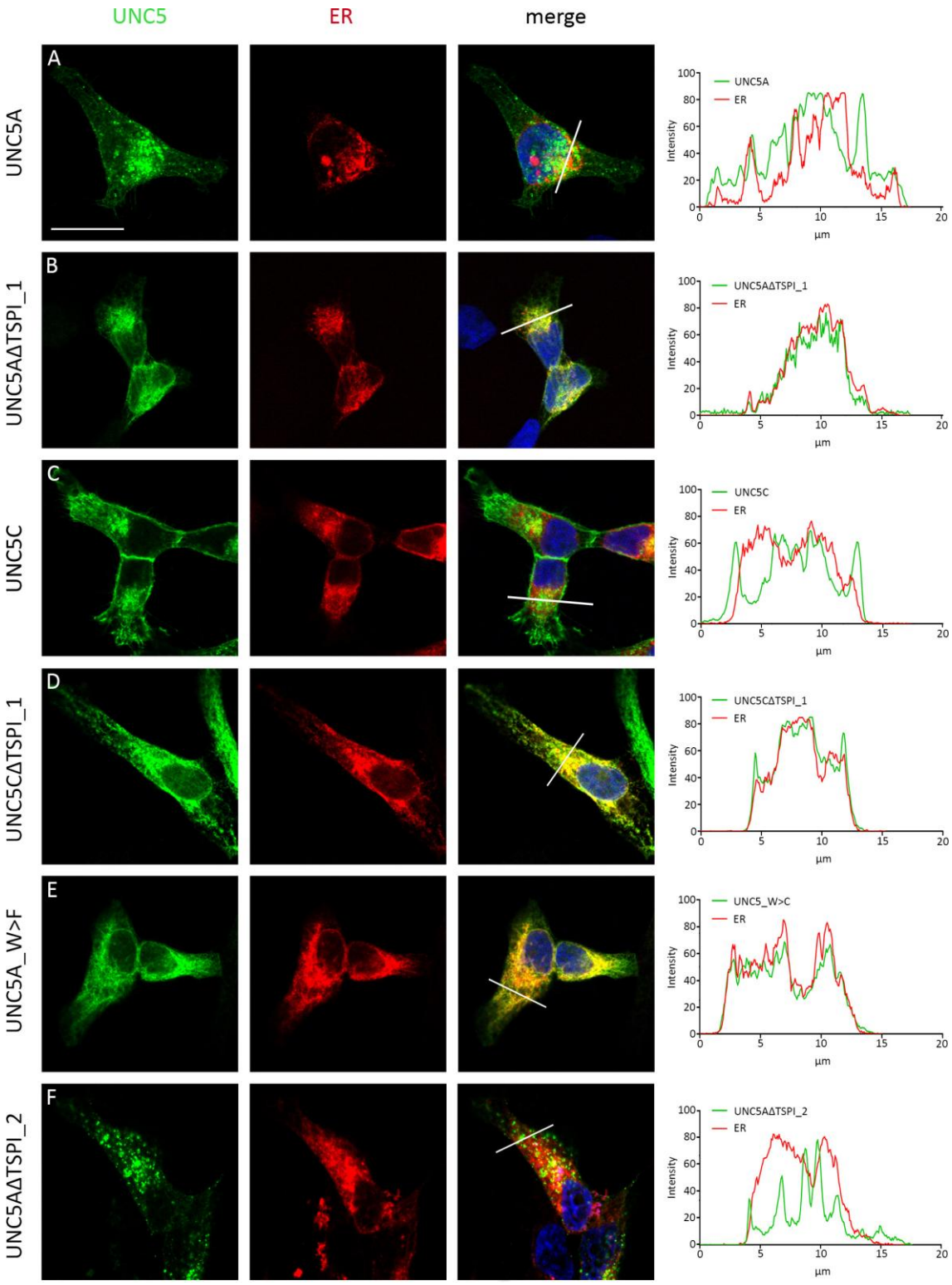

Figure 29 | ER localization of UNC5 constructs involving integrity of TSPI_1. Confocal images of HEK293T cells expressing UNC5A (**A**), UNC5AΔTSPI_1 (**B**), UNC5C (**C**) and UNC5CΔTSPI_1 (**D**), UNC5A_W>F (**E**), UNC5AΔTSPI_2 (**F**) YFP-labeled constructs. Cells were labeled with a ER tracker, a ER marker (**A**-**F** central panels). Images were merged with both channels and with nuclei labeling (blue). Optical sections correspond to the relative middle of each cell. Intensities for each channel were plotted in a xy graph, illustrating intensities where the drawn line was placed, UNC5 constructs (green line) and ER tracker (red line) (**A**-**F**). Scale bar: 20µm.

2. 3. DISTRIBUTION OF UNC5A AND UNC5AΔTSPI_1 IN HIPPOCAMPAL NEURONS

Because RT-PCR experiments to assess expression of both forms of UNC5A were done using different tissues from the CNS, we wanted to analyze distribution of UNC5A and UNC5CΔTSPI_1 in hippocampal neurons. We transfected cells with both YFP tagged constructs and labeled neurons with Tetramethylrhodamine (TRITC) (532nm)-tagged Phalloidin, that specifically binds to polymerized actin filaments, to better distinguish neuronal structures. Expression of UNC5A can be observed in the developing neurites of neurons and presumably the prospecting axon. On the other hand, UNC5CΔTSPI_1 localization is restricted in the soma of the hippocampal cells.

In hippocampal neurons, UNC5A is distributed in the neurites while UNC5CΔTSPI_1 is only observed in the soma of the neurons, which leads to the conclusion that UNC5CΔTSPI_1 does not target properly to neural structures where UNC5A typically localizes.

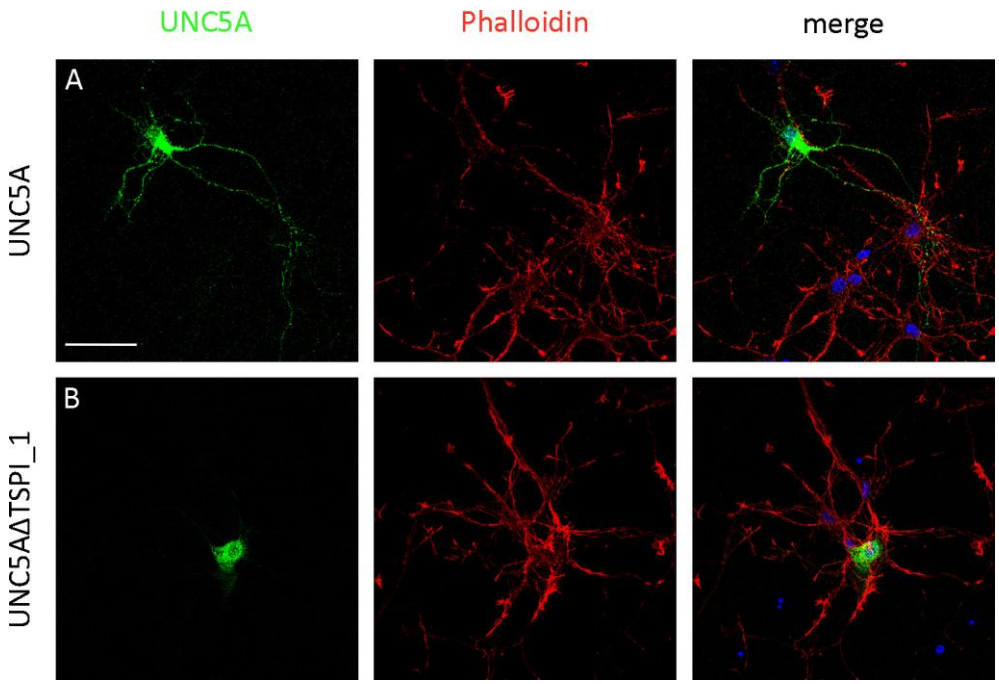

Figure 30 | Localization of UNC5A and UNC5AΔTSPI_1 in hippocampal neurons mimics what was observed in HeLa cells. Hippocampal neurons from E17 mice were transfected after 3DIV. YFP-labeled constructs, UNC5A (**A**) and UNC5AΔTSPI_1 (**B**) were transfected (green, left panels) (**A**, **B**). Neurons were labeled with Phalloidin (red, central panels) and images were merged along with nuclei detection (blue, right panels) (**A**, **B**). Scale bar: 30µm.

2. 4. QUANTIFICATION OF CELL SURFACE EXPRESSION OF UNC5A AND UNC5AΔTSPI_1

In order to measure cell surface expression of UNC5A and UNC5AΔTSPI_1 we used HEK293T cells, in which UNC5A forms were verified to mimic the distribution observed in HeLa cells. HEK293T cells are vastly used as an expression tool for recombinant protein expression, since they are capable of carry out most of the post-translational folding and processing required to generate functional and mature mammalian proteins, as well as producing a high amount of protein upon transfection[225].

In this experiment, transfected HEK293T cells with different constructs were biotinylated. Biotin binds specifically and covalently Glycine residues of proteins, which further, can be detected due to its ability to specifically bind streptavidin. Briefly (see Materials and Methods), living HEK293T cells were incubated at 4^{o}C with biotin to avoid internalization of cell surface proteins. Protein lysates were immunoprecipitated with a GFP antibody and detected by polyacrylamide gel electrophoresis, with both streptavidin-Horseradish peroxidase (HRP) and anti-GFP to calculate cell surface expression.

We transfected both, UNC5A and UNC5AΔTSPI_1, into HEK293T cells and several experimental controls, YFP-tagged UNC5B; as a positive control of a membrane surface receptor, GFP-tagged Alex3; a mitochondrial associated protein as a negative control, a cherry-tagged UNC5C; to ensure specificity of GFP antibody and a YFP-tagged UNC5B with no biotin; to test streptavidin specificity for biotin.

UNC5A and UNC5AΔTSPI_1 expression was detected with a GFP antibody. However, streptavidin signal in UNC5AΔTSPI_1 was practically absent, contrarily to UNC5A receptor. The intensity of the bands were analyzed and found to be significantly different. As expected, UNC5B was detected in the cell membrane, Alex3 was not found in the cell surface and UNC5C-cherry was not detected by GFP antibody nor UNC5B with streptavidin when lacking biotin incubation.

So far, this quantifiable technique allowed us to calculate and corroborate that TSPI_1 is an important structural domain to target UNC5A receptor to the cell membrane.

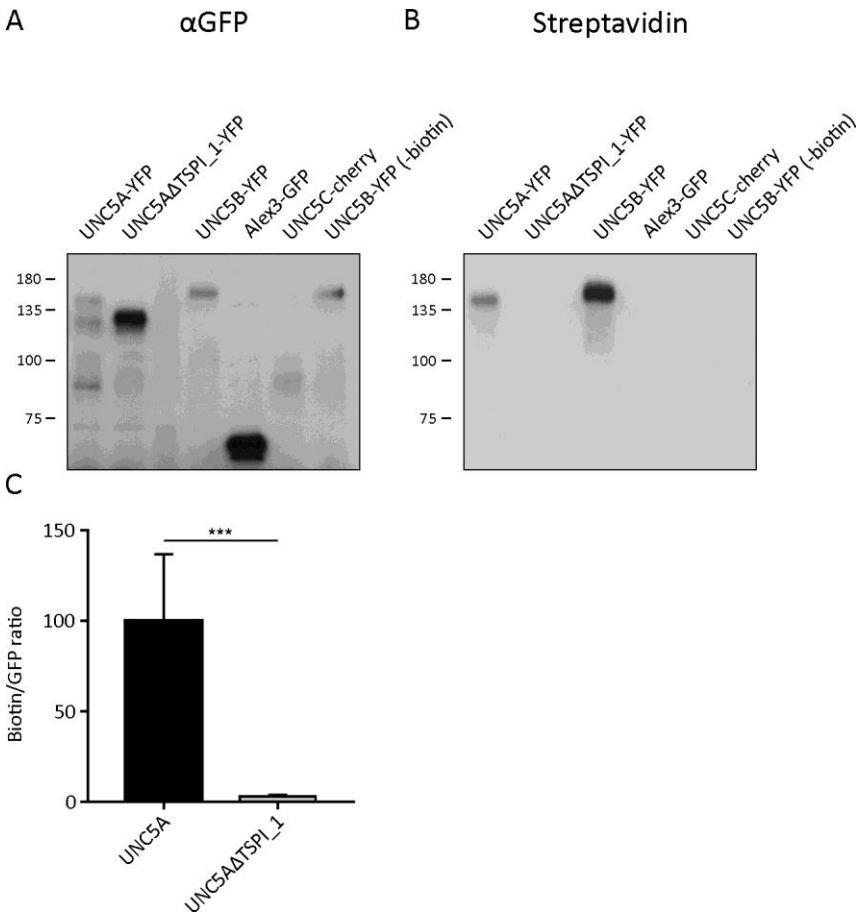

Figure 31 | Biotin labeling of surface proteins evidences different targeting of UNC5A forms to the cell membrane. HEK293T cells were transfected with UNC5A and UNC5AΔTSPI_1 YFP-labeled constructs. Control constructs were also transfected into HEK293T cells: UNC5B-YFP, Alex3-GFP, UNC5C-cherry and UNC5B-YFP with no biotin labeling. Cells were treated with biotin at 4°C to avoid internalization of biotin. After total protein extraction, a immunoprecipitation was performed against GFP and detected by immunoblotting against GFP (**A**) and biotinylated proteins detected by Streptavidin (**B**). Immunoblotting was quantified and the ratio between biotin and GFP signals was calculated. When ratios between UNC5A and UNC5AΔTSPI_1 were compared, significative differences were found (**C**). Data represents means ± SD ($^{***}p \leq 0.001$).

2. 5. DIFFERENCES IN TURNOVER RATES OF UNC5A ISOFORMS

In transfected HeLa and HEK293T cells, we observed that UNC5AΔTSPI_1 does not progress beyond the ER and forms aggregates in this organelle.

Since misfolded proteins tend to have a shorter Half Life than functional proteins, in the next experiment we wanted to analyze the turnover rate of both isoforms. We expected UNC5AΔTSPI_1 to exhibit a shorter Half Life than UNC5A full length form. Nevertheless, when transfected HEK293T cells were transfected with both UNC5A and UNC5AΔTSPI_1 and treated with cycloheximide (CHX), a *de novo* protein synthesis blocker, the turnover rate we observed for UNC5A was faster than for UNC5AΔTSPI_1.

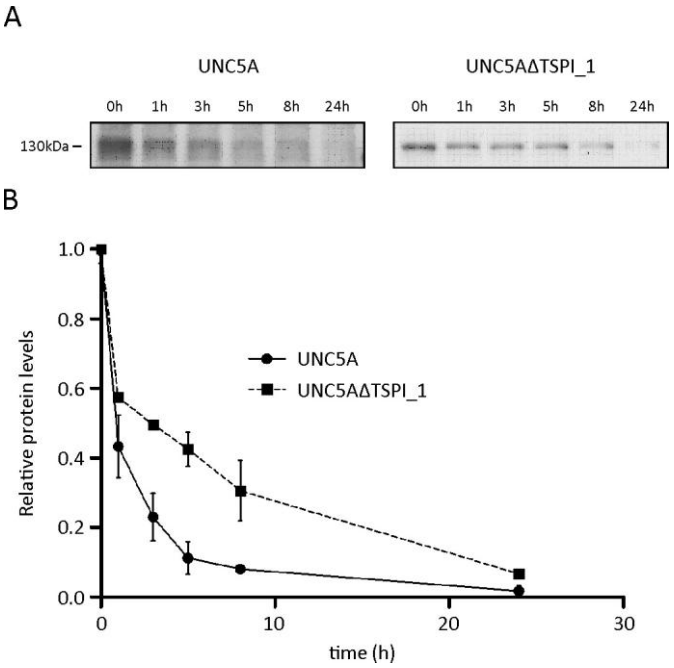

Figure 32 | CHX treatment revealed different turnover constants of UNC5A and UNC5AΔTSPI_1. Lysates from different transfected UNC5A constructs into HEK293T cells were obtained at different time points after CHX treatment (0, 1, 3, 5, 8 and 24 hours). Then, protein levels were detected by immunoblotting with GFP antibody (**A**). Immunoblots for UNC5A (left panel) and UNC5AΔTSPI_1 (right panel) are shown (**A**). Calculated intensities from immunoblots were plotted as survival curves (**B**).

2. 6. FUNCTIONALITY OF UNC5A AND UNC5AΔTSPI_1

UNC5 receptors are responsible for two known processes in nervous cells. They mediate axon repulsion upon Netrin-1 binding[61] and they act as dependence receptors, triggering cell death signaling cascades when Netrin-1 is not bound to them[226]. Thus, next series of experiments will be focused to test the ability of both isoforms performing these well known cellular processes.

Following results are preliminary, due to scarce number of samples analyzed. More experiments are needed to assert differential functions for UNC5AΔTSPI_1. Nevertheless, we

present here some results that may be helpful to understand functions in axon guidance and cell death induction of the short isoform of UNC5A.

2. 6. 1. AXON GUIDANCE

Hippocampal neurons from E16 mice embryos were isolated and after 3 days *in vitro* (DIV), neurons were transfected with UNC5A, UNC5AΔTSPI_1, UNC5B and UNC5C YFP-tagged constructs along with a YFP empty vector as a negative control. After 4 DIV hippocampampal neurons were stimulated or not with Netrin-1 for 45 minutes and fixed. Neurons were labeled with Phalloidin and collapsed growth cones from transfected neurons were counted, as an indicative of UNC5 mediated repulsion driven by Netrin-1.

We observed collapsed growth cones in UNC5A, UNC5B and UNC5C transfected neurons only after treatment with Netrin-1 supplemented media treatment. Although we only detected statistical differences in growth cone collapse in UNC5B transfected hippocampal neurons when treated with Netrin-1, there is a clear tendency of UNC5A and UNC5C mediated growth cone collapse. A tendency that clearly cannot be observed in the negative control, YFP transfected neurons and neither in UNC5AΔTSPI_1 transfected neurons.

Therefore, these results suggest that UNC5AΔTSPI_1 fail to mediate repulsion in the presence of Netrin-1, most probably due to not being capable to bind Netrin-1 in the cell surface a repulsion that can be observed in other UNC5 family full length members.

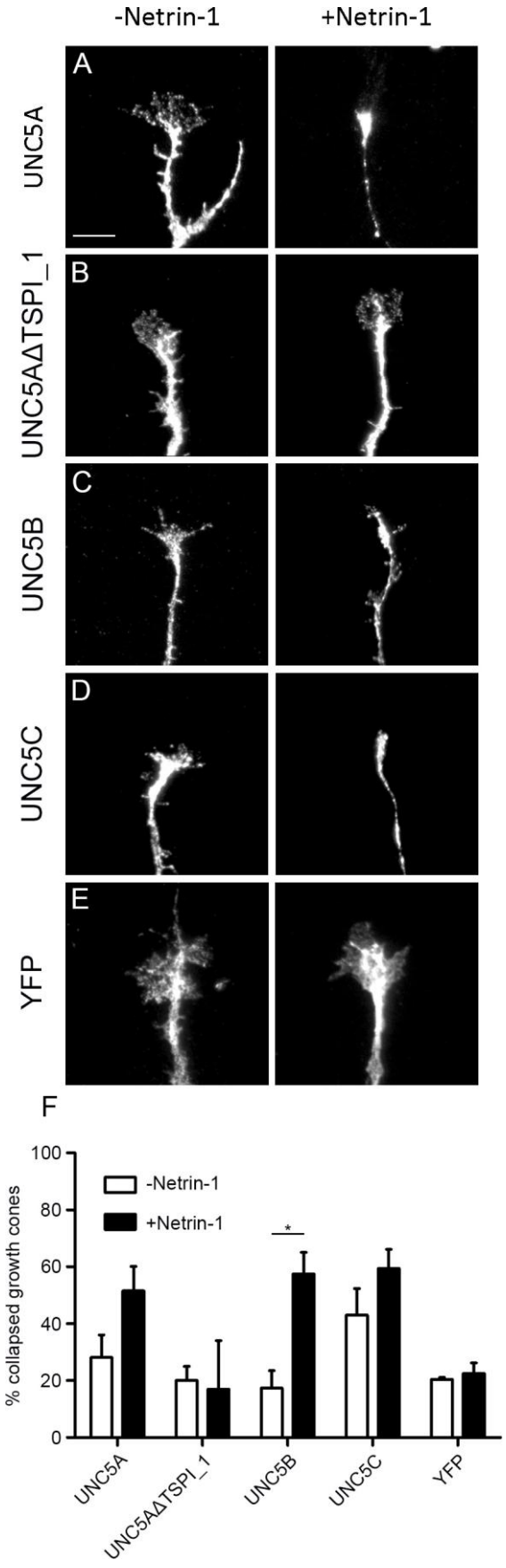

Figure 33 | UNC5AΔTSPI_1 fails to induce growth cone collapse after Netrin-1 treatment in hippocampal neurons. Hippocampal neurons from E16 mice embryos were labeled with Phalloidin (**A**-**E**) and transfected after 3DIV with UNC5A (**A**), UNC5AΔTSPI_1 (**B**), UNC5B (**C**), UNC5C (**D**) and empty vector YFP (**E**). Neurons were treated with control media (left panels) or Netrin-1 supplemented media (right panels). Fixed neurons were observed under fluorescence microscope and the ratio expressed in % between collapsed growth cones and total transfected neurons was calculated (**F**). Data represents means ± SD ($^{ns}p > 0.05$, $^{*}p \leq 0.05$). Scale bar: 10µm.

2. 6. 2. CELL DEATH

UNC5A is among all UNC5 family members, the receptor that has the ability to induce cell death in a greater extent, this is thought to be due to the interaction with NRAGE[199]. This cell death induction is independent of Netrin-1 availability and it is found in some regions in the spinal cord during development[227]. In this experiment we transfected UNC5A and UNC5AΔTSPI_1 YFP-tagged constructs into HeLa cells. As negative controls we also transfected UNC5C, reported to induce lower rates of cell death when Netrin-1 is absent[199], and YFP empty construct, which *per se* does not induce cell death.

HeLa cells were transfected, fixed and labeled with Hoesch, a nuclei marker. The idea of labeling nuclei with Hoesch was to identify pyknotic nuclei, which can be clearly identified due to its fragmented morphology. Transfected cells in three different and independent wells were counted and we established a ratio between observed pyknotic nuclei and total transfected cells. As described before[199], we found UNC5A to be the receptor that upon transfection in HeLa cells, causes cell death in a greater extent, being 16.5% the ratio of pyknotic nuclei, a significative higher value than that observed in cell death induction by UNC5C (6%) or the control empty vector YFP (9.1%). Most importantly cell death caused by UNC5AΔTSPI_1 (5.4%) was dramaticaly lower compared to the calculated percentage for UNC5A.

To sum up, these results indicate that UNC5A has the ability to induce cell death in absence of Netrin-1 in a higher degree than UNC5C. Moreover, the ability of UNC5AΔTSPI_1 to induce cell death is almost absent, suggesting that subcellular localization of these receptors is crucial for their ability to induce cell death.

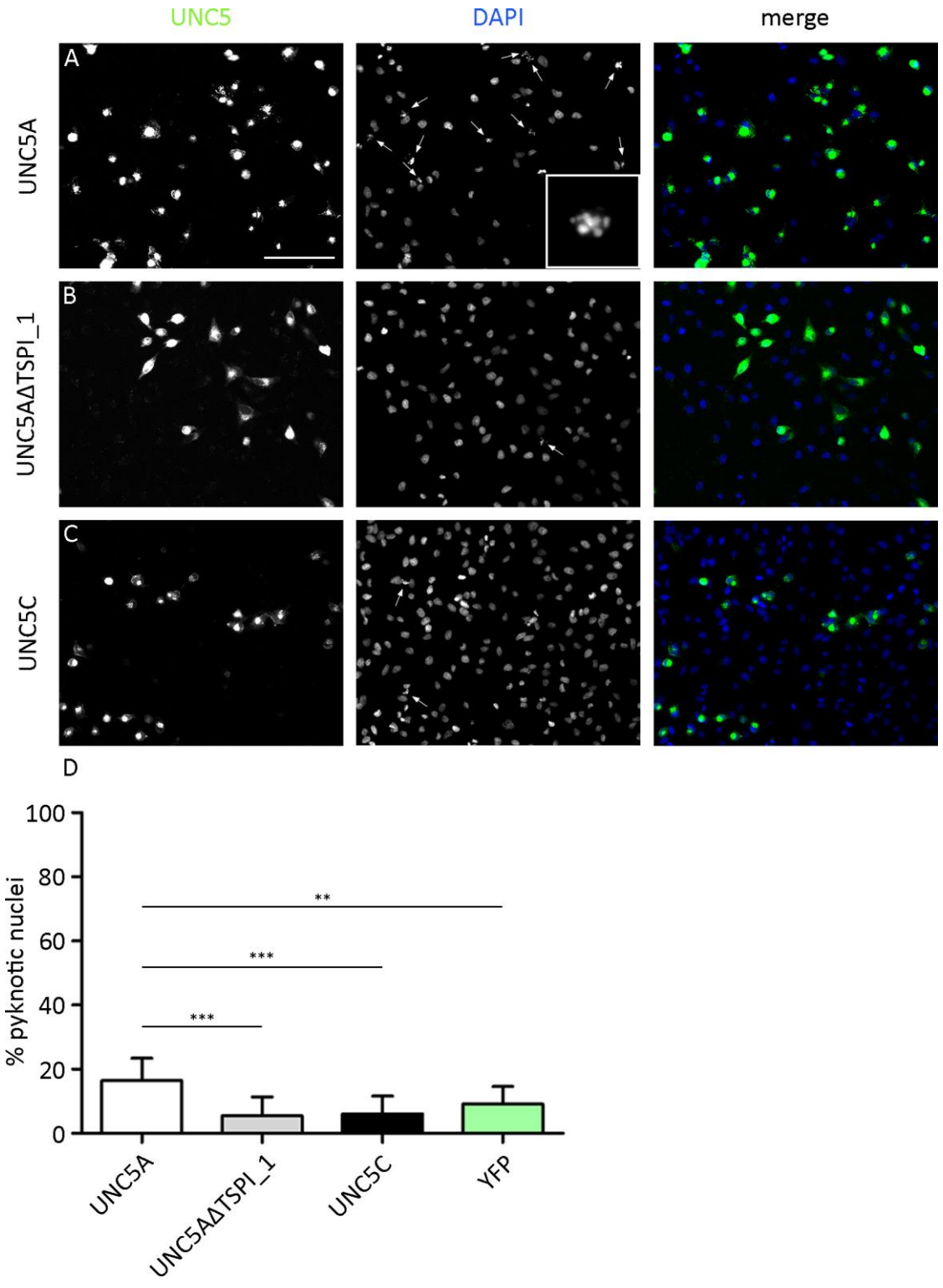

Figure 34 | Cell death induced by UNC5AUNC5AΔTSPI_1 does not occur in transfected HeLa cells. HeLa cells were transfected with UNC5A, UNC5AΔTSPI_1 and YFP empty vector (**C**). 48h after transfection, cells were fixed and nuclei were labeled. Three independent coverslips were used (n=3) and total transfected cells (green) were counted. Apoptotic cells were identifyied by pyknotic nuclei counting (magnification in A DAPI). A percentage of pyknotic nuclei over transfected cells was calculated and compared (**D**). Data represents means ± SD ($^{**}p \leq 0.01$, $^{***}p \leq 0.001$). Scale bar: 80µm.

DISCUSSION

1. IMPLICATIONS IN AXON GUIDANCE OF UNC5 RECEPTORS ASSOCIATION TO LIPID RAFTS

1. 1. DIFFERENTIAL SUBCELLULAR DISTRIBUTION OF UNC5 RECEPTORS

Transmembrane receptors implicated in axon guidance processes are mainly located in the growth cone. These receptors need to be embedded in the cell membrane in order to sense extracellular cues that are translated in intracellular signals which are finally translated into cytoskeletal modifications. UNC5 is a family of transmembrane receptors that are involved in axon guidance and specifically in repulsion processes during axon pathfinding. UNC5 are Netrin-1 receptors which coordinate with DCC transmembrane receptor to give adequate responses during axon elongation. During cerebellar development, UNC5B and UNC5C are key receptors in the extension of GCs parallel fibers in restraining axon elongation in the ML[83].

In our first experiment, we subcloned UNC5(A-D) receptors into a pEYFP vector in order to transfect HEK293T cells and assess its subcellular localization. Since UNC5 receptors are transmembrane proteins we expected them to be located within the cell membrane. For this reason, we also labeled transfected cells with the membrane marker WGA. UNC5A and UNC5C were found to be distributed into membrane clusters, a localization that was evidenced in xyz image reconstructions. UNC5B was distributed evenly in the cell membrane, with no evidence of protein aggregation in distinct puncta in the cell membrane. Contrarily, UNC5D was found to be retained in intracellular compartments compared to their counterpartners. Although UNC5 membars exhibitted differences in subcellular distributions, all of them colocalized with the membrane marker. Therefore, subcloning UNC5 receptors into a pEYFP vector does not affect the ability of UNC5 proteins to reach the membrane surface.

For the first time, differences in subcellular distribution have been described for UNC5 receptors, a feature that may influence in their role in axon guidance. The degree in which different UNC5 receptors seggregate differently in transfected HEK293T cells is striking.

Nonetheless, nothing is known to date about the distributions of these receptors in native tissues, and more importantly in growth cones where they perform their roles. HEK293T cells are the most common system for protein expression. Even in this simplified system UNC5 receptors are found segregated into different cell membrane compartments.

Structural domains are conserved across all UNC5 receptors, they all contain two Ig domains, two TSPI repeats, a transmembrane domain, a DB, a ZU5 and a DD domain. Nonetheless amino acid sequence is highly divergent across UNC5 receptors. Such differences support the hypothesis that unique domains may play a role in intracellular trafficking and/or in cell membrane clustering. UNC5 receptors are known to be associated in lipid raft microdomains, which are typically ~10-200nm in size, a measure that cannot be resolved with conventional confocal microscopy, and much smaller than the macro-sized clusters observed in UNC5A and UNC5C transfected cells. In some cases, the cell uses membranes to distribute and concentrate certain class of membrane proteins[228]. For instance, direct interaction with cortical actin may drive integral membrane proteins to associate into macroscopic clusters[229]. Another explanation for large scale sized protein clusters can be explained by a steric confinement, where cortical actin bundles organize transmembrane proteins, independently of membrane lipidic composition, in a way such as to corral and confined membrane areas, restraining movements of proteins within these membrane domains[230].

Further experiments are required to test the hypothesis that the difference of subcellular localization of UNC5 members are due to divergences in the sequence of amino acids, and whether such differences may drive to a specific interaction with cortical actin, a fact that could explain the formation of clusters of UNC5A and UNC5C proteins.

1. 2. DISTRIBUTION OF UNC5 RECEPTORS INTO LIPID RAFTS MICRODOMAINS

Netrin-1 receptors, UNC5 and DCC, have been shown to be specifically associated to lipid rafts microdomains by biochemical membrane fractionation[149]. However, the molecular mechanisms involved into this specialized membrane localization are not fully understood. To

date, this localization into cholesterol enriched microdomains, has only been proved for UNC5A, UNC5B and UNC5C receptors[215]. This association to lipid rafts has been reported to be necessary for UNC5 receptors to exert its ability in promoting cell death when Netrin-1 is absent[215].

Taking advantage of several techniques such as biochemical membrane fractionation, lipid rafts membrane labeling and biophysical approaches, we addressed the localization, lateral diffusion and mobility of these receptors within the cellular membrane.

Many lines of evidence have identified CTxB a *bona fide* lipid raft marker. Therefore, we specificaly labeled UNC5 YFP-tagged transfected HEK293T cells with CTxB. All UNC5 members, partially, at least, colocalized with the CTxB labeling. UNC5C receptor, found to be distributed into membrane clusters did colocalize with highly enriched fractions in CTxB as shown in Fig. C (arrowheads). Nonetheless, CTxB is able, by binding with high avidity up to five molecules of GM_1, to cross-link lipid rafts domains and consequently modulate architecture and dynamics of cell membranes. This ability of CTxB, can potentially cause a redistribution of cell membrane components, in this case, as CTxB labeling was performed in living cells, making UNC5C clusters even larger than we found in our first localization experiments.

In the present thesis, UNC5 membrane dynamics were assessed by expressing UNC5 receptors in HEK293T cells, a cell line that do not express endogenous UNC5 receptors. Mobility in the cell membrane of UNC5 receptors was assessed with FRAP methodology. This technique allowed us to quantify the proportion of protein in the cell membrane that is able to freely diffuse, concluding the proportion of the protein that is retained in specific cell membrane compartments. FRAP experiments are designed to assess the mobility of fluorescently labeled proteins in a discrete cellular compartment, in our case, the cell membrane, by measuring the mobility of non-bleached molecules. This is why incorporation of newly synthesized proteins *en route* to the cell membrane must be avoid in order to strictly observe fluorescence recovery from adjacent intact proteins. In the present study, HEK293T

cells that presented high vesicle trafficking were directly discarded and moreover, histogram analysis allowed us to corroborate that fluorescence recovery after photobleaching started from the flanks of the photobleached regions. However, some other controls could have been performed in order to rule out that the fluorescence recovery was due to intracellular trafficking protein. For instance, by treating the cells with Brefeldin A, the formation of COPI-mediated transport vesicles can be prevented, thus, exocytosis and trafficking of proteins to the cell membrane would be inhibited.

The idea behind the designed protocol of FRAP experiments was to acquire images of the cell prior photobleaching to measure fluorescence intensity of the prebleached area, thus, recovery could be calculated related to the prebleach intensity. Following rapid photobleaching, image acquisition was performed every 0.4 seconds, to gather as much as information camera was able to obtain, as the first phase of the fluorescence recovery happens at a really fast pace. UNC5 receptors were found to reach a plateau after 240 seconds of photobleaching, this is why we decided to stop image acquisition at this time point, when fluorescence recovery reached a steady state.

Image analysis from FRAP recordings were done using IgorPro, a software that allows to take into account background intensity and photobleaching of the cell due to time acquisition. Therefore, three different intensity values were calculated when processing FRAP images, bleached area, background and total cell intensity fluorescence at each timepoint. These corrections when calculating fluorescence recovery inside the photobleached area allowed us to ensure that fluorescence recovery was only due to lateral mobility of intact proteins.

There is a striking correlation between distribution of UNC5 receptors in the cell membrane with the calculated fraction that freely diffuses in our FRAP experiments. Receptors that were found to exhibit a clustered organization in HEK293T cells (UNC5A and UNC5C) resulted in a very limited diffusion coefficients in FRAP curves. Contrarily, UNC5B and UNC5D

receptors, which were observed to distribute homogenously along the cell membrane, showed higher rates of free lateral movement in FRAP experiments. Thus, a clear correlation exists between the organization in macro-clusters of these receptors and their restricted dynamics within the cell membrane, possibly, due to arresting in certain membrane domains.

1. 3. COMPARABLE MOBILITY OF UNC5B AND UNC5C BETWEEN HEK293T CELLS AND HIPPOCAMPAL NEURONS

During postnatal cerebellar development, both UNC5B and UNC5C receptors are expressed in neurons from the external granule layer EGL. Immediately after birth, postmitotic granule cells descend to the deep EGL and extend tangentially their axons, the parallel fibers, that will ultimately contact the Purkinje cells dendritic arbors. The soma of granule cells will then re-orientate perpendicularly to the axons and migrate radially through the ML in a Bergmann glia dependent manner, to form the IGL. Secreted Netrin-1 by EGL and interneurons of the molecular layer, repels parallel fibers from granule cells, preventing their aberrant growing toward deeper layers of the cerebellum. This effect has been described when downregulating Cdc42, the Rho GTPase immediately downstream of UNC5 activation[231], or Trio, a GEF modulator that activates Rho GTPases. Parallels fibers of granule neurons from Cdc42 or Trio knock out (KO) animals are disorganized and defasciculated compared with those of wild types[232].

Subcellular localization observations and FRAP experiments with UNC5 receptors were performed using transfected HEK293T cells. Many authors claim that neuronal-like features and gene expression signature, make HEK293T cells a good model to study proteins involved in functions of the CNS[233]. Nonetheless, HEK293T cells may differ in many aspects to neuronal cells. For instance, an important feature in this study is the lipid composition of cell membranes, that favors the formation of lipid raft structures and alters the membrane fluidity.

Since GCs are one of the smallest cell types in the CNS, we decided to perform FRAP experiments in transfected hippocampal neurons. Photobleaching in the growth cone was not

possible in FRAP experiments in neurons, (1) the growth cone collapsed after photobleaching, most probable due to phototoxicity and (2) motility of intact growth cones, made them to be impossible to record as they went out of focus easily. With this, we directed photobleaching in the axon initial segment. Calculated curves from fluorescence recovery in between HEK293T cells and hippocampal neurons did not deferred in UNC5B and UNC5C dynamics. It is worth to mention that described clusters observed in UNC5C HEK293T cells, were confirmed in the soma and the axon initial segment of the transfected hippocampal neurons.

1. 4. A WELL KNOWN LIPID RAFT RESIDENT. DCC DYNAMICS IN HEK293T CELLS AND HIPPOCAMPAL NEURONS

Netrin-1 receptor DCC, is known to be associated to lipid rafts microdomains. Moreover, this association is necessary for the mediated attraction response towards a Netrin-1 source[149]. Protein dynamics not only depend on the association of certain microdomains, for instance, Mf of certain GPI-anchored proteins like Thy-1, exhibits a Mf of 50%[234], while Cav protein, a hallmark in lipid raft composition, has a Mf of 16% in the cell membrane[235].

We performed FRAP experiments in both, DCC YFP-tagged transfected HEK293T cells and hippocampal neurons, so we could compare dynamics of a well known Netrin-1 receptor associated to lipid rafts. DCC receptor distributed homogeneously along the cell membrane, resembling the distribution observed for UNC5B, and as we expected Mf calculated in HEK293T cells were similar to that calculated for UNC5B. Nonetheless, Mf in hippocampal neurons was significantly lower when compared to transfected HEK293T cells.

1. 5. BIOCHEMICAL FRACTIONATION, A NON-QUANTIFIABLE TOOL TO ASSESS LIPID RAFT ASSOCIATION

The association of certain membrane proteins can be assessed by biochemical fractionation of the cell membrane. After cold detergent solubilization, some membrane fractions remain intact and float in a sucrose gradient. These insolubility is a common treat of lipid raft fractions. In fact, floating fractions are enriched in lipid raft membrane proteins such as

caveolin and flotillin. On the other hand, heavy fractions are normally enriched in clathrin proteins, which are used as a DSM marker.

With this knowledge, we transfected HEK293T cells with UNC5B and UNC5C and performed membrane biochemical fractionation. In both assays, we detected clathrin, the DSM marker, confined to the 9-12 fractions. When cells were treated with MβCD, clathrin marker was slightly shifted occupying 8 fraction. On the other hand, caveolin, the DRM marker, was preferentially found in 3-5 fractions, a localization that was completely shifted to 7 fraction in one of the assays (Fig. 8D). In control conditions, both receptors were present in the same fractions that we detected lipid rafts marker (Fig. 8A, C). The presence of receptors in DRM fractions was either, absent in DRM fractions or shifted to DSM fraction domains after MβCD treatment (Fig. 8B, D).

Next, we wanted to assess lipid raft association by biochemical fractionation in native tissue by using the same protocol in directly dissected cortex and cerebellum from P4 mice. This is a good approach since receptors are not overexpressed in an *in vitro* model and lipid raft association is assessed in native conditions. Although fractionation was successful, DSMs were enriched in both, caveolin and flotillin and found in 4-5 fractions and 9-12 fractions were enriched in clathrin, we failed in detecting UNC5B or UNC5C by conventional immunoblot (Fig. 8E). This is possible due to technical limitations such as low concentration of the receptors in each fraction or the antibody itself.

Traditionally, lipid rafts have been defined by their insolubility in ice cold Triton X-100. Although biochemical fractionation is an accepted methodology and a good preliminary approach to assess lipid raft association of transmembrane proteins, it has its limitations. First, this is only a qualitative method, proportion of a certain protein associated to lipid rafts domains are not quantifiable. Second, DRMs do not reflect the native composition and organization of lipid rafts in living cells. The protein composition found in DRMs can widely vary depending on the detergent that has been used for solubilization[236]. Moreover, subtle

variations in buffer temperatures can drastically influence protein composition in DRMs[154], which can lead to contradictory reports about lipid raft associations.

1. 6. CELL MEMBRANE CHOLESTEROL COMPOSITION AFFECTS UNC5B AND UNC5C DYNAMICS

As previously stated, cell membrane microdomains are mainly enriched in cholesterol, among other membrane lipids. These enriched fractions in the cell membrane affect the fluidity and dynamics of the plasma membrane and therof, lateral mobility of transmembrane proteins associated to lipid rafts. After membrane cholesterol depletion, we could observe that mobility for both receptors, UNC5B and UNC5C, increased, which led us to the conclusion that receptors were partially released from these domains.

We used three different drugs that have different mechanisms of action to deplete membrane cholesterol. MβCD and ChoA did affect the mobility of UNC5B and UNC5C. Contrarily, nystatin did not affect the Mf calculated in HEK293T transfected cells.

UNC5C distribution into clusters has been first described in this thesis. Therefore, mechanisms of trafficking underlying this distribution are still unknown. After cell membrane cholesterol depletion we examined UNC5C clusters, noteworthy, they remained intact. Thus, the integrity of the clusters after cholesterol depletion suggests that this organization do not depend on lipid rafts but on other cellular mechanisms.

Drugs used to deplete membrane cholesterol are widely accepted for the assessment of protein association to lipid rafts. However, one potential artifact of depleting membrane cholesterol may be to affect the overall health of the cells. MβCD is the most common drug to acutely deplete membrane cholesterol, it is compatible with living cells experiments and it is known to act only in the membrane surface[237]. ChoA converts cholesterol molecules into cholest-4-en-3-one, which does not have the same membrane-ordering properties as cholesterol. ChoA is also used as an acute procedure to deplete cell membrane cholesterol and it is less harmful than MβCD. Yet, cell membrane cholesterol present in living cells is a poor substrate for ChoA and thus this treatment is not as efficient as MβCD in disrupting lipid rafts.

Nystatin is also used to disrupt lipid rafts, nonetheless in our experiments we did not identified considerable changes in UNC5 receptors dynamics after nystatin treatment. An alternative of using drugs to deplete membrane cholesterol is to grow cells in lipoprotein-deficient medium. However, this methodology is time consuming, as intracellular cholesterol needs days to be reallocated.

Treatment of cells with lipid rafts disrupting agents is a powerful tool in the study of proteins associated to raft microdomains. Many controls are needed though, for instance, to assess the viability of treated cells or ensure that the treatments are efficiently depleting cell membrane cholesterol.

With this data, we were able to quantify the ammount of UNC5B and UNC5C receptors that are linked to cholesterol enriched microdomains, since depletion of membrane cholesterol affects the dynamics in the cell membrane of these receptors.

1. 7. DD, MORE THAN A STRUCTURAL DOMAIN

DD domain was described to be necessary for the localization in lipid rafts of UNC5B[215]. After deleting DD, was faound in DSM fractions in membrane biochemical fractionation[215]. In addition to drug experiments, we deleted DD of UNC5B and UNC5C. In our FRAP experiments with UNC5BΔDD and UNC5CΔDD Mf was increased. These results are in line with what was found in biochemical experiments, where deleting DD of these receptors prevents lipid raft localization. Strikingly, Mf of both UNC5BΔDD and UNC5CΔDD, increased in a greater extent rather than when membrane cholesterol was depleted. Data obtained from these FRAP experiments, suggests that DD is, together with cholesterol membrane levels, an important feature to retain both receptors within lipid rafts microdomains.

Other mechanisms may be involved in raft localization. For instance, it is known that cytoskeletal structures such as actin, are important cellular components to maintain or clusterize raft structures. The DDs of UNC5s are similar to those present in ankyrin or PIDD[198], which mediate the attachment of integral membrane proteins to the spectrin-actin based

membrane cytoskeleton. The reported differences in the sequences of UNC5 DDs might explain their specific mobility parameters through controlling their interaction with endogenous proteins. The removal of the DDs may prevent the binding of UNC5 to scaffolding proteins or actin cytoskeleton, affecting their lateral membrane mobility and their interaction with cholesterol-enriched microdomains.

1. 8. TO CLUSTER OR NOT TO CLUSTER...

Since we observed differential dynamics for UNC5C that correlated with observable macro-clusters in the cell membrane, we decided to perform a detailed study of the mobility of UNC5C clusters. We found that UNC5C clusters are highly enriched in CTxB lipid raft marker, that UNC5C non-bleached proteins have preference to occupy these areas and that mobility constants are atrikingly higher outside these clusters.

Lipid rafts, due to its size, are undetectable by using a conventional confocal microscope. Therefore it is unlikely that the structures we identified in UNC5C transfected cells are lipid rafts themselves. Nonetheless, raft structures can associate to build large-scaled platforms mostly through cytoskeletal interactions[238]. It is possible that UNC5C macro-clusters may be associations of several raft platforms.

1. 9. SPTPALM: A POWERFUL TOOL TO IDENTIFY UNC5B SUBPOPULATIONS

sptPALM experiments revealed not only what we could see in FRAP experiments, which UNC5C is less mobile than UNC5B, as it is represented in the MSD curves, but we could also distinguish two populations of UNC5B molecules when analyzing their mobility. It still to be identified the domain or domains of the aminoacid sequence that makes UNC5B and UNC5C to have preferred domains within the cell membrane. Nonetheless, with sptPALM experiments we have shown that a fraction of UNC5B behaves in terms of diffusion the same way a high proportion of UNC5C does. By ligand union and the action of scaffolding proteins such as Cav, receptors that may be sparse throughout the cell membrane, become closer and therefore

clusterized in certain microdomains that will ultimately activate and start a signalling cascade. This could be a regulatory mechanism in which UNC5B only in cooperation with UNC5C in certain membrane microdomains can be activated.

1. 10. EFFECTS OF CHOLESTEROL DEPLETION IN UNC5 MEDIATED AXON GUIDANCE PROCESSES

Raft cholesterol-enriched structures are important both for developmental axonal guidance[150] and for regeneration post-spinal cord injury[239, 240]. For instance, The peroxisome assembly gene (PEX2) deficiency in mouse brain as a model of the Zellweger syndrome[241] is characterized by abnormal cerebellar histogenesis with marked abnormalities in granule neuron population[242]. This specific phenotype might reflect the importance of cholesterol-enriched membrane microdomains during cerebellar development.

Whereas the importance of raft integrity in Netrin-1 neuronal function has been identified for DCC[149] and Neogenin[243], nothing has been reported to UNC5-dependent Netrin-1 axon chemorepulsion. To evaluate the functional importance of the distribution of UNC5 receptors in lipid rafts during axon guidance we studied the chemorepulsive response to Netrin-1 from postnatal cerebellar granule cells, depleting the levels of endogenous cholesterol combining pharmacological and genetical approaches. Upon Netrin-1 binding to UNC5 receptors, growth cones of ELG neurons collapse and their axons are repelled. However, the pre-treatment with cholesterol depleting agents such as MβCD or CO prevented the collapse of growth cones and the repulsion of EGL axons. Interestingly, even though the action mechanisms of both drugs are different, both are able to undermine membrane cholesterol, resulting in the inhibition of the chemorepulsive effects from Netrin-1. These results are in line with the disruption of Netrin-1 attraction in dorsal spinal cord neurons upon lipid raft destabilization[244], suggesting that analogously to DCC, the repulsive function of UNC5 receptors depends on the integrity of cholesterol-enriched raft microdomains. The specificity and reversibility of cholesterol depletion with MβCD treatment is demonstrated by the restoration of the Netrin-1-repulsion upon cholesterol reloaded. Alternatively, downregulation

the expression of Cyp46A1 in hippocampal neurons increases the concentration of cholesterol[221, 222], and overexpressing Cyp46A1 decreases the levels of cholesterol in neurons[221]. Only the overexpression of Cyp46A1 decreased the repulsiveness against Netrin-1 in EGL neurons. These results reinforced the idea that intact cholesterol-enriched membrane microdomains are required for the proper chemorepulsive response of EGL axons to Netrin-1.

Netrin-1 is known to be expressed in the developing spinal cord and adult spinal cord by cells in the central canal and the floor plate[245]. After spinal cord injury high levels of Netrin-1 are still detected during 3 months after lesion in the adult spinal cord[245]. The attractive function of Netrin-1 could be utilized to promote peripheral regeneration. However, the predominant expression of UNC5A–D in spinal cord adult neurons (corticospinal and lateral motor neurons) will activate Netrin-1 repulsive signaling to slow down the rate of axon regeneration. Moreover, raft disruption with cholesterol modifying agents favors peripheral nerve regeneration after lesion[240], a fact that together with our results reported here, may promote the axonal regeneration in spinal cord injury models.

2. ALTERNATIVE SPLICING OF UNC5A. SUBCELLULAR LOCALIZATION AND FUNCTIONALITY OF THE SHORT SPLICE VARIANT

2. 1. EXPRESSION SHIFT OF THE UNC5A RECEPTOR IS DEVELOPMENTALLY REGULATED

Two alternative splice variants were detected for the UNC5A gene in the CNS. In RT-PCR experiments using mice tissue from the CNS we detected the canonical form of UNC5A (long form) and a mRNA of UNC5A that was lacking the first TSPI repeat (short form). The first TSPI domain is located in the extracellular portion of the receptor and accounts for 54bp. This domain corresponds to the exon 6 of the UNC5A gene, which was previously predicted to suffer alternative splicing[246]. The mentioned splice variant was previously detected in embryonic rat spinal cord[223].

In RT-PCR experiments we observed that the expression pattern of both isoforms seems to be regulated during development and adulthood and their expression is tissue-specific. UNC5AΔTSPI_1 is restricted to the cortex and the cerebellum in postnatal development and adult animals. However, we were able to detect expression of UNC5A in the cerebellum but in lower levels than the short isoform. On the other hand, during development, in spinal cord both forms were equally detected but the expression shifted in postnatal and adult individuals, where we only detected the upper band, corresponding to the full length UNC5A. The upper and lower bands, which corresponded to the predicted amplification product length, were then sequenced and upon alignment we ensured that the lower band lacked the first TSPI repeat. It is worth to mention that we also detected a band in between these two mentioned bands. This band was also sequenced and strikingly it corresponded to the full length isoform of UNC5A.

RT-PCR was also performed with UNC5B primers targeting the same region we used for UNC5A RT-PCR, as expected we only detected one single band corresponding to a UNC5B mRNA with both TSPI repeats.

Comparison of mouse TSPI_1 sequence with *D. melanogaster* and *C. elegans* resulted in a 52% and 55% of homology respectively in the amino acid identity. This fact suggests that at least the first TSPI has a conserved function throughout species. Nonetheless, the importance of this domain is still not known.

2. 2. A DOMAIN THAT CHANGES SUBCELLULAR LOCALIZATION

At this point we were interested in the effects for UNC5A of skipping the TSPI domain. For this reason we deleted the first TSPI repeat of our UNC5A full lenght construct. Localization of both constructs were dramaticaly different when we transfected both forms into HeLa cells. Full lenght targeted to the cell membrane, as we observed in previous experiments, but UNC5AΔTSPI_1 was unable to progress beyond the ER, as it perfect co-localized with a ER tracker. Although UNC5C does not suffer this kind of alternative splicing, we wanted to assess

whether the function of TSPI_1 in membrane targeting was conserved in other UNC5 counterpartners. Indeed, when deleting TSPI_1 from UNC5C the resulting phenotype was exactly the same.

A recently published paper[224] claimed that C-mannosyltransferases are necessary to target UNC5A to the cell membrane. When these C-mannosyltransferases are knocked-out UNC5A does not reach the cell membrane. Monnosylation occurs in three Tryptophan residues in the consensus sequence (WxxWxxWxxC) within the TSPI domain. When point mutating these three Tryptophan residues, UNC5A construct was redistributed as we observed for UNC5AΔTSPI_1 or UNC5CΔTSPI_1. Because this consensus sequence was conserved in the TSPI_2 repeat of UNC5A we deleted this domain and observed that localization did not change when compared with UNC5A.

In transfected hippocampal neurons we obtained the same results. UNC5A is able to distribute along the developing neurites while UNC5AΔTSPI_1 could only be detected in the soma of these neurons. Thus, both isoforms distribute in the same subcellular compartments in HeLa cells and in hippocampal neurons.

Taken together, these results evidenced that TSPI_1 is an essential structural domain for UNC5A to reach the cell surface. Specifically three Tryptophan resisdues within the TSPI_1 domain are needed for the cell membrane localization. Based on the observations in which intracellular forms co-localize with the ER marker, mannosylation could be a crucial posttranslational modification that, if it does not take place the result is likely to be a truncated protein that cannot progress beyond the ER.

2. 3. QUANTIFICATION OF CELL SURFACE EXPRESSION OF UNC5A ISOFORMS

Biotinylation assay of cell surface proteins revealed that, as we expected, UNC5A targets efficiently to the cell membrane while UNC5AΔTSPI_1 fails to reach the membrane surface, which most likely is retained in the ER. Biotin is a non-permeable membrane vitamin that binds Glycine residues with high avidity. Biotin can also be detected with a coupled-Horseradish

Peroxidase (HRP) streptavidin due to its high affinity in a polyacrilamide electrophoresis gel. This assay was performed at 4^{o}C to avoid mainly biotin internalization.

Intensities detected with streptavidin-HRP may vary due to number of Cysteine residues present in the proteins of interest. In our case, compared receptors, UNC5A and UNC5AΔTSPI_1, differ in 7 Glycine residues which may not be enough at least to observe a variation of detected intensity due to a different number Glycine residues. Strikingly, we detected a higher amount of biotin bound to UNC5B receptor, our positive control. UNC5B TSPI_1 contains the same number of Glycine residues as UNC5A TSPI_1 which may lead to the conclusion that UNC5B receptor is by far, more abundant in the cell surface than UNC5A. These differences in cell surface expression may be due to different membrane trafficking mechanisms involved in UNC5A and UNC5B plasmatic membrane targeting. Curiously, these two receptors were found to be distributed differently in the cell membrane, a feature that may involve distinct intracellular mechanisms.

2. 4. PROTEIN STABILITY

CHX interferes with the protein synthesis *de novo* by blocking eukaryotic translational elongation. Thus, newly synthesized proteins are avoided and therefore, only proteins present in the cell from the moment of CHX treatment will be detected. This is a widely natural occuring fungicide to study protein stability.

As it is known, the majority of misfolded proteins undergo degradation via autophagy or ubiquitin-proteasome system. Whereas, the proteasome system is involved in the rapid degradation of ubiquitinated proteins, autophagy processes can selectively remove protein aggregates or damaged from certain organelles, a fact that does not match with our observations in the CHX experiments. In this experiment we first assessed the stability of UNC5A and UNC5AΔTSPI_1 in single transfection. Unlike we expected, UNC5A protein levels decreased drastically comparing with UNC5AΔTSPI_1 protein levels.

Accumulations of misfolded proteins in the ER are often associated with adult-onset diseases including Alzheimer's, Parkinson's or Huntington's. ER is a highly susceptible organelle to suffer stress from eventual protein misfolding. In the ER proteins begin to fold and posttranslational modifications and disulfide bonds are formed. Misfolded proteins tend to accumulate in the ER, causing the activation of special machinery called unfolded protein response (UPR). This response includes upregulation of a set of genes that among other processes, are required for ER expansion, ER-Golgi trafficking and protein degradation, with the goal to relief stress from the ER. Nonetheless, more experiments are required to test the hypothesis that UNC5AΔTSPI_1 do activate the UPR.

Noteworthy, bands detected for UNC5A are blurring, suggesting that full length protein is posttranslationally modified. UNC5AΔTSPI_1 bands have a sharp shape, which may suggest no posttranslational modifications occurring. Thus, these findings may corroborate the fact that TSPI_1 domain is necessary for posttranslational modifications, such as mannose addition, as previously discussed.

2. 5. Is UNC5ΔTSPI_1 functional?

As a cell membrane receptor UNC5A needs to be in the cell surface in order to bind to its ligand and initiate signaling cascades. This requirement is not accomplished in the case of UNC5AΔTSPI_1, that as we have observed, it is retained in intracellular compartments.

In our preliminary experiments regarding UNC5AΔTSPI_1 functionality in axon guidance repulsion in presence of Netrin-1, growth cones did not collapse when hippocampal neurons were treated with Netrin-1. These are only preliminary results, and more experiments in this direction are needed, to understand the underlying mechanisms of UNC5AΔTSPI_1 in axon pathfinding. Nevertheless, our results match with what other authors have described. For instance, it is known that Netrin-1 binds to the two Ig domains of the extracellular domain of UNC5A[64]. However, in a knock out model of *D. melanogaster* for UNC5, the aberrant axon

developmental phenotype in the midline cannot be reverted when UNC5 lacking the first TSPI is expressed in commissural neurons[61].

To assess the ability of UNC5A to trigger cell death, we transfected HeLa cells and counted pyknotic nuclei. More experiments are needed to corroborate that UNC5AΔTSPI_1 fails in triggering apoptosis. For example, caspase activation could be analyzed in order indentify whether intracellular machinery is activated or propidium iodide incorporation to assess the viability of these cells. Experiments carried out by Megan E. Williams and collaborators, identified that association of UNC5A and NRAGE is responsible for apoptosis induced by UNC5A and that level of apoptosis is by far greater than amount induced by UNC5B or UNC5C[199]. We observed a significant increment in apoptosis induced by UNC5A when compared to that induced by UNC5C, nevertheless, our results are far from the 80% of apoptotic cells that the authors claim. Researchers used transfected cos cells, which express high levels of NRAGE. On the other hand we were unable to efficiently transfect cos cells, for this reason we used HeLa cells in these experiments. It is possible that HeLa cells do not express these levels of NRAGE protein and thus, the potentiated cell death activity was attenuated. It is also worth to mention that UNC5A is able to trigger apoptosis independent of Netrin-1 in the developmental spinal cord of mice embryos[227]. Knocking out UNC5A results in supernumerary neurons located in certain spinal cord nuclei[227]. These results match with our findings that the canonical form of UNC5A is mainly expressed in the spinal cord, in both embryos and adult individuals.

CONCLUSIONS

1. UNC5 receptors are distributed in a different fashion within the cell membrane. UNC5A and UNC5C are distributed into distinguishable macro-clusters while UNC5B and UNC5D distribute evenly within the plasmatic membrane.

2. FRAP technique enabled us to quantify differences in membrane distribution of UNC5 receptors. Such differences were not previously identified by using classical lipid raft assays.

3. Lipid raft localization of UNC5B and UNC5C is abolished after cell membrane cholesterol removal.

4. Lipid raft destabilization by membrane cholesterol depletion efficiently affects UNC5B and UNC5C membrane dynamics.

5. DD deletion increases lateral membrane mobility of UNC5B and UNC5C receptors.

6. Clustered fractions of UNC5C exhibited lower mobility than non-clustered UNC5C molecules. This study determined that UNC5C receptor had preference to occupy pre-built structures in the cell membrane.

7. Netrin-1 induced growth cone collapse in cerebellar granule neurons, depends on cell membrane cholesterol composition

8. Axonal chemorepulsion mediated by Netrin-1 is dependent on lipid raft microdomains integrity in cerebellar granule cell axons.

9. CYP46A1 efficiently blocks Netrin-1 mediated chemorepulsion in cerebellar granule cell axons, by genetically modulating levels of cholesterol.

10. Alternative splicing of UNC5A results in a shorter isoform lacking the first TSPI repeat. These isoforms are differentially expressed throughout the CNS and during development and postnatal stages.

11. Integrity of the TSPI_1 is necessary for the expression of UNC5A in the cell membrane.

12. Protein turnover of UNC5A and UNC5AΔTSPI_1 is significantly different.

13. Preliminary experiments suggest different functions for both isoforms.

MATERIALS AND METHODS

REAGENTS AND ANTIBODIES

The following antibodies were used: anti-tubulin beta-III (MMS-435P,Covance), anti-UNC5B (ab54430, abcam), anti-UNC5C (ab106949, abcam). Wheat germ agglutinin (WGA) alexa® 594 (Invitrogen, W11262), cholera toxin B-subunit (CTxB) alexa® 488 (Invitrogen, C34775) and alexa® 555 (Invitrogen, C34776), poly-D-Lysine (PDL) (P7280, Sigma), recombinant Mouse Netrin-1 (1109-N1-025, R&D Systems, Inc), rat Tail Colagen Type I (354236, BD Biosciences), Cholesterol Oxidase, Streptomyces sp. (228250, Calbiochem), Methyl-β-cyclodextrin (C4555, Sigma), nystatin (N6261, Sigma), Phalloidin–TRITC (P1951, Sigma), DMSO (D5879, Sigma), Dapi (D9542, Sigma).

PLASMIDS AND CONSTRUCTS

UNC5(A-D) receptors were subcloned into a pEYFP plasmid (Clontech), EYFP was placed at the C terminus of each receptor. UNC5A using flanking restriction sites *HindIII* and *EcoRI* (*forward primer* 5' CCC AAG CTT ATG GCC GTC CGG CCC GGC CTG and *reverse primer* 5' CCG GAA TTC TCC GCA CTC GGC CTC TGA CAC), UNC5B using flanking restriction sites *HindIII* and *EcoRI* (*forward primer* 5' CCC AAG CTT ATG AGG GCC CGG AGC GGG GTG and *reverse primer* 5' CCG GAA TTC TCC GCA ATC GCC ATC TGT GG), UNC5C using flanking restriction sites *XhoI* and *EcoRI* (*forward primer* 5' CCG CTC GAG ATG AGG AAA GGT CTG AGG GC and *reverse primer* 5' CCG GAA TTC TCC ATA CTG TCC TTC TGC TG), UNC5D using flanking restriction sites *NheI* and *HindIII* (*forward primer* 5' CTA GCT AGC ATG GGG ACA GGG GCT GCA GAC G and *reverse primer* 5' CCC AAG CTT TAG AGT CCA TTT TGC CTG CTG) or into a pmCherry plasmid only for UNC5C gene using the same pair of primers mentioned above. UNC5B and UNC5C were also subcloned into pmEos2.1 vector to perform sptPALM experiments. mEos2 was placed at the C terminus of both molecules, UNC5B was subcloned using *EcoRI* and *SalI* restriction sites (*forward primer* 5'

GGA ATT CCG ATG AGG GCC CGG AGC GGG GTG and *reverse primer* 5’ CGC GTC GAC GTG CAA TCG CCA TCT GTG GCC AT) and UNC5C was subcloned using *NheI* and *XhoI* restriction sites (*forward primer* 5’ GGC TAG CCA TGA GGA AAG GTC TGA GGG CG and *reverse primer* 5’ GGC TCG AGA TAC TGT CCT TCT GCT GCC AA). Inserts were purchased (Source Bioscience) and subcloned into the mentioned vectors. pCDNA3-hDCC was generously provided by E. Stein (Yale University, New Haven, CT) and subcloned into a pEYFP plasmid using *NheI* and *XhoI* as flanking regions (*forward primer* 5’ CTA GCT AGC ATG GAG AAT AGT CTT AGA TG and *reverse primer* 5’ CCG CTC GAG TAA AAG GCT GAG CCT GTG ATG) shRNA against Cyp46A1, shRNA scramble control and Cyp46a1-GFP were a generous gift from Dr. Carlos Dotti (Centro de Biologıa Molecular 'Severo Ochoa' (CSIC/UAM), Madrid, Spain). ER tracker plasmid and Alex3-GFP were a kinf gift from Dr. Serena Mirra (University of Barcelona, Barcelona, Spain).

MUTAGENESIS

Mutagenesis was performed following manufacturer instructions. We used the kit QuikChange II XL Site-Directed Mutagenesis Kit (Agilent 200522). Primers used for site directed mutagenesis to delete DD were *forward primer* 5’ CTG TCC ATC CGC CAA GAA TTC TGC AGC AGC CTG and *reverse primer* 5’ CAG GCT GCT GCA GAA TTC TTG GCG GAT GGA CAG for UNC5B targeting 2560 position to create a *EcoRI* restriction site and delete the DD (UNC5BΔDD); *forward primer* 5’ CCC TAT CCG GCA GGA ATT CTG CAG CAG CCT GGA TG and *reverse primer* 5’ CAT CCA GGC TGC TGC AGA ATT CCT GCC GGA TAG GG for UNC5C targeting 2594 position to create a *EcoRI* restriction site and delete the DD (UNC5CΔDD). Primers used for TSPI deletions were *forward primer* 5' CTG CAG CGG TCA TTG TTT ATG TGA ATT CTG GGT GGT CGA CGT and *reverse primer* 5' ACG TCG ACC ACC CAG AAT TCA CAT AAA CAA TGA CCG CTG CAG for UNC5A targeting 711 position to create *EcoRI* restriction site; *forward primer* 5' CAC TCT GTG CCC AGT GAA TTC GAG CTG GAG TTC GTG G and *reverse primer* 5' CCA CGA ACT CCA GCT CGA ATT CAC TGG GCA CAG AGT G for UNC5A targeting 874 position to create *EcoRI* restriction site and

delete TSPI_1. To delete TSPI_1 of UNC5C we used *forward primer* 5' AAA AAG CAC CAC AGC CAC TGT CGG CGC GCC TGT TAA TGG TGG CTG GTC CAC C and *reverse primer* 5' GGT GGA CCA GCC ACC ATT AAC AGG CGC GCC GAC AGT GGC TGT GGT GCT TTT T targeting 768 position to create a *AscI* restriction site; *forward primer* 5' CAC TAC GTT ATG TCC AGT GGA TGG CGC GCC GAC TTC ATG GAG CAA ATG GTC AAC and *reverse primer* 5' GTT GAC CAT TTG CTC CAT GAA GTC GGC GCG CCA TCC ACT GGA CAT AAC GTA GTG targeting 951 position to create *AscI* restriction site and delete TSPI_1. To delete TSPI_2 from UNC5A we used *forward primer* 5' ATG GGC TCC AGC TGG CGC GCA CTG GGC ACC GAG TGG CGC AGG C and *reverse primer* 5' GCC TGC GCC ACT CGG TGC CCA GTG CGC GCC AGC TGG AGC CCA T to target 891 position and create a *AscI* restriction site; *forward primer* 5' GGG GCC GGA AGA GGC GCG CCG GCA GAG GTC ACT G and *reverse primer* 5' CAG TGA CCT CTG CCG GCG CGC CTC TTC CGG CCC C to target position 1050 and create a *AscI* restriction site and delete TSPI_2 from UNC5A. Three Tryptophan residues of UNC5A within the TSPI_1 domain were changed by Phenylalanine residues, *forward primer* 5' CAT TGT TTA TGT GAA CGG TGG GTT CTC GAC GTT CAC CGA GTT CTC CGT CTG CAG T and *reverse primer* 5' ACT GCA GAC GGA GAA CTC GGT GAA CGT CGA GAA CCC ACC GTT CAC ATA AAC AAT G.

RT-PCR PRIMERS

To amplify regions comprising the TSPI_1 domain of UNC5A and UNC5B from CNS tissues we used for UNC5A *forward primer* 5' CAC TGG AGC AAG GCA TTG TG to target position 482 and *reverse primer* 5' GCT GAG CAG GTG ACC ATT AG to target position 1371. For UNC5B we used *forward primer* 5' AAC TTT GAC CAG GAG CCT CT to target position 467 and *reverse primer* 5' CAC TGG CCG TTA GGT CTG GA to target position 1334.

HETEROLOGOUS CELL CULTURES

HEK293T and HeLa cells were maintained in DMEM media supplemented with Fetal Bovine Serum (FBS) (10%), glutamine 1% (GIBCO 25030-024) and penicillin/streptomycin 1% (GIBCO, 15140-122).

PRIMARY NEURONAL CULTURES

Primary cultures of mouse cerebellar EGL neurons were prepared from P4-P5 CD1 mice. Animals were sacrificed by decapitation in accordance with relevant institutional and governmental ethical guidelines and regulations. Cerebellums were isolated, mechanically disaggregated and trypsinized. After the centrifugation, neurons were resuspended in 2 mL in DMEM (GIBCO 41966-029) media and EGL were isolated by centrifugation in a percol gradient (35% and 60% of percol and centrifuged at 3000rpm, during 10 minutes at 4ºC). After washing excess of percol with PBS, EGL neurons were placed on poly-D-lysine pre-coated dishes in plating medium. The composition of the plating medium is DMEM, penicillin/streptomycin 1%, Glutamine 1%, D-(+)-Glucose 4.5% (Sigma, G-8769), NHS 5% (GIBCO 26050-088), FBS 10% (GIBCO, 16000-044). Plating medium was maintained during 24h and then changed to culture medium. Culture medium has the same composition as plating medium except for NHS and FBS, who were replaced by B27 2% (GIBCO 17504-044) and N2 1% (GIBCO, 17502-048). Primary cultures of mouse hippocampal neurons were prepared from E16 OF1 mice.

EGL explants were obtained from P4-P5 mice. Animals were sacrificed by decapitation in accordance with relevant institutional and governmental ethical guidelines and regulations. Cerebellums were isolated and chopped in 300 µm slices. Selected slices were further dissected using fine tungsten needles to extract small tissue pieces to extract small tissue pieces from the external granular layer from the cerebellum. Explants were carefully placed inside a 3D collagen matrix prepared as previously described[219]. The collagen matrix was formed on poly-D-lysine pre-coated dishes and cultured in culture medium for 24h.

Primary cultures of mouse hippocampal neurons were prepared from E16-E17 CD1 mice. Animals were sacrificed by decapitation in accordance with relevant institutional and governmental ethical guidelines and regulations. Hippocampus were isolated, mechanically disaggregated and trypsinized. After the centrifugation (800rpm during 5 minutes at 4^{o}C), neurons were resuspended in 1 mL in DMEM (GIBCO 41966-029). Hippocampal neurons were placed on poly-D-lysine pre-coated dishes in plating medium. The composition of the plating medium is Neurobasal, penicillin/streptomycin 1%, Glutamax 1%, B27 1%.

All the experiments using animals were performed in accordance with the European Community Council directive and the National Institute of Health guidelines for the care and use of laboratory animals. Experiments were also approved by the local ethical committees.

TRANSFECTION OF HEK-293T CELLS, NEURONS AND ELECTROPORATION OF EXPLANTS

One day prior to transfection, cells were counted and plated in previously PDL coated 35 mm coverslips, to have a 70% of confluence on the day of transfection. HEK293T cells were transfected with Lipofectamine 2000® (4µg of DNA and 8µL of Lipofectamine 2000®) following manufacturer instructions.

After 2DIV, the cultures were transfected with UNC5(B-D)-YFP, using Lipofectamine 2000®. Prior to transfection procedure, 2:5 of medium was removed and kept aside to be returned after transfection. For each 35 mm plate, 4 µg of DNA and 8 µL of Lipofectamine 2000® were used. As with HEK393T cells, following manufacturer instructions. The final mixture of DNA- Lipofectamine 2000® was carefully added to the cultures and further incubated at 37ºC and 5% CO_2 for 50 minutes. The medium was replaced for that removed at the beginning and equal amount of fresh Neurobasal® medium (penicillin/streptomycin 1%, Glutamax 1%, B27 2%). Cultures were incubated until the following day.

Explants were electroporated with the Invitrogen Neon® system, briefly dissected explants were washed three times in PBS and suspended in buffer R with 5µg of DNA.

Conditions of the electroporation were voltage: 500V; width: 50ms; 5 pulses. Explants were incubated for 1 hour in Neurobasal and then mounted in a 3D collagen matrix.

IMMUNOCYTOCHEMISTRY

HEK-293T cells and primary neurons were fixed with a solution of 4% paraformaldehyde in PBS during 10 min at room temperature. Neuronal explants were fixed by incubation with the same solution during 30 min at room temperature. Cells were rinsed with PBS, and permeabilized with a solution of Triton-X-100 0.1% in PBS during 10min, or during 30 min for the explants. Afterwards, cells were washed with PBS and incubated in blocking solution (NHS 10% in PBS) during 1 hour at room temperature, of during 3 hours for the explants. After blocking, the cells were incubated with the respective primary antibodies diluted in blocking solution for 2h at room temperature, or overnight at 4C for the explants. Cells and explants were washed with PBS and incubated in the secondary antibody solution (PBS 1x with 10% NHS) during 1h at room temperature, or 3 hours for the explants. Finally, cells and explants were washed and mounted in Mowiol for imaging.

Colocalization of UNC5 receptors with the WGA membrane marker and CTxB lipid raft membrane marker was performed at 4^{o}C to avoid internalization of the marker for 30 minutes.

BIOCHEMICAL MEMBRANE FRACTIONATION

HEK293T cells were cultured in growth medium until reaching 80% of confluence. Cells were the transfected with either UNC5B or UNC5C and harvested 24 hours after transfection. MβCD treatment was performed during 45 minutes prior solubilization (1mM). Cells were treated in 1mL of lysis buffer (Membrane Blocking solution (MBS) 1x, Triton X-100 1% and proteases inhibitor 1x). Lysed cells were the transfered into a suitable 12mL tube for ultracentrifugation. Prior transfer of the cell lysates, 3mL of 50% sucrose in MBS1x were placed in the 12mL tube. Sucrose gradient was built by adding 30% and 5% sucrose solution in MBS with a gradient tool.

Ultracentrifugation was performed at 4^{o}C, at 39000rpm during 16 hours. Fractions were collected every 1mL and samples were prepared for immunoblotting analysis.

FRAP ANALYSIS OF UNC5 MEMBRANE DYNAMICS

FRAP experiments were performed in different days but always following the same protocol. Cells expressing the YFP-tagged receptor were placed in a cell chamber Attofluor®, with preheated at 37ºC imaging medium (MEM®, Hepes 30mM, pH: 7.4). All FRAP experiments were performed in phenol-red and serum-free media to decrease non-specific fluorescence intensity. Living cells were always in the incubator at 37ºC and 5% CO2. Cells were imaged using a iXon EMCCD Andor DU-897 camera with a 100×/1.4 Oil objective. Cells were excited with a 488 nm diode laser 25%. The FRAP protocol was divided into three sections: initially cells were scanned 50 times every 0.4 seconds at three different Z levels (Δ0.75 µm) (prebleach). Then, a small selected region of the cytoplasmic membrane was photobleached, using a 488 nm diode laser 80% and a ROI line (10 µm) (Dwell time: 60 µs, 10 repeats) and scanned 300 times at maximum speed (one frame each 0.136 seconds) (postbleach), named fast acquisition phase. Thereafter, cells were scanned 90 times each 2 seconds (postbleach) at three different Z levels (Δ0.75 µm). Fiji software was used to measure intensities from the recordings, while IGORpro v6.0 (WaveMetrics) software was used to process the measurements. Three different measurements for each time point were taken with Fiji: whole cell integrated density, background integrated density and fluorescence recovery integrated density. Then, data was treated with IGORpro v6.0 (WaveMetrics). First, recovery intensities were normalized to 1, taking the prebleach intensities as absolute. Moreover, whole cell and recovery intensities were corrected by subtracting background intensities. Finally, whole cell intensities were used to correct the recovery intensities, needed to correct photobleaching due to acquisition protocol. To better understand calculations, this is the formula that was used to correct and normalize the FRAP curve to 1:

$$I_{FRAP\ norm}(t) = \frac{I_{whole-prebleach}}{I_{whole}(t) - I_{background}(t)} \times \frac{I_{FRAP}(t) - I_{background}(t)}{I_{FRAP-prebleach}}$$

Once the normalized points were calculated at each time point, averages and SD values for each condition were plotted in a graph and FRAP curve was then fitted to a single exponential. y_0 is the y value at the photobleaching point, τ is the time constant and *A* is the amplitude of each component. Finally mobile fraction Mf was calculated as:

$$I(t) = y_0 + Ae^{-\tau t}$$

$$M_f = \frac{-A}{1 - (y_0 + A)}$$

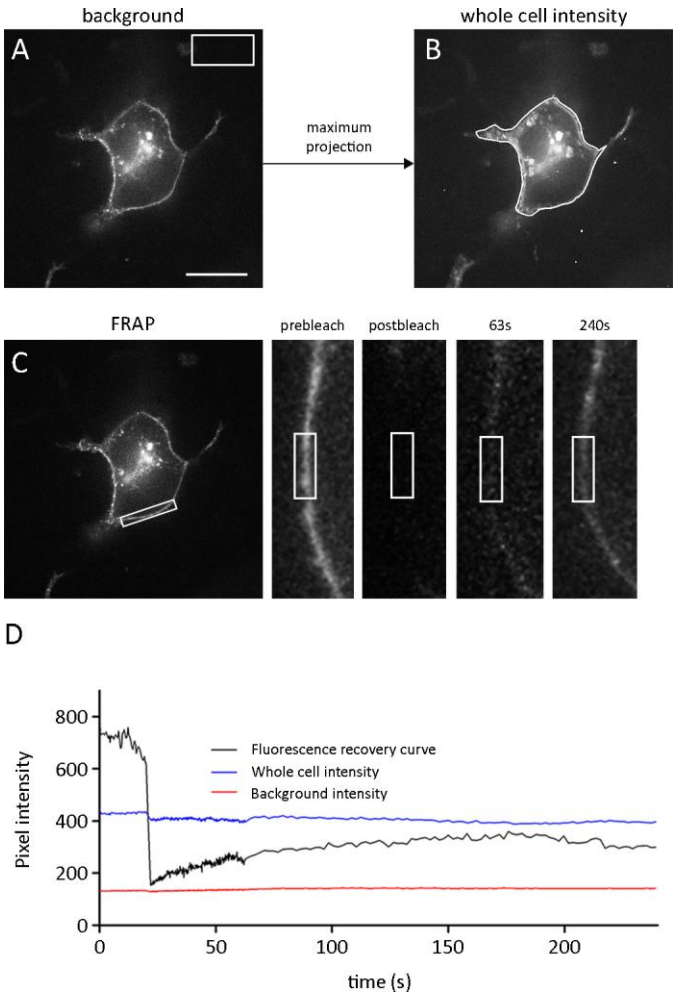

Figure 35 | FRAP protocol illustrated step by step. Squared ROI with which background intensities were measured (**A**) Stacks were projected. Then, a ROI was drawn around the cell and intensities were measured for each frame (**B**). Photobleached area is highlighted and magnified (**C**). Four different time lines are shown (prebleach, postbleach , 63 seconds and 240 seconds) as well as ROI with which recovery intensities were measured (**C**). Measurements plotted in a graph, fluorescence recovery curve (black line), whole cell intensity (blue line) and background intensity (red line) (**D**). Scale bar: 20µm.

SPTPALM EXPERIMENTS OF UNC5B AND UNC5C RECEPTORS

sptPALM experiments were performed on an Elyra PS1 STORM/SIM microscope (Carl Zeiss Microscopy GmbH) equipped with a 100× objective (α Plan-Apochromat 100× 1.46 NA oil-immersion), a focus lock system and an EMCCD camera Andor iXon Ultra 897 (Andor Technologies). A LF488/561-A-000 beam splitter and a FF01–523/610–25 emission filter (Semrock) were used to record SEpH and mEos2 fluorescence. Cells were imaged in total internal reflection microscopy (TIRFM) or highly inclined illumination mode in an enclosed chamber at (36.0 ± 1.5)°C.

For sptPALM measurements were performed as previously described[247]. A 560 nm laser was adjusted to 9–14 W/cm2. mEos2 molecules were continuously converted with a 405

nm laser, the power of which was gradually increased to maintain the density of photoconverted molecules. This ensured that only single mEos2 molecules were converted and imaged at 560 nm while keeping their number constant, and well separated during the acquisition. The density of fluorescent particles was kept below 0.2 molecules/µm2. Images were acquired every 0.032 seconds.

Single molecule fluorescent spots were localized in each frame and their position was followed over time using the TrackMate tracking algorithm[248]. A custom written MatLab (Math Works) routine was used to visualize individual trajectories and their corresponding mean-squared displacement (MSD) plots and to generate an average MSD vs. lag time plot. To improve the relative statistical error of individual MSD curves, only trajectories with 15 points or more were included in the analysis. It has previously been shown that when the diffusion coefficient is calculated from a linear fit to the first four points of the MSD vs. time plot, the relative error of the fit increases as the number of points decreases. As a consequence, the size of the diffusion coefficient distribution increases and the range of measured diffusion coefficients can still differ by a factor of two. In such cases the best estimate for the diffusion coefficient corresponds to the mean value[249, 250]. We therefore, calculated the diffusion coefficients from the mean MSD vs. time plot of all trajectories recorded per cell.

Diffusion coefficient (D) was calculated by fitting the first four points of the average MSD curve to the equation:

$$MSD(t) = 4Dt + b$$

An average confinement size was calculated by fitting MSD vs. time plot to the equation:

$$MSD(t) = \frac{L^2}{3}\left(1 - exp\left(-\frac{12Dt}{L^2}\right)\right) + 4D_{mac}t$$

Where L^2 is confinement area in which diffusion is constricted and D_{mac} is diffusion coefficient at long timescale. An average localization precision if fluorescence spots was 40–60 nm.

GROWTH CONE COLLAPSE EXPERIMENTS

EGL primary cultures were cultured during 3 days *in vitro* (3DIV) and then treated with MβCD (0.5 mM) for 10 min, CO (2U) for 2h, or the respective controls (PBS for MβCD and DMSO for CO). Neurons then were incubated with Netrin-1 (300 ng/ml) or the control (BSA 0.1%) during 45 min at 37C in culture media (DMEM). After this incubation, neurons were fixed with PFA 4% and permeabilized with PBS-Triton-X-100 (0.1%). Finally, actin filaments were stained by incubation with Phalloidin-TRITC (1μM) during 30 minutes. Cells were mounted on Mowiol and used for imaging.

REPULSION EXPERIMENTS

During the plating procedure, explants were embedded into the 3D collagen matrix and confronted at a distance of (200-600 μm) with aggregates of Netrin-1-stable expressing HEK-293T cells[251]. Netrin-1 expression in stable cells was regularly tested by western blot. Explants were cultured during 24h. Then they are fixed and immunocytochemistry was performed. To remove cholesterol, the explants were plated and treated with MβCD (1%) during 30 min. After the treatment, explants were washed 3 times with culture medium and grown during 24 hours. To replace removed cholesterol, MβCD-treated explants were grown in culture medium supplemented with cholesterol (5mM).

STATISTICS

Results were analyzed statistically by GraphPad Prism software. Data are presented as means ± SEM or means ± SD. Means were compared with two-tailed, unpaired Student's t-test or

analysis of variance following Tukey's Multiple Comparison Test or Mantel-Cox test. A p value less than 0.05 was accepted as significant.

RNA EXTRACTION AND RT-PCR

Total RNA from CNS tissues were extracted by using TRIzol® reagent (15596026, Invitrogen) and following manufacturer instructions. Briefly, all the materials and reagents used in this protocol were RNase-free. 1mL of TRIzol® was used per 50mg of tissue and samples were homogenized. 0.5mL of isopropanol were added per 1mL of TRIzol®. After centrifugation at 4^{o}C, supernatant was discarded. Pellet was resuspended in 75% ethanol and centrifuged. Supernatant was discarded and pellet was finally resuspended in 20µL of RNase-free water to further quantify total RNA isolated.

RT-PCR was performed using 2µg of RNA from the tissue isolation and following manufacturer instructions, RETROscript® (AM1710, Invitrogen). Shortly, a mix of Oligo(dT) and Random Decamers were used for the RT-PCR reaction. Afterwards, samples were heated at 70^{o}C and the remaining components of the RT-PCR were added. Mixes were incubated for 1 hour at 43^{o}C ending with a 10 minute extension at 92^{o}C to inactivate the reverse transcriptase.

The resulting product was further amplified with UNC5A and UNC5B primers designed to target the TSPI_1 domain (see RT-PCR primers section) and amplification product resolved with an agarose gel.

BIOTINYLATION OF CELL SURFACE PROTEINS

HEK293T cells were transfected with the mentioned constructs. 24 hours after transfection cells were washed three times with ice-cols PBS (pH 8.0) to remove any amine-containing madia and proteins from the cells. 2mM of biotin (EZ-Link® Sulfo-NHS-LC-Biotin) (21335, Thermo Scientific) in PBS was added to the cells at 4^{o}C to avoid biotin internalization, during 30

minutes. After biotin incubation, cells were washed three times with PBS + 100mM Glycine to quench and remove excess biotin reagent and byproducts.

Cells were then lysed (50mM Hepes pH 7.5, 150mM NaCl, 1.5mM $MgCl_2$, 1mM EGTA, 10% glycerol, 1% Triton X-100) in and prepared for immunoprecipitation. Briefly, samples were first pre-cleared with 30µL of protein A-sepharose (P3391, Sigma). Protein A-sepharose was blocked in 5% Bovine serum albumin (BSA). After 1 hour of pre-clearing and blocking, samples were mixed with blocked protein A-sepharose and 1µL of anti-GFP antibody was added. Incubation was performed overnight and at 4°C. Beads were then washed three times with RIPA buffer (50mM Tris-HCl pH 7.0, 1% Triton X-100, 0.25% Na-deoxycholate, 150mM NaCl, 1mM EDTA, 0.1% SDS). Beads were finally eluted and loaded in a polyacrylamide gel.

Protein detection was performed by using anti-GFP antibody and biotin was detected with Streptavidin-Biotinylated HRP Complex (GERPN1051, GE Healthcare).

CYCLOHEXIMIDE TREATMENT OF HEK293T CELLS

HEK293T cells were transfected with the tested constructs. 24 hours after transfection growing medium was replaced with medium lacking FBS, and cells were treated with CHX (C7698, Sigma) (20µg/mL). Cells were harvested and lysed (50mM Hepes pH 7.5, 150mM NaCl, 1.5mM $MgCl_2$, 1mM EGTA, 10% glycerol, 1% Triton X-100) every 2 hours (0, 1, 3, 5, 7 and 9 time points in hours). Samples were the prepared for immunoblotting and YFP signal from constructs was detected and quantified.

REFERENCES

1. Beddington, R. S. Induction of a second neural axis by the mouse node. *Development* **120**, 613–620 (1994).
2. Colas, J. F. and Schoenwolf, G. C. Towards a cellular and molecular understanding of neurulation. *Dev. Dyn.* **221**, 117–145 (2001).
3. Schoenwolf, G. C. and Alvarez, I. S. Roles of neuroepithelial cell rearrangement and division in shaping of the avian neural plate. *Development* **106**, 427–439 (1989).
4. Holland, P. W. H., Booth, H. A. F. and Bruford, E. A. Classification and nomenclature of all human homeobox genes. *BMC Biol.* **5**, 47 (2007).
5. Millet, S., Bloch-Gallego, E., Simeone, A. and Alvarado-Mallart, R. M. The caudal limit of Otx2 gene expression as a marker of the midbrain/hindbrain boundary: a study using in situ hybridisation and chick/quail homotopic grafts. *Development* **122**, 3785–3797 (1996).
6. Wassarman, K. M., Lewandoski, M., Campbell, K., Joyner, A. L., Rubenstein, J. L., Martinez, S. and Martin, G. R. Specification of the anterior hindbrain and establishment of a normal mid/hindbrain organizer is dependent on Gbx2 gene function. *Development* **124**, 2923–2934 (1997).
7. Hidalgo-Sanchez, M., Millet, S., Simeone, A. and Alvarado-Mallart, R. M. Comparative analysis of Otx2, Gbx2, Pax2, Fgf8 and Wnt1 gene expressions during the formation of the chick midbrain/hindbrain domain. *Mech. Dev.* **81**, 175–178 (1999).
8. Sgaier, S. K., Millet, S., Villanueva, M. P., Berenshteyn, F., Song, C. and Joyner, A. L. Morphogenetic and cellular movements that shape the mouse cerebellum; insights from genetic fate mapping. *Neuron* **45**, 27–40 (2005).
9. White, J. J. and Sillitoe, R. V. Development of the cerebellum: from gene expression patterns to circuit maps. *Wiley Interdiscip. Rev. Dev. Biol.* **2**, 149–164 (2013).
10. Sudarov, A. and Joyner, A. L. Cerebellum morphogenesis: the foliation pattern is orchestrated by multi-cellular anchoring centers. *Neural Dev.* **2**, 26 (2007).
11. Sillitoe, R. V and Joyner, A. L. Morphology, molecular codes, and circuitry produce the three-dimensional complexity of the cerebellum. *Annu. Rev. Cell Dev. Biol.* **23**, 549–577 (2007).

12. Fu, Y., Tvrdik, P., Makki, N., Paxinos, G. and Watson, C. Precerebellar cell groups in the hindbrain of the mouse defined by retrograde tracing and correlated with cumulative Wnt1-cre genetic labeling. *Cerebellum* **10**, 570–584 (2011).

13. Rahimi-Balaei, M., Afsharinezhad, P., Bailey, K., Buchok, M., Yeganeh, B. and Marzban, H. Embryonic stages in cerebellar afferent development. *Cerebellum & ataxias* **2**, 7 (2015).

14. Grishkat, H. L. and Eisenman, L. M. Development of the spinocerebellar projection in the prenatal mouse. *J. Comp. Neurol.* **363**, 93–108 (1995).

15. Paradies, M. A. and Eisenman, L. M. Evidence of early topographic organization in the embryonic olivocerebellar projection: a model system for the study of pattern formation processes in the central nervous system. *Dev. Dyn.* **197**, 125–145 (1993).

16. Kalinovsky, A., Boukhtouche, F., Blazeski, R., Bornmann, C., Suzuki, N., Mason, C. A. and Scheiffele, P. Development of axon-target specificity of ponto-cerebellar afferents. *PLoS Biol.* **9**, e1001013 (2011).

17. Schweighofer, N., Lang, E. J. and Kawato, M. Role of the olivo-cerebellar complex in motor learning and control. *Front. Neural Circuits* **7**, 94 (2013).

18. Voogd, J. and Ruigrok, T. J. H. The organization of the corticonuclear and olivocerebellar climbing fiber projections to the rat cerebellar vermis: the congruence of projection zones and the zebrin pattern. *J. Neurocytol.* **33**, 5–21 (2004).

19. Miyata, T., Ono, Y., Okamoto, M., Masaoka, M., Sakakibara, A., Kawaguchi, A., Hashimoto, M. and Ogawa, M. Migration, early axonogenesis, and Reelin-dependent layer-forming behavior of early/posterior-born Purkinje cells in the developing mouse lateral cerebellum. *Neural Dev.* **5**, 23 (2010).

20. Sillitoe, R. V, Gopal, N. and Joyner, A. L. Embryonic origins of ZebrinII parasagittal stripes and establishment of topographic Purkinje cell projections. *Neuroscience* **162**, 574–588 (2009).

21. Middleton, F. A. and Strick, P. L. Cerebellar projections to the prefrontal cortex of the primate. *J. Neurosci.* **21**, 700–712 (2001).

22. Wang, V. Y., Rose, M. F. and Zoghbi, H. Y. Math1 expression redefines the rhombic lip derivatives and reveals novel lineages within the brainstem and cerebellum. *Neuron* **48**, 31–43 (2005).

23. Chizhikov, V. V, Lindgren, A. G., Currle, D. S., Rose, M. F., Monuki, E. S. and Millen, K. J. The roof

plate regulates cerebellar cell-type specification and proliferation. *Development* **133**, 2793–2804 (2006).

24. Miale, I. L. and Sidman, R. L. An autoradiographic analysis of histogenesis in the mouse cerebellum. *Exp. Neurol.* **4**, 277–296 (1961).

25. Gilthorpe, J. D., Papantoniou, E.-K., Chedotal, A., Lumsden, A. and Wingate, R. J. T. The migration of cerebellar rhombic lip derivatives. *Development* **129**, 4719–4728 (2002).

26. Zhu, Y., Yu, T. and Rao, Y. Temporal regulation of cerebellar EGL migration through a switch in cellular responsiveness to the meninges. *Dev. Biol.* **267**, 153–164 (2004).

27. Kuramoto, T., Kuwamura, M. and Serikawa, T. Rat neurological mutations cerebellar vermis defect and hobble are caused by mutations in the netrin-1 receptor gene Unc5h3. *Brain Res. Mol. Brain Res.* **122**, 103–108 (2004).

28. Przyborski, S. A., Knowles, B. B. and Ackerman, S. L. Embryonic phenotype of Unc5h3 mutant mice suggests chemorepulsion during the formation of the rostral cerebellar boundary. *Development* **125**, 41 LP – 50 (1998).

29. Goldowitz, D., Hamre, K. M., Przyborski, S. A. and Ackerman, S. L. Granule cells and cerebellar boundaries: analysis of Unc5h3 mutant chimeras. *J. Neurosci.* **20**, 4129–4137 (2000).

30. Chedotal, A. Slits and their receptors. *Adv. Exp. Med. Biol.* **621**, 65–80 (2007).

31. Marillat, V., Cases, O., Nguyen-Ba-Charvet, K. T., Tessier-Lavigne, M., Sotelo, C. and Chedotal, A. Spatiotemporal expression patterns of slit and robo genes in the rat brain. *J. Comp. Neurol.* **442**, 130–155 (2002).

32. Altman, J. Postnatal development of the cerebellar cortex in the rat. 3. Maturation of the components of the granular layer. *J. Comp. Neurol.* **145**, 465–513 (1972).

33. Espinosa, J. S. and Luo, L. Timing neurogenesis and differentiation: insights from quantitative clonal analyses of cerebellar granule cells. *J. Neurosci.* **28**, 2301–2312 (2008).

34. Komuro, H., Yacubova, E., Yacubova, E. and Rakic, P. Mode and tempo of tangential cell migration in the cerebellar external granular layer. *J. Neurosci.* **21**, 527–540 (2001).

35. Zmuda, J. F. and Rivas, R. J. The Golgi apparatus and the centrosome are localized to the sites of newly emerging axons in cerebellar granule neurons in vitro. *Cell Motil. Cytoskeleton* **41**, 18–38 (1998).

36. Chedotal, A. Should I stay or should I go? Becoming a granule cell. *Trends Neurosci.* **33**, 163–172 (2010).

37. Edmondson, J. C. and Hatten, M. E. Glial-guided granule neuron migration in vitro: a high-resolution time-lapse video microscopic study. *J. Neurosci.* **7**, 1928–1934 (1987).

38. Stoeckli, E. T. Understanding axon guidance: are we nearly there yet? *Development* **145**, (2018).

39. Dent, E. W. and Gertler, F. B. Cytoskeletal dynamics and transport in growth cone motility and axon guidance. *Neuron* **40**, 209–227 (2003).

40. Suter, D. M. and Forscher, P. Substrate-cytoskeletal coupling as a mechanism for the regulation of growth cone motility and guidance. *J. Neurobiol.* **44**, 97–113 (2000).

41. Marsh, L. and Letourneau, P. C. Growth of neurites without filopodial or lamellipodial activity in the presence of cytochalasin B. *J. Cell Biol.* **99**, 2041–2047 (1984).

42. Medeiros, N. A., Burnette, D. T. and Forscher, P. Myosin II functions in actin-bundle turnover in neuronal growth cones. *Nat. Cell Biol.* **8**, 215–226 (2006).

43. Letourneau, P. C. Cell-substratum adhesion of neurite growth cones, and its role in neurite elongation. *Exp. Cell Res.* **124**, 127–138 (1979).

44. Bridgman, P. C., Dave, S., Asnes, C. F., Tullio, A. N. and Adelstein, R. S. Myosin IIB is required for growth cone motility. *J. Neurosci.* **21**, 6159–6169 (2001).

45. Tanaka, E. M. and Kirschner, M. W. Microtubule behavior in the growth cones of living neurons during axon elongation. *J. Cell Biol.* **115**, 345–363 (1991).

46. Lee, A. C. and Suter, D. M. Quantitative analysis of microtubule dynamics during adhesion-mediated growth cone guidance. *Dev. Neurobiol.* **68**, 1363–1377 (2008).

47. Suter, D. M., Schaefer, A. W. and Forscher, P. Microtubule dynamics are necessary for SRC family kinase-dependent growth cone steering. *Curr. Biol.* **14**, 1194–1199 (2004).

48. Buck, K. B. and Zheng, J. Q. Growth cone turning induced by direct local modification of microtubule dynamics. *J. Neurosci.* **22**, 9358–9367 (2002).

49. Barallobre, M. J., Pascual, M., Del Rio, J. A. and Soriano, E. The Netrin family of guidance factors: emphasis on Netrin-1 signalling. *Brain Res. Brain Res. Rev.* **49**, 22–47 (2005).

50. Kullander, K. and Klein, R. Mechanisms and functions of Eph and ephrin signalling. *Nat. Rev. Mol. Cell Biol.* **3**, 475–486 (2002).

51. Raper, J. A. Semaphorins and their receptors in vertebrates and invertebrates. *Curr. Opin. Neurobiol.* **10**, 88–94 (2000).

52. Barber, M., Di Meglio, T., Andrews, W. D., Hernandez-Miranda, L. R., Murakami, F., Chedotal, A. and Parnavelas, J. G. The role of Robo3 in the development of cortical interneurons. *Cereb. Cortex* **19 Suppl 1**, i22-31 (2009).

53. Govek, E.-E., Newey, S. E. and Van Aelst, L. The role of the Rho GTPases in neuronal development. *Genes Dev.* **19**, 1–49 (2005).

54. Hall, A. Rho GTPases and the actin cytoskeleton. *Science* **279**, 509–514 (1998).

55. Moon, S. Y. and Zheng, Y. Rho GTPase-activating proteins in cell regulation. *Trends Cell Biol.* **13**, 13–22 (2003).

56. Schmidt, A. and Hall, A. Guanine nucleotide exchange factors for Rho GTPases: turning on the switch. *Genes Dev.* **16**, 1587–1609 (2002).

57. Miner, J. H. and Yurchenco, P. D. Laminin functions in tissue morphogenesis. *Annu. Rev. Cell Dev. Biol.* **20**, 255–284 (2004).

58. Wang, Q. and Wadsworth, W. G. The C domain of netrin UNC-6 silences calcium/calmodulin-dependent protein kinase- and diacylglycerol-dependent axon branching in Caenorhabditis elegans. *J. Neurosci.* **22**, 2274–2282 (2002).

59. Chan, S. S., Zheng, H., Su, M. W., Wilk, R., Killeen, M. T., Hedgecock, E. M. and Culotti, J. G. UNC-40, a C. elegans homolog of DCC (Deleted in Colorectal Cancer), is required in motile cells responding to UNC-6 netrin cues. *Cell* **87**, 187–195 (1996).

60. Hong, K., Hinck, L., Nishiyama, M., Poo, M., Tessier-Lavigne, M. and Stein, E. A Ligand-Gated Association between Cytoplasmic Domains of UNC5 and DCC Family Receptors Converts Netrin-Induced Growth Cone Attraction to Repulsion. *Cell* **97**, 927–941 (1999).

61. Keleman, K. and Dickson, B. J. Short- and Long-Range Repulsion by the Drosophila Unc5 Netrin Receptor. *Neuron* **32**, 605–617 (2001).

62. Purohit, A. A., Li, W., Qu, C., Dwyer, T., Shao, Q., Guan, K.-L. and Liu, G. Down Syndrome Cell Adhesion Molecule (DSCAM) Associates with Uncoordinated-5C (UNC5C) in Netrin-1-Mediated Growth Cone Collapse. *J. Biol. Chem.* (2012).

63. Keino-Masu, K., Masu, M., Hinck, L., Leonardo, E. D., Chan, S. S., Culotti, J. G. and Tessier-

Lavigne, M. Deleted in Colorectal Cancer (DCC) encodes a netrin receptor. *Cell* **87**, 175–185 (1996).

64. Geisbrecht, B. V, Dowd, K. A., Barfield, R. W., Longo, P. A. and Leahy, D. J. Netrin binds discrete subdomains of DCC and UNC5 and mediates interactions between DCC and heparin. *J. Biol. Chem.* **278**, 32561–32568 (2003).

65. Stein, E., Zou, Y., Poo, M. and Tessier-Lavigne, M. Binding of DCC by netrin-1 to mediate axon guidance independent of adenosine A2B receptor activation. *Science* **291**, 1976–1982 (2001).

66. Li, X., Saint-Cyr-Proulx, E., Aktories, K. and Lamarche-Vane, N. Rac1 and Cdc42 but not RhoA or Rho kinase activities are required for neurite outgrowth induced by the Netrin-1 receptor DCC (deleted in colorectal cancer) in N1E-115 neuroblastoma cells. *J. Biol. Chem.* **277**, 15207–15214 (2002).

67. Finci, L. I., Kruger, N., Sun, X., Zhang, J., Chegkazi, M., Wu, Y., Schenk, G., Mertens, H. D. T., Svergun, D. I., Zhang, Y., Wang, J.-H. and Meijers, R. The crystal structure of netrin-1 in complex with DCC reveals the bifunctionality of netrin-1 as a guidance cue. *Neuron* **83**, 839–849 (2014).

68. Killeen, M., Tong, J., Krizus, A., Steven, R., Scott, I., Pawson, T. and Culotti, J. UNC-5 function requires phosphorylation of cytoplasmic tyrosine 482, but its UNC-40-independent functions also require a region between the ZU-5 and death domains. *Dev. Biol.* **251**, 348–366 (2002).

69. Xu, K., Wu, Z., Renier, N., Antipenko, A., Tzvetkova-Robev, D., Xu, Y., Minchenko, M., Nardi-Dei, V., Rajashankar, K. R., Himanen, J., Tessier-Lavigne, M. and Nikolov, D. B. Neural migration. Structures of netrin-1 bound to two receptors provide insight into its axon guidance mechanism. *Science* **344**, 1275–1279 (2014).

70. Fitzgerald, D. P., Seaman, C. and Cooper, H. M. Localization of Neogenin protein during morphogenesis in the mouse embryo. *Dev. Dyn.* **235**, 1720–1725 (2006).

71. Hattori, D., Millard, S. S., Wojtowicz, W. M. and Zipursky, S. L. Dscam-mediated cell recognition regulates neural circuit formation. *Annu. Rev. Cell Dev. Biol.* **24**, 597–620 (2008).

72. Ly, A., Nikolaev, A., Suresh, G., Zheng, Y., Tessier-Lavigne, M. and Stein, E. DSCAM is a netrin receptor that collaborates with DCC in mediating turning responses to netrin-1. *Cell* **133**, 1241–1254 (2008).

73. Liu, G., Li, W., Wang, L., Kar, A., Guan, K.-L., Rao, Y. and Wu, J. Y. DSCAM functions as a netrin

receptor in commissural axon pathfinding. *Proc. Natl. Acad. Sci. U. S. A.* **106**, 2951–2956 (2009).

74. Boyer, N. P. and Gupton, S. L. Revisiting Netrin-1: One Who Guides (Axons). *Front. Cell. Neurosci.* **12**, 221 (2018).

75. Kennedy, T. E., Serafini, T., de la Torre, J. R. and Tessier-Lavigne, M. Netrins are diffusible chemotropic factors for commissural axons in the embryonic spinal cord. *Cell* **78**, 425–435 (1994).

76. Serafini, T., Colamarino, S. A., Leonardo, E. D., Wang, H., Beddington, R., Skarnes, W. C. and Tessier-Lavigne, M. Netrin-1 is required for commissural axon guidance in the developing vertebrate nervous system. *Cell* **87**, 1001–1014 (1996).

77. Colamarino, S. A. and Tessier-Lavigne, M. The axonal chemoattractant netrin-1 is also a chemorepellent for trochlear motor axons. *Cell* **81**, 621–629 (1995).

78. Varela-Echavarria, A., Tucker, A., Puschel, A. W. and Guthrie, S. Motor axon subpopulations respond differentially to the chemorepellents netrin-1 and semaphorin D. *Neuron* **18**, 193–207 (1997).

79. Dillon, A. K., Fujita, S. C., Matise, M. P., Jarjour, A. A., Kennedy, T. E., Kollmus, H., Arnold, H.-H., Weiner, J. A., Sanes, J. R. and Kaprielian, Z. Molecular control of spinal accessory motor neuron/axon development in the mouse spinal cord. *J. Neurosci.* **25**, 10119–10130 (2005).

80. Deiner, M. S., Kennedy, T. E., Fazeli, A., Serafini, T., Tessier-Lavigne, M. and Sretavan, D. W. Netrin-1 and DCC mediate axon guidance locally at the optic disc: loss of function leads to optic nerve hypoplasia. *Neuron* **19**, 575–589 (1997).

81. Lin, L., Rao, Y. and Isacson, O. Netrin-1 and slit-2 regulate and direct neurite growth of ventral midbrain dopaminergic neurons. *Mol. Cell. Neurosci.* **28**, 547–555 (2005).

82. Barallobre, M. J., Del Rio, J. A., Alcantara, S., Borrell, V., Aguado, F., Ruiz, M., Carmona, M. A., Martin, M., Fabre, M., Yuste, R., Tessier-Lavigne, M. and Soriano, E. Aberrant development of hippocampal circuits and altered neural activity in netrin 1-deficient mice. *Development* **127**, 4797–4810 (2000).

83. Alcantara, S., Ruiz, M., De Castro, F., Soriano, E. and Sotelo, C. Netrin 1 acts as an attractive or as a repulsive cue for distinct migrating neurons during the development of the cerebellar system. *Development* **127**, 1359 LP – 1372 (2000).

84. Lange, Y. Tracking cell cholesterol with cholesterol oxidase. *J. Lipid Res.* **33**, 315–321 (1992).

85. Dietschy, J. M. and Turley, S. D. Control of cholesterol turnover in the mouse. *J. Biol. Chem.* **277**, 3801–3804 (2002).

86. Dietschy, J. M., Turley, S. D. and Spady, D. K. Role of liver in the maintenance of cholesterol and low density lipoprotein homeostasis in different animal species, including humans. *J. Lipid Res.* **34**, 1637–1659 (1993).

87. Dietschy, J. M. and Turley, S. D. Cholesterol metabolism in the central nervous system during early development and in the mature animal. **45**, (2004).

88. Rubin, L. L. and Staddon, J. M. The cell biology of the blood-brain barrier. *Annu. Rev. Neurosci.* **22**, 11–28 (1999).

89. Dehouck, B., Fenart, L., Dehouck, M. P., Pierce, A., Torpier, G. and Cecchelli, R. A new function for the LDL receptor: transcytosis of LDL across the blood-brain barrier. *J. Cell Biol.* **138**, 877–889 (1997).

90. Quan, G., Xie, C., Dietschy, J. M. and Turley, S. D. Ontogenesis and regulation of cholesterol metabolism in the central nervous system of the mouse. *Brain Res. Dev. Brain Res.* **146**, 87–98 (2003).

91. Suzuki, S., Kiyosue, K., Hazama, S., Ogura, A., Kashihara, M., Hara, T., Koshimizu, H. and Kojima, M. Brain-derived neurotrophic factor regulates cholesterol metabolism for synapse development. *J. Neurosci.* **27**, 6417–6427 (2007).

92. Vance, J. E., Pan, D., Campenot, R. B., Bussiere, M. and Vance, D. E. Evidence that the major membrane lipids, except cholesterol, are made in axons of cultured rat sympathetic neurons. *J. Neurochem.* **62**, 329–337 (1994).

93. Hayashi, H., Campenot, R. B., Vance, D. E. and Vance, J. E. Glial lipoproteins stimulate axon growth of central nervous system neurons in compartmented cultures. *J. Biol. Chem.* **279**, 14009–14015 (2004).

94. Karten, B., Campenot, R. B., Vance, D. E. and Vance, J. E. Expression of ABCG1, but not ABCA1, correlates with cholesterol release by cerebellar astroglia. *J. Biol. Chem.* **281**, 4049–4057 (2006).

95. Zhang, J., Akwa, Y., el-Etr, M., Baulieu, E. E. and Sjovall, J. Metabolism of 27-, 25- and 24-hydroxycholesterol in rat glial cells and neurons. *Biochem. J.* **322 (Pt 1**, 175–184 (1997).

96. Bjorkhem, I., Diczfalusy, U. and Lutjohann, D. Removal of cholesterol from extrahepatic sources by oxidative mechanisms. *Curr. Opin. Lipidol.* **10**, 161–165 (1999).

97. Lund, E. G., Guileyardo, J. M. and Russell, D. W. cDNA cloning of cholesterol 24-hydroxylase, a mediator of cholesterol homeostasis in the brain. *Proc. Natl. Acad. Sci.* **96**, 7238 LP – 7243 (1999).

98. Lund, E. G., Xie, C., Kotti, T., Turley, S. D., Dietschy, J. M. and Russell, D. W. Knockout of the Cholesterol 24-Hydroxylase Gene in Mice Reveals a Brain-specific Mechanism of Cholesterol Turnover. *J. Biol. Chem.* **278**, 22980–22988 (2003).

99. Singer, S. J. and Nicolson, G. L. The fluid mosaic model of the structure of cell membranes. *Science* **175**, 720–731 (1972).

100. De Craene, J.-O., Bertazzi, D. L., Bar, S. and Friant, S. Phosphoinositides, Major Actors in Membrane Trafficking and Lipid Signaling Pathways. *Int. J. Mol. Sci.* **18**, (2017).

101. Singer, S. J. The Molecular Organization Of Biological Membranes. *Struct. Funct. Biol. Membr.* 145–222 (1971). doi:10.1016/B978-0-12-598650-2.50009-0

102. Nicolson, G. L. Transmembrane control of the receptors on normal and tumor cells: I. Cytoplasmic influence over cell surface components. *Biochim. Biophys. Acta - Rev. Biomembr.* **457**, 57–108 (1976).

103. Zhang, F., Lee, G. M. and Jacobson, K. Protein lateral mobility as a reflection of membrane microstructure. *BioEssays* **15**, 579–588 (1993).

104. Cho, W. Building Signaling Complexes at the Membrane. *Sci. STKE* **2006**, pe7 LP-pe7 (2006).

105. Marcelja, S. Lipid-mediated protein interaction in membranes. *Biochim. Biophys. Acta* **455**, 1–7 (1976).

106. Bagatolli, L. A., Ipsen, J. H., Simonsen, A. C. and Mouritsen, O. G. An outlook on organization of lipids in membranes: searching for a realistic connection with the organization of biological membranes. *Prog. Lipid Res.* **49**, 378–389 (2010).

107. Silvius, J. R. Partitioning of membrane molecules between raft and non-raft domains: insights from model-membrane studies. *Biochim. Biophys. Acta* **1746**, 193–202 (2005).

108. Dumas, F., Lebrun, M. C. and Tocanne, J. F. Is the protein/lipid hydrophobic matching principle relevant to membrane organization and functions? *FEBS Lett.* **458**, 271–277 (1999).

109. Pasenkiewicz-Gierula, M., Subczynski, W. K. and Kusumi, A. Influence of phospholipid unsaturation on the cholesterol distribution in membranes. *Biochimie* **73**, 1311–1316 (1991).

110. Kusumi, A. and Hyde, J. S. Spin-label saturation-transfer electron spin resonance detection of transient association of rhodopsin in reconstituted membranes. *Biochemistry* **21**, 5978–5983 (1982).

111. Grouleff, J., Irudayam, S. J., Skeby, K. K. and Schiott, B. The influence of cholesterol on membrane protein structure, function, and dynamics studied by molecular dynamics simulations. *Biochim. Biophys. Acta* **1848**, 1783–1795 (2015).

112. Aittoniemi, J., Niemela, P. S., Hyvonen, M. T., Karttunen, M. and Vattulainen, I. Insight into the putative specific interactions between cholesterol, sphingomyelin, and palmitoyl-oleoyl phosphatidylcholine. *Biophys. J.* **92**, 1125–1137 (2007).

113. Kusumi, A., Koyama-Honda, I. and Suzuki, K. Molecular dynamics and interactions for creation of stimulation-induced stabilized rafts from small unstable steady-state rafts. *Traffic* **5**, 213–230 (2004).

114. Ramstedt, B. and Slotte, J. P. Sphingolipids and the formation of sterol-enriched ordered membrane domains. *Biochim. Biophys. Acta* **1758**, 1945–1956 (2006).

115. Hancock, J. F. Lipid rafts: contentious only from simplistic standpoints. *Nat. Rev. Mol. Cell Biol.* **7**, 456–462 (2006).

116. Lindblom, G. and Oradd, G. Lipid lateral diffusion and membrane heterogeneity. *Biochim. Biophys. Acta* **1788**, 234–244 (2009).

117. Lucero, H. A. and Robbins, P. W. Lipid rafts–protein association and the regulation of protein activity. *Arch. Biochem. Biophys.* **426**, 208–224 (2004).

118. Simons, K. and Ikonen, E. Functional rafts in cell membranes. *Nature* **387**, 569–572 (1997).

119. Pike, L. J. Rafts defined: a report on the Keystone Symposium on Lipid Rafts and Cell Function. *Journal of lipid research* **47**, 1597–1598 (2006).

120. Maeda, Y. and Kinoshita, T. Structural remodeling, trafficking and functions of glycosylphosphatidylinositol-anchored proteins. *Prog. Lipid Res.* **50**, 411–424 (2011).

121. Kinoshita, T., Fujita, M. and Maeda, Y. Biosynthesis, Remodelling and Functions of Mammalian GPI-anchored Proteins: Recent Progress. *J. Biochem.* **144**, 287–294 (2008).

122. Orlean, P. and Menon, A. K. Thematic review series: lipid posttranslational modifications. GPI anchoring of protein in yeast and mammalian cells, or: how we learned to stop worrying and love glycophospholipids. *J. Lipid Res.* **48**, 993–1011 (2007).

123. Pike, L. J. Lipid rafts: bringing order to chaos. *J. Lipid Res.* **44**, 655–667 (2003).

124. Aicart-Ramos, C., Valero, R. A. and Rodriguez-Crespo, I. Protein palmitoylation and subcellular trafficking. *Biochim. Biophys. Acta - Biomembr.* **1808**, 2981–2994 (2011).

125. McCabe, J. B. and Berthiaume, L. G. N-terminal protein acylation confers localization to cholesterol, sphingolipid-enriched membranes but not to lipid rafts/caveolae. *Mol. Biol. Cell* **12**, 3601–3617 (2001).

126. Yamada, E. The fine structure of the gall bladder epithelium of the mouse. *J. Biophys. Biochem. Cytol.* **1**, 445–458 (1955).

127. Harder, T. and Simons, K. Caveolae, DIGs, and the dynamics of sphingolipid-cholesterol microdomains. *Curr. Opin. Cell Biol.* **9**, 534–542 (1997).

128. Couet, J., Li, S., Okamoto, T., Ikezu, T. and Lisanti, M. P. Identification of peptide and protein ligands for the caveolin-scaffolding domain. Implications for the interaction of caveolin with caveolae-associated proteins. *J. Biol. Chem.* **272**, 6525–6533 (1997).

129. Sargiacomo, M., Scherer, P. E., Tang, Z., Kubler, E., Song, K. S., Sanders, M. C. and Lisanti, M. P. Oligomeric structure of caveolin: implications for caveolae membrane organization. *Proc. Natl. Acad. Sci. U. S. A.* **92**, 9407–9411 (1995).

130. Das, K., Lewis, R. Y., Scherer, P. E. and Lisanti, M. P. The membrane-spanning domains of caveolins-1 and -2 mediate the formation of caveolin hetero-oligomers. Implications for the assembly of caveolae membranes in vivo. *J. Biol. Chem.* **274**, 18721–18728 (1999).

131. Dietzen, D. J., Hastings, W. R. and Lublin, D. M. Caveolin is palmitoylated on multiple cysteine residues. Palmitoylation is not necessary for localization of caveolin to caveolae. *J. Biol. Chem.* **270**, 6838–6842 (1995).

132. Parton, R. G. and Richards, A. A. Lipid Rafts and Caveolae as Portals for Endocytosis: New Insights and Common Mechanisms. *Traffic* **4**, 724–738 (2003).

133. Hering, H., Lin, C.-C. and Sheng, M. Lipid rafts in the maintenance of synapses, dendritic spines, and surface AMPA receptor stability. *J. Neurosci.* **23**, 3262–3271 (2003).

134. He, Q. and Meiri, K. F. Isolation and Characterization of Detergent-Resistant Microdomains Responsive to NCAM-Mediated Signaling from Growth Cones. *Mol. Cell. Neurosci.* **19**, 18–31 (2002).

135. Edidin, M. The state of lipid rafts: from model membranes to cells. *Annu. Rev. Biophys. Biomol. Struct.* **32**, 257–283 (2003).

136. Paratcha, G. and Ibanez, C. F. Lipid rafts and the control of neurotrophic factor signaling in the nervous system: variations on a theme. *Curr. Opin. Neurobiol.* **12**, 542–549 (2002).

137. Huang, C. S., Zhou, J., Feng, A. K., Lynch, C. C., Klumperman, J., DeArmond, S. J. and Mobley, W. C. Nerve growth factor signaling in caveolae-like domains at the plasma membrane. *J. Biol. Chem.* **274**, 36707–36714 (1999).

138. Tansey, M. G., Baloh, R. H., Milbrandt, J. and Johnson, E. M. J. GFRalpha-mediated localization of RET to lipid rafts is required for effective downstream signaling, differentiation, and neuronal survival. *Neuron* **25**, 611–623 (2000).

139. Suzuki, S., Numakawa, T., Shimazu, K., Koshimizu, H., Hara, T., Hatanaka, H., Mei, L., Lu, B. and Kojima, M. BDNF-induced recruitment of TrkB receptor into neuronal lipid rafts. *J. Cell Biol.* **167**, 1205 LP – 1215 (2004).

140. Besshoh, S., Bawa, D., Teves, L., Wallace, M. C. and Gurd, J. W. Increased phosphorylation and redistribution of NMDA receptors between synaptic lipid rafts and post-synaptic densities following transient global ischemia in the rat brain. *J. Neurochem.* **93**, 186–194 (2005).

141. Golub, T., Wacha, S. and Caroni, P. Spatial and temporal control of signaling through lipid rafts. *Curr. Opin. Neurobiol.* **14**, 542–550 (2004).

142. Palazzo, A. F., Eng, C. H., Schlaepfer, D. D., Marcantonio, E. E. and Gundersen, G. G. Localized stabilization of microtubules by integrin- and FAK-facilitated Rho signaling. *Science* **303**, 836–839 (2004).

143. Nakai, Y. and Kamiguchi, H. Migration of nerve growth cones requires detergent-resistant membranes in a spatially defined and substrate-dependent manner. *J. Cell Biol.* **159**, 1097–1108 (2002).

144. Guirland, C. and Zheng, J. Q. Membrane lipid rafts and their role in axon guidance. *Adv. Exp. Med. Biol.* **621**, 144–155 (2007).

145. Huber, A. B., Kolodkin, A. L., Ginty, D. D. and Cloutier, J.-F. Signaling at the growth cone: ligand-receptor complexes and the control of axon growth and guidance. *Annu. Rev. Neurosci.* **26**, 509–563 (2003).

146. Dekker, L. V and Segal, A. W. Perspectives: signal transduction. Signals to move cells. *Science* **287**, 982-983,985 (2000).

147. Gauthier, L. R. and Robbins, S. M. Ephrin signaling: One raft to rule them all? One raft to sort them? One raft to spread their call and in signaling bind them? *Life Sci.* **74**, 207–216 (2003).

148. Yu, W., Guo, W. and Feng, L. Segregation of Nogo66 receptors into lipid rafts in rat brain and inhibition of Nogo66 signaling by cholesterol depletion. *FEBS Lett.* **577**, 87–92 (2004).

149. Herincs, Z., Corset, V., Cahuzac, N., Furne, C., Castellani, V., Hueber, A.-O. and Mehlen, P. DCC association with lipid rafts is required for netrin-1-mediated axon guidance. *J. Cell Sci.* **118**, 1687–1692 (2005).

150. Guirland, C., Suzuki, S., Kojima, M., Lu, B. and Zheng, J. Q. Lipid Rafts Mediate Chemotropic Guidance of Nerve Growth Cones. *Neuron* **42**, 51–62 (2004).

151. van Meer, G. and Simons, K. Lipid polarity and sorting in epithelial cells. *J. Cell. Biochem.* **36**, 51–58 (1988).

152. Yu, J., Fischman, D. A. and Steck, T. L. Selective solubilization of proteins and phospholipids from red blood cell membranes by nonionic detergents. *J. Supramol. Struct.* **1**, 233–248 (1973).

153. Hanada, K., Nishijima, M., Akamatsu, Y. and Pagano, R. E. Both sphingolipids and cholesterol participate in the detergent insolubility of alkaline phosphatase, a glycosylphosphatidylinositol-anchored protein, in mammalian membranes. *J. Biol. Chem.* **270**, 6254–6260 (1995).

154. Mayor, S. and Maxfield, F. R. Insolubility and redistribution of GPI-anchored proteins at the cell surface after detergent treatment. *Mol. Biol. Cell* **6**, 929–944 (1995).

155. Komura, N., Suzuki, K. G. N., Ando, H., Konishi, M., Koikeda, M., Imamura, A., Chadda, R., Fujiwara, T. K., Tsuboi, H., Sheng, R., Cho, W., Furukawa, K., Furukawa, K., Yamauchi, Y., Ishida, H., Kusumi, A. and Kiso, M. Raft-based interactions of gangliosides with a GPI-anchored receptor. *Nat. Chem. Biol.* **12**, 402–410 (2016).

156. Day, C. A. and Kenworthy, A. K. Functions of cholera toxin B-subunit as a raft cross-linker. *Essays Biochem.* **57**, 135–145 (2015).

157. Van, H. S. Cholera toxin: interaction of subunits with ganglioside GM1. *Science* **183**, 656–657 (1974).

158. Gupta, N. and DeFranco, A. L. Visualizing lipid raft dynamics and early signaling events during antigen receptor-mediated B-lymphocyte activation. *Mol. Biol. Cell* **14**, 432–444 (2003).

159. Sezgin, E. and Schwille, P. Model membrane platforms to study protein-membrane interactions. *Mol. Membr. Biol.* **29**, 144–154 (2012).

160. Bagatolli, L. A., Sanchez, S. A., Hazlett, T. and Gratton, E. Giant vesicles, Laurdan, and two-photon fluorescence microscopy: evidence of lipid lateral separation in bilayers. *Methods Enzymol.* **360**, 481–500 (2003).

161. Sezgin, E. and Schwille, P. Fluorescence techniques to study lipid dynamics. *Cold Spring Harb. Perspect. Biol.* **3**, a009803 (2011).

162. Eggeling, C. Super-resolution optical microscopy of lipid plasma membrane dynamics. *Essays Biochem.* **57**, 69–80 (2015).

163. Axelrod, D., Ravdin, P., Koppel, D. E., Schlessinger, J., Webb, W. W., Elson, E. L. and Podleski, T. R. Lateral motion of fluorescently labeled acetylcholine receptors in membranes of developing muscle fibers. *Proc. Natl. Acad. Sci. U. S. A.* **73**, 4594–4598 (1976).

164. Reits, E. A. and Neefjes, J. J. From fixed to FRAP: measuring protein mobility and activity in living cells. *Nat. Cell Biol.* **3**, E145-7 (2001).

165. Staras, K., Mikulincer, D. and Gitler, D. Monitoring and quantifying dynamic physiological processes in live neurons using fluorescence recovery after photobleaching. *J. Neurochem.* **126**, 213–222 (2013).

166. Sprague, B. L. and McNally, J. G. FRAP analysis of binding: proper and fitting. *Trends Cell Biol.* **15**, 84–91 (2005).

167. Yildiz, A., Forkey, J. N., McKinney, S. A., Ha, T., Goldman, Y. E. and Selvin, P. R. Myosin V walks hand-over-hand: single fluorophore imaging with 1.5-nm localization. *Science* **300**, 2061–2065 (2003).

168. Manley, S., Gillette, J. M., Patterson, G. H., Shroff, H., Hess, H. F., Betzig, E. and Lippincott-Schwartz, J. High-density mapping of single-molecule trajectories with photoactivated localization microscopy. *Nat. Methods* **5**, 155 (2008).

169. Wiedenmann, J., Ivanchenko, S., Oswald, F., Schmitt, F., Rocker, C., Salih, A., Spindler, K.-D. and Nienhaus, G. U. EosFP, a fluorescent marker protein with UV-inducible green-to-red fluorescence conversion. *Proc. Natl. Acad. Sci. U. S. A.* **101**, 15905–15910 (2004).

170. Rust, M. J., Bates, M. and Zhuang, X. Sub-diffraction-limit imaging by stochastic optical reconstruction microscopy (STORM). *Nat. Methods* **3**, 793–796 (2006).

171. Cheezum, M. K., Walker, W. F. and Guilford, W. H. Quantitative comparison of algorithms for tracking single fluorescent particles. *Biophys. J.* **81**, 2378–2388 (2001).

172. Neumann, A. K., Itano, M. S. and Jacobson, K. Understanding lipid rafts and other related membrane domains. *F1000 Biol. Rep.* **2**, 31 (2010).

173. Jacobson, K., Liu, P. and Lagerholm, B. C. The Lateral Organization and Mobility of Plasma Membrane Components. *Cell* **177**, 806–819 (2019).

174. van de Manakker, F., Vermonden, T., van Nostrum, C. F. and Hennink, W. E. Cyclodextrin-Based Polymeric Materials: Synthesis, Properties, and Pharmaceutical/Biomedical Applications. *Biomacromolecules* **10**, 3157–3175 (2009).

175. Li, Z., Wang, M., Wang, F., Gu, Z., Du, G., Wu, J. and Chen, J. gamma-Cyclodextrin: a review on enzymatic production and applications. *Appl. Microbiol. Biotechnol.* **77**, 245–255 (2007).

176. Mahammad, S. and Parmryd, I. Cholesterol depletion using methyl-beta-cyclodextrin. *Methods Mol. Biol.* **1232**, 91–102 (2015).

177. Nishijo, J., Moriyama, S. and Shiota, S. Interactions of cholesterol with cyclodextrins in aqueous solution. *Chem. Pharm. Bull. (Tokyo).* **51**, 1253–1257 (2003).

178. Leventis, R. and Silvius, J. R. Use of cyclodextrins to monitor transbilayer movement and differential lipid affinities of cholesterol. *Biophys. J.* **81**, 2257–2267 (2001).

179. Mahammad, S., Dinic, J., Adler, J. and Parmryd, I. Limited cholesterol depletion causes aggregation of plasma membrane lipid rafts inducing T cell activation. *Biochim. Biophys. Acta* **1801**, 625–634 (2010).

180. Ahn, K. and Sampson, N. S. Cholesterol Oxidase Senses Subtle Changes in Lipid Bilayer Structure. *Biochemistry* **43**, 827–836 (2004).

181. Fernanandez-Garayzabal, J. F., Delgado, C., Blanco, M. M., Suarez, G. and Dominguez, L. Cholesterol oxidase from Rhodococcus equi is likely the major factor involved in the cooperative

lytic process (CAMP reaction) with Listeria monocytogenes. *Lett. Appl. Microbiol.* **22**, 249–252 (1996).

182. Fielding, C. J. and Fielding, P. E. Relationship between cholesterol trafficking and signaling in rafts and caveolae. *Biochim. Biophys. Acta - Biomembr.* **1610**, 219–228 (2003).

183. Sampson, N. S., Kass, I. J. and Ghoshroy, K. B. Assessment of the role of an omega loop of cholesterol oxidase: a truncated loop mutant has altered substrate specificity. *Biochemistry* **37**, 5770–5778 (1998).

184. Hillyard, D. Z., Nutt, C. D., Thomson, J., McDonald, K. J., Wan, R. K., Cameron, A. J. M., Mark, P. B. and Jardine, A. G. Statins inhibit NK cell cytotoxicity by membrane raft depletion rather than inhibition of isoprenylation. *Atherosclerosis* **191**, 319–325 (2007).

185. Coutinho, A., Silva, L., Fedorov, A. and Prieto, M. Cholesterol and ergosterol influence nystatin surface aggregation: relation to pore formation. *Biophys. J.* **87**, 3264–3276 (2004).

186. Fujii, G., Chang, J. E., Coley, T. and Steere, B. The formation of amphotericin B ion channels in lipid bilayers. *Biochemistry* **36**, 4959–4968 (1997).

187. Park, H., Go, Y. M., St John, P. L., Maland, M. C., Lisanti, M. P., Abrahamson, D. R. and Jo, H. Plasma membrane cholesterol is a key molecule in shear stress-dependent activation of extracellular signal-regulated kinase. *J. Biol. Chem.* **273**, 32304–32311 (1998).

188. Akhtar, R. S., Ness, J. M. and Roth, K. A. Bcl-2 family regulation of neuronal development and neurodegeneration. *Biochim. Biophys. Acta - Mol. Cell Res.* **1644**, 189–203 (2004).

189. Minnt, A. J., Boise, L. H. and Thompson, C. B. Bcl-XS Antagonizes the protective effects of Bcl-xL. *J. Biol. Chem.* **271**, 6306–6312 (1996).

190. Xiao, Q., Ford, A. L., Xu, J., Yan, P., Lee, K.-Y., Gonzales, E., West, T., Holtzman, D. M. and Lee, J.-M. Bcl-x Pre-mRNA Splicing Regulates Brain Injury after Neonatal Hypoxia-Ischemia. *J. Neurosci.* **32**, 13587–13596 (2012).

191. Bredesen, D. E., Ye, X., Tasinato, A., Sperandio, S., Wang, J. J., Assa-Munt, N. and Rabizadeh, S. p75NTR and the concept of cellular dependence: seeing how the other half die. *Cell Death Differ.* **5**, 365–371 (1998).

192. Ellerby, L. M., Hackam, A. S., Propp, S. S., Ellerby, H. M., Rabizadeh, S., Cashman, N. R., Trifiro, M. A., Pinsky, L., Wellington, C. L., Salvesen, G. S., Hayden, M. R. and Bredesen, D. E. Kennedy's

disease: caspase cleavage of the androgen receptor is a crucial event in cytotoxicity. *J. Neurochem.* **72**, 185–195 (1999).

193. Bredesen, D. E., Mehlen, P., Rabizadeh, S., Snipas, S. J., Assa-Munt, N. and Salvesen, G. S. The DCC gene product induces apoptosis by a mechanism requiring receptor proteolysis. *Nature* **395**, 801–804 (1998).

194. Liu, J., Yao, F., Wu, R., Morgan, M., Thorburn, A., Finley, R. L. J. and Chen, Y. Q. Mediation of the DCC apoptotic signal by DIP13 alpha. *J. Biol. Chem.* **277**, 26281–26285 (2002).

195. Forcet, C., Ye, X., Granger, L., Corset, V., Shin, H., Bredesen, D. E. and Mehlen, P. The dependence receptor DCC (deleted in colorectal cancer) defines an alternative mechanism for caspase activation. *Proc. Natl. Acad. Sci. U. S. A.* **98**, 3416–3421 (2001).

196. Llambi, F., Calheiros-Lourenço, F., Gozuacik, D., Guix, C., Pays, L., Del Rio, G., Kimchi, A. and Mehlen, P. The dependence receptor UNC5H2 mediates apoptosis through DAP-kinase. *EMBO J.* **24**, 1192–1201 (2005).

197. Llambi, F., Causeret, F., Bloch-Gallego, E. and Mehlen, P. Netrin-1 acts as a survival factor via its receptors UNC5H and DCC. *EMBO J.* **20**, 2715–2722 (2001).

198. Wei, Z., Wang, R., Wu, H., Zhang, M., Jin, H., Chan, L.-N., Wen, W., Yu, C. and Wen, Z. Autoinhibition of UNC5b Revealed by the Cytoplasmic Domain Structure of the Receptor. *Mol. Cell* **33**, 692–703 (2009).

199. Williams, M. E., Strickland, P., Watanabe, K. and Hinck, L. UNC5H1 induces apoptosis via its juxtamembrane region through an interaction with NRAGE. *J. Biol. Chem.* **278**, 17483–17490 (2003).

200. Meyerhardt, J. A., Caca, K., Eckstrand, B. C., Hu, G., Lengauer, C., Banavali, S., Look, A. T. and Fearon, E. R. Netrin-1: interaction with deleted in colorectal cancer (DCC) and alterations in brain tumors and neuroblastomas. *Cell Growth Differ.* **10**, 35–42 (1999).

201. Fearon, E. R., Cho, K. R., Nigro, J. M., Kern, S. E., Simons, J. W., Ruppert, J. M., Hamilton, S. R., Preisinger, A. C., Thomas, G. and Kinzler, K. W. Identification of a chromosome 18q gene that is altered in colorectal cancers. *Science* **247**, 49–56 (1990).

202. Ekstrand, B. C., Mansfield, T. A., Bigner, S. H. and Fearon, E. R. DCC expression is altered by multiple mechanisms in brain tumours. *Oncogene* **11**, 2393–2402 (1995).

203. Klingelhutz, A. J., Hedrick, L., Cho, K. R. and McDougall, J. K. The DCC gene suppresses the malignant phenotype of transformed human epithelial cells. *Oncogene* **10**, 1581–1586 (1995).

204. Narayanan, R., Lawlor, K. G., Schaapveld, R. Q., Cho, K. R., Vogelstein, B., Bui-Vinh Tran, P., Osborne, M. P. and Telang, N. T. Antisense RNA to the putative tumor-suppressor gene DCC transforms Rat-1 fibroblasts. *Oncogene* **7**, 553–561 (1992).

205. Thiebault, K., Mazelin, L., Pays, L., Llambi, F., Joly, M.-O., Scoazec, J.-Y., Saurin, J.-C., Romeo, G. and Mehlen, P. The netrin-1 receptors UNC5H are putative tumor suppressors controlling cell death commitment. *Proc. Natl. Acad. Sci. U. S. A.* **100**, 4173–4178 (2003).

206. Human Genome Sequencing Consortium I International Human Genome Sequencing C, corp-author. Finishing the euchromatic sequence of the human genome. *Nature* **431**, 931–945 (2004).

207. Gilbert, W. Why genes in pieces? *Nature* **271**, 501 (1978).

208. Kim, E., Goren, A. and Ast, G. Alternative splicing: current perspectives. *Bioessays* **30**, 38–47 (2008).

209. Jensen, K. B., Dredge, B. K., Stefani, G., Zhong, R., Buckanovich, R. J., Okano, H. J., Yang, Y. Y. L. and Darnell, R. B. Nova-1 regulates neuron-specific alternative splicing and is essential for neuronal viability. *Neuron* **25**, 359–371 (2000).

210. Li, Y. I., Sanchez-Pulido, L., Haerty, W. and Ponting, C. P. RBFOX and PTBP1 proteins regulate the alternative splicing of micro-exons in human brain transcripts. *Genome Res.* **25**, 1–13 (2015).

211. Wahl, M. C., Will, C. L. and Luhrmann, R. The spliceosome: design principles of a dynamic RNP machine. *Cell* **136**, 701–718 (2009).

212. Zhang, X., Yan, C., Zhan, X., Li, L., Lei, J. and Shi, Y. Structure of the human activated spliceosome in three conformational states. *Cell Res.* **28**, 307 (2018).

213. Kim, E., Magen, A. and Ast, G. Different levels of alternative splicing among eukaryotes. *Nucleic Acids Res.* **35**, 125–131 (2007).

214. Leggere, J. C., Saito, Y., Darnell, R. B., Tessier-Lavigne, M., Junge, H. J. and Chen, Z. NOVA regulates Dcc alternative splicing during neuronal migration and axon guidance in the spinal cord. *Elife* **5**, 1–25 (2016).

215. Maisse, C., Rossin, A., Cahuzac, N., Paradisi, A., Klein, C., Haillot, M.-L., Hérincs, Z., Mehlen, P. and Hueber, A.-O. Lipid raft localization and palmitoylation: Identification of two requirements

for cell death induction by the tumor suppressors UNC5H. *Exp. Cell Res.* **314**, 2544–2552 (2008).

216. OHTANI, Y., IRIE, T., UEKAMA, K., FUKUNAGA, K. and PITHA, J. Differential effects of α-, β- and γ-cyclodextrins on human erythrocytes. *Eur. J. Biochem.* **186**, 17–22 (1989).

217. Richmond, W. Preparation and Properties of a Cholesterol Oxidase from Nocardia sp. and Its Application to the Enzymatic Assay of Total Cholesterol in Serum. *Clin. Chem.* **19**, 1350 LP – 1356 (1973).

218. Bademosi, A. T., Steeves, J., Karunanithi, S., Zalucki, O. H., Gormal, R. S., Liu, S., Lauwers, E., Verstreken, P., Anggono, V., Meunier, F. A. and van Swinderen, B. Trapping of Syntaxin1a in Presynaptic Nanoclusters by a Clinically Relevant General Anesthetic. *Cell Rep.* **22**, 427–440 (2018).

219. Gil, V. and del Río, J. A. Analysis of axonal growth and cell migration in 3D hydrogel cultures of embryonic mouse CNS tissue. *Nat. Protoc.* **7**, 268 (2012).

220. de la Torre, J. R., Höpker, V. H., Ming, G., Poo, M., Tessier-Lavigne, M., Hemmati-Brivanlou, A. and Holt, C. E. Turning of Retinal Growth Cones in a Netrin-1 Gradient Mediated by the Netrin Receptor DCC. *Neuron* **19**, 1211–1224 (1997).

221. Martin, M. G., Perga, S., Trovò, L., Rasola, A., Holm, P., Rantamäki, T., Harkany, T., Castrén, E., Chiara, F., Dotti, C. G. and Parton, R. Cholesterol Loss Enhances TrkB Signaling in Hippocampal Neurons Aging in Vitro. *Mol. Biol. Cell* **19**, 2101–2112 (2008).

222. Djelti, F. *et al.* CYP46A1 inhibition, brain cholesterol accumulation and neurodegeneration pave the way for Alzheimer's disease. *Brain* **138**, 2383–2398 (2015).

223. Manitt, C., Thompson, K. M. and Kennedy, T. E. Developmental shift in expression of netrin receptors in the rat spinal cord: Predominance of UNC-5 homologues in adulthood. *J. Neurosci. Res.* **77**, 690–700 (2004).

224. Shcherbakova, A., Tiemann, B., Buettner, F. F. R. and Bakker, H. Distinct C- mannosylation of netrin receptor thrombospondin type 1 repeats by mammalian DPY19L1 and DPY19L3. *Proc. Natl. Acad. Sci.* **114**, 2574–2579 (2017).

225. Thomas, P. and Smart, T. G. HEK293 cell line: a vehicle for the expression of recombinant proteins. *J. Pharmacol. Toxicol. Methods* **51**, 187–200 (2005).

226. Llambi, F., Causeret, F., Bloch-Gallego, E. and Mehlen, P. Netrin-1 acts as a survival factor via its

receptors UNC5H and DCC. *EMBO J.* **20**, 2715–2722 (2001).

227. Williams, M. E., Lu, X., McKenna, W. L., Washington, R., Boyette, A., Strickland, P., Dillon, A., Kaprielian, Z., Tessier-Lavigne, M. and Hinck, L. UNC5A promotes neuronal apoptosis during spinal cord development independent of netrin-1. *Nat. Neurosci.* **9**, 996–998 (2006).

228. Johannes, L., Pezeshkian, W., Ipsen, J. H. and Shillcock, J. C. Clustering on Membranes: Fluctuations and More. *Trends Cell Biol.* **28**, 405–415 (2018).

229. Raghupathy, R., Anilkumar, A. A., Polley, A., Singh, P. P., Yadav, M., Johnson, C., Suryawanshi, S., Saikam, V., Sawant, S. D., Panda, A., Guo, Z., Vishwakarma, R. A., Rao, M. and Mayor, S. Transbilayer lipid interactions mediate nanoclustering of lipid-anchored proteins. *Cell* **161**, 581–594 (2015).

230. Goiko, M., de Bruyn, J. R. and Heit, B. Short-Lived Cages Restrict Protein Diffusion in the Plasma Membrane. *Sci. Rep.* **6**, 34987 (2016).

231. Picard, M., Petrie, R. J., Antoine-Bertrand, J., Saint-Cyr-Proulx, E., Villemure, J. F. and Lamarche-Vane, N. Spatial and temporal activation of the small GTPases RhoA and Rac1 by the netrin-1 receptor UNC5a during neurite outgrowth. *Cell. Signal.* **21**, 1961–1973 (2009).

232. Govek, E.-E., Wu, Z., Acehan, D., Molina, H., Rivera, K., Zhu, X., Fang, Y., Tessier-Lavigne, M. and Hatten, M. E. Cdc42 Regulates Neuronal Polarity during Cerebellar Axon Formation and Glial-Guided Migration. *iScience* **1**, 35–48 (2018).

233. Shaw, G., Morse, S., Ararat, M. and Graham, F. L. Preferential transformation of human neuronal cells by human adenoviruses and the origin of HEK 293 cells. *FASEB J.* **16**, 869–871 (2002).

234. Zhang, F., Crise, B., Su, B., Hou, Y., Rose, J. K., Bothwell, A. and Jacobson, K. Lateral diffusion of membrane-spanning and glycosylphosphatidylinositol-linked proteins: toward establishing rules governing the lateral mobility of membrane proteins. *J. Cell Biol.* **115**, 75–84 (1991).

235. Blouin, C. M., Le Lay, S., Eberl, A., Kofeler, H. C., Guerrera, I. C., Klein, C., Le Liepvre, X., Lasnier, F., Bourron, O., Gautier, J.-F., Ferre, P., Hajduch, E. and Dugail, I. Lipid droplet analysis in caveolin-deficient adipocytes: alterations in surface phospholipid composition and maturation defects. *J. Lipid Res.* **51**, 945–956 (2010).

236. Schuck, S., Honsho, M., Ekroos, K., Shevchenko, A. and Simons, K. Resistance of cell membranes to different detergents. *Proc. Natl. Acad. Sci. U. S. A.* **100**, 5795–5800 (2003).

237. Lopez, C. A., de Vries, A. H. and Marrink, S. J. Molecular mechanism of cyclodextrin mediated cholesterol extraction. *PLoS Comput. Biol.* **7**, e1002020 (2011).

238. Viola, A. and Gupta, N. Tether and trap: regulation of membrane-raft dynamics by actin-binding proteins. *Nat. Rev. Immunol.* **7**, 889–896 (2007).

239. Kaplan, A. and Sanz, R. L. Axotomy-Induced Ganglioside Processing: A Mediator of Axon Regeneration Restricted to the PNS. *J. Neurosci.* **34**, 8659–8661 (2014).

240. Roselló-Busquets, C., de la Oliva, N., Martínez-Mármol, R., Hernaiz-Llorens, M., Pascual, M., Muhaisen, A., Navarro, X., del Valle, J. and Soriano, E. Cholesterol Depletion Regulates Axonal Growth and Enhances Central and Peripheral Nerve Regeneration . *Frontiers in Cellular Neuroscience* **13**, 40 (2019).

241. Muller, C. C., Nguyen, T. H., Ahlemeyer, B., Meshram, M., Santrampurwala, N., Cao, S., Sharp, P., Fietz, P. B., Baumgart-Vogt, E. and Crane, D. I. PEX13 deficiency in mouse brain as a model of Zellweger syndrome: abnormal cerebellum formation, reactive gliosis and oxidative stress. *Dis. Model. Mech.* **4**, 104–119 (2010).

242. Faust, P. L. Abnormal cerebellar histogenesis in PEX2 Zellweger mice reflects multiple neuronal defects induced by peroxisome deficiency. *J. Comp. Neurol.* **461**, 394–413 (2003).

243. Tassew, N. G., Mothe, A. J., Shabanzadeh, A. P., Banerjee, P., Koeberle, P. D., Bremner, R., Tator, C. H. and Monnier, P. P. Modifying lipid rafts promotes regeneration and functional recovery. *Cell Rep.* **8**, 1146–1159 (2014).

244. Hérincs, Z., Corset, V., Cahuzac, N., Furne, C., Castellani, V., Hueber, A.-O. and Mehlen, P. DCC association with lipid rafts is required for netrin-1-mediated axon guidance. *J. Cell Sci.* **118**, 1687 LP – 1692 (2005).

245. Low, K., Culbertson, M., Bradke, F., Tessier-Lavigne, M. and Tuszynski, M. H. Netrin-1 Is a Novel Myelin-Associated Inhibitor to Axon Growth. *J. Neurosci.* **28**, 1099–1108 (2008).

246. Engelkamp, D. Cloning of three mouse Unc5 genes and their expression patterns at mid-gestation. *Mech. Dev.* **118**, 191–197 (2002).

247. Manley, S., Gillette, J. M. and Lippincott-Schwartz, J. Single-particle tracking photoactivated localization microscopy for mapping single-molecule dynamics. *Methods Enzymol.* **475**, 109–120 (2010).

248. Jaqaman, K., Loerke, D., Mettlen, M., Kuwata, H., Grinstein, S., Schmid, S. L. and Danuser, G. Robust single-particle tracking in live-cell time-lapse sequences. *Nat. Methods* **5**, 695–702 (2008).

249. Qian, H., Sheetz, M. P. and Elson, E. L. Single particle tracking. Analysis of diffusion and flow in two-dimensional systems. *Biophys. J.* **60**, 910–921 (1991).

250. Ernst, D. and Köhler, J. Measuring a diffusion coefficient by single-particle tracking: statistical analysis of experimental mean squared displacement curves. *Phys. Chem. Chem. Phys.* **15**, 845–849 (2013).

251. Cotrufo, T., Pérez-Brangulí, F., Muhaisen, A., Ros, O., Andrés, R., Baeriswyl, T., Fuschini, G., Tarrago, T., Pascual, M., Ureña, J., Blasi, J., Giralt, E., Stoeckli, E. T. and Soriano, E. A Signaling Mechanism Coupling Netrin-1/Deleted in Colorectal Cancer Chemoattraction to SNARE-Mediated Exocytosis in Axonal Growth Cones. *J. Neurosci.* **31**, 14463 LP – 14480 (2011).